2021

The role of DAXX in the selective autophagy receptor SQSTM1/p62 phase condensation

Yang, Yi

Copyright statement

b

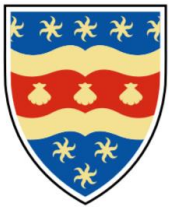

UNIVERSITY OF
PLYMOUTH

The role of DAXX in the selective autophagy receptor SQSTM1/p62 phase condensation

By

Yi Yang

A thesis submitted to the University of Plymouth in partial fulfilment

for the degree of

DOCTOR OF PHILOSOPHY

Peninsula Medical School

April 2021

Acknowledgements

There are so many people, without whom I would not have made it to this point.

First and foremost, I would like to acknowledge my Director of Studies, Professor Shouqing Luo, not only for offering me the opportunity to undertake a PhD and become part of your research group but also for sharing your experience, training me as a research scientist, defining the path of my research, and being patient with all my stupid questions. Your passion and enthusiasm for scientific research encourage me every single day to get the most of it and to achieve the goal I did not expect I would ever achieve. I will be grateful all my life for your unconditional support and help during the last four years. My thanks also go to my second supervisor, Professor Robert Fern, for your time and guidance in each stage throughout my study. There are several academics outside my supervisory team that I would like to thank. I would like to extend my thanks to Professor Bing Hu, Dr Xinpeng Dun and Dr Xinzhong Li, for your generous help and support to both my work and my life, giving me the warmth of family. I would like to acknowledge Dr Claudia Barros for your instruction of *Drosophila* experiments and Dr Torsten Bossing for your excellent support on microscopy. To Mr Waldemar Woznica, I would like to thank you for offering me the opportunity to work in the Animal House and being supportive every time I was in trouble. My thanks also go to Dr Fang Lin, your courage and passion for research have been motivated me through all these years.

I have been so fortunate to have met great people in Plymouth. It is my great pleasure working with a great research crew. To Robert Button, thank you for introducing me to everyone in JBB on my first day and helping me get familiar

with all the reagents and equipment. To Tracey Evans, thank you for caring about both my physical and mental health. My thanks also go to both the past and present members in our group: Sheridan Roberts, Thea Willis, Rebecca Sipthorpe, Evelina Valionyte, Katrina Cowan and Jack Kelly. I would also like to thank Foram, Jemma, Gabi, Liyam and Bora for encouraging me to talk, being really nice to me and listening to me patiently even I could only speak ‘survival English’. Your kindness has made me feel that I was not alone, and I am grateful for all the warmth and hugs you kindly offered. To academic visitors from China, Xiaoyan, Yan, Yuying, Qishuai, Jianlan and Ying, I cherish the days we have had, the problems we have solved and the day trips we have enjoyed. We did become a family in this country, and I hope I make the same impact in your lives as you have in mine. I am sorry that I cannot name every person in the lab who has helped and supported me through these years, but I am grateful to all of you.

I would also like to thank my parents for inspiring my love of science, life-long hobbies, and I cannot thank you both enough. To my mum, thank you for giving me every opportunity to explore my hobbies since I was 4 years old, inspiring me, encouraging me and believing in me, and thank you for the listening you have endured like a friend. I am so lucky to have a dad who is definitely a superhero in my heart, taking me for day trips exploring nature when I was a child, sharing with me your knowledge and experience. I would not have had the courage to travel to the UK and stay far away from home pursuing my dreams without your selfless financial and spiritual support. I am so fortunate to have invaluable encouragement from all my family. My grandparents, who have kept telling me to eat properly and take care of myself. My uncles and aunts, who have always sent

me positive messages and ‘red pocket’ money to support my life. Ye and Liu, my cousins, have always been there for me and listened to me incredibly patiently.

I would also like to thank my friends who have been there for me over these years. I would like to thank my friends from home, particularly Ying, Meng, Yangxin and Ming, for sharing with me funny stories to cheer me up almost every single day in the past four years and satisfying my desire of gossiping. Thank you for being there for me, you have made the jet lags disappear. I would also like to thank my friends in Plymouth for being all around. I cherish the night outs we have had and the songs we have sung together; I wish you all good in your study and work. Yinfei and Zehan, I cannot imagine how I could survive this pandemic lockdown without your supportive talks and company. I truly admire your scientific abilities and professional thoughts and hope one day we really do work together, and of course, continue our whiskey tasting together.

Without funding, this PhD thesis would not have existed. I would like to thank the University of Plymouth for offering me the opportunity to study in this beautiful ocean city and awarding me the scholarship, which made my life so much easier.

Lastly, in this COVID-19 pandemic situation, I would like to show my deepest gratitude to all the doctors, nurses, police, other key workers and volunteers all over the world. Thank you for devoting yourselves to fighting against the virus.

Thank you, the reader, for taking the time to look through this thesis. I wish you all the best in your careers.

Author's declaration

At no time during the registration for the research degree has the author been registered for any other University award, without prior agreement of the Doctoral College Quality Sub-Committee.

Work submitted for this research degree at the University of Plymouth has not formed part of any other degree either at the University of Plymouth or at another establishment.

This study was financed with the aid of a studentship from the University of Plymouth.

Publications (or public presentation of creative research outputs):

Yang, Y., Willis, T. L., Button, R. W., Strang, C. J., Fu, Y., Wen, X., Grayson, P. R. C., Evans, T., Sipthorpe, R. J., Roberts, S. L., Hu, B., Zhang, J., Lu, B., & Luo, S. (2019). Cytoplasmic DAXX drives SQSTM1/p62 phase condensation to activate Nrf2-mediated stress response. Nat Commun, 10(1), 3759. doi:10.1038/s41467-019-11671-2

Yang, Y., Valionyte, E., Kelly, J., & Luo, S. (2020). Histone H3F3/H3.3 chaperone DAXX converts to modulate SQSTM1 phase condensation for NFE2L2 activation. Autophagy, 16(1), 171-172. doi:10.1080/15548627.2019.1677323

Li, Z., Wang, C., Wang, Z., Zhu, C., Li, J., Sha, T., Ma, L., Gao, C., **Yang, Y.**, Sun, Y., Wang, J., Sun, X., Lu, C., Difiglia, M., Mei, Y., Ding, C., Luo, S., Dang, Y., Ding, Y., Fei, Y., & Lu, B. (2019). Allele-selective lowering of mutant HTT protein

by HTT-LC3 linker compounds. Nature, 575(7781), 203-209. doi:10.1038/s41586-019-1722-1

Roberts, S. L., Evans, T., **Yang, Y.**, Fu, Y., Button, R. W., Sipthorpe, R. J., Cowan, K., Valionyte, E., Anichtchik, O., Li, H., Lu, B., & Luo, S. (2020). Bim contributes to the progression of Huntington's disease-associated phenotypes. Hum Mol Genet, 29(2), 216-227. doi:10.1093/hmg/ddz275

Valionyte, E., **Yang, Y.**, Roberts, S. L., Kelly, J., Lu, B., & Luo, S. (2020). Lowering Mutant Huntingtin Levels and Toxicity: Autophagy-Endolysosome Pathways in Huntington's Disease. J Mol Biol, 432(8), 2673-2691. doi:10.1016/j.jmb.2019.11.012

Conferences Attended:

The 3rd UK Autophagy Network Meeting, University College London, UK (2017)

The 24th Annual Conference of Chinese Life Scientists Society in the UK, University of Cambridge, UK (2018)

The 25th Annual Conference of Chinese Life Scientists Society in the UK, University College London, UK (2019)

Word count of the main body of thesis: 34,199 words

Signed: Yi Yang

Date: 26.04.2021

Yi Yang

The role of DAXX in the selective autophagy receptor SQSTM1/p62 phase condensation

Abstract

Macroautophagy ('autophagy' hereafter) is a lysosome-dependent degradation system for intracellular protein quality control. Autophagy can selectively remove cargo materials, which is dependent on cargo receptors. SQSTM1/p62 ('p62' hereafter) is one of the best characterised receptors mediating the autophagic degradation of misfolded proteins, and its body formation is essential for its cargo recognition and clearance.

Mounting evidence has revealed that membraneless compartments, participating in various biological processes, are assembled via liquid-liquid phase separation (LLPS). These phase-separated condensates ensure that cellular activities occur in a spatiotemporally controlled manner and provide a method for concentrating and segregating cellular components. Liquid-like non-membrane condensates present dynamic properties and can exchange macromolecules with surroundings. The formation of non-membrane-bound p62 bodies is mediated by liquid-liquid phase separation. It has been yet poorly characterised the regulation of p62 liquid-liquid phase separation, and the molecular details of the assembly and functions of p62 bodies remain elusive. This study aims to identify a mechanism of it. Via an unbiased yeast two-hybrid screening, DAXX is found a p62 binding protein. Further experiments confirmed that cytoplasmic DAXX promotes p62 puncta formation and drives p62 liquid

phase condensation. *In vitro* experiments also confirmed that DAXX promotes p62 phase condensation. Evidence has suggested the critical role of the p62-Keap1-Nrf2 pathway in combating the oxidative stress and maintaining the cellular redox homeostasis. To examine whether DAXX has an effect on redox homeostasis, Reactive Oxygen Species (ROS) assays and Dual-luciferase assays were applied, and results showed that the DAXX-induced p62 phase condensation promotes p62 recruitment of Keap1 and subsequent Nrf2-mediated stress responses.

Collectively, this study suggests that cytoplasmic DAXX drives p62 phase condensation and regulates cellular redox homeostasis, providing a mechanistic insight into p62 phase separation and the prosurvival function of DAXX. Further investigation would reveal if DAXX-induced p62 phase condensation is implicated in ROS-relevant human diseases.

Table of contents

Table of figures

Table of abbreviations

3-MA: 3-methyladenine

AD: Alzheimer's Disease

ALS: Amyotrophic lateral sclerosis

ATG: Autophagy-related

AMP: Adenosine monophosphate

AMPK: AMP-activated protein kinase

ANOVA: Analysis of variance

aPKC: atypical protein kinase C

APP: Amyloid precursor protein

ARE: Antioxidant response elements

Atg: Autophagy-related

ATP: Adenosine triphosphate

Bcl-XL: B-cell lymphoma-extra large

BLAST: Basic local alignment search tool

BSA: Bovine serum albumin

CAG: cysteine, adenine and guanine

CHX: Cycloheximide

CMA: Chaperone-mediated autophagy

CQ: Chloroquine

Cvt: Cytoplasm-to-vacuole targeting

DAPI: 4′,6-diamidino-2-phenylindole

DCF: 2′,7′-dichlorofluorescein

$DCFH_2$: 2′,7′-dichlorodihydrofluorescein

$DCFH_2$-DA: 2′-7′-Dichlorodihydrofluorescein diacetate

DAXX: Death domain-associated protein 6

DEPTOR: DEP domain-containing mTOR-interacting protein

DMEM: Dulbecco’s modified Eagle’s medium

DNA: Deoxyribonucleic acid

Dox: doxycycline

DTT: Dithiothreitol

ECL: Enhanced chemiluminescence

ER: Endoplasmic reticulum

ERK: extracellular signal-regulated kinase

EM: Electron microscopy

FBS: Fetal bovine serum

FRAP: Fluorescence recovery after photobleaching

FTD: Frontotemporal dementia

GAPDH: Glyceraldehyde 3-phosphate dehydrogenase

GFP: Green fluorescent protein

GST: Glutathione-S-Transferase

GSTM1: Glutathione S-transferase Mu 1

H_2O_2: Hydrogen peroxide

HA: Hemagglutinin

HBD: Histone-binding domain

HD: Huntington disease

HDAC: Histone deacetylases

HEK: Human embryonic kidney

HSC70: Heat shock-cognate protein of 70 kDa

Htt: Huntingtin

IDR: Intrinsically disordered region

IP: Immunoprecipitation

IPTG: Isopropyl β-d-1-thiogalactopyranoside

JNK: Jun N-terminal kinase

Keap1: Kelch-like ECH-associated protein 1

KIR: Keap1-interacting region

KD: Knockdown

KO: Knockout

LAMP-2A: Lysosome-associated membrane protein type 2A

LC3: Microtubule-associated protein 1A/1B-light chain 3

LIR: LC3-interacting region

LLPS: Liquid-liquid phase separation

LRRK2: Leucine-rich repeat kinase 2

MAPK: Mitogen-activated protein kinase

MEF: Mouse embryonic fibroblast

MEK: MAPK/ERK kinase

mLST8: mammalian lethal with SEC13 protein 8

mTOR: mechanistic target of rapamycin

NBR1: Neighbor of Brca1 gene 1 (NBR1)

NCO4A: Nuclear receptor coactivator 4

NDP52: Nuclear domain 10 protein 52

NES: Nuclear export signal

NEMO: Nuclear factor-kappa-B essential modulator

NF-κB: Nuclear factor kappa-light-chain-enhancer of activated B cells

NIX: Nip3-like protein X

NLS: Nuclear localisation signal

NP-40: Nonyl phenoxypolyethoxylethanol

NTA: Nitrilotriacetic acid

NQO1: NAD(P)H: quinone oxidoreductase 1

Nrf2: Nuclear factor erythroid 2–related factor 2

OCT: Optimal cutting temperature

PAS: Preautophagosomal structure

PB1: Phox1 and Bem1p

PBS: Phosphate-buffered saline

PCR: Polymerase chain reaction

PD: Parkinson’s disease

PE: Phosphatidylethanolamine

PFA: Paraformaldehyde

PGAM5: Phosphoglycerate mutase 5

PINK1: PTEN-induced putative kinase 1

PML: Promyelocytic leukaemia

polyQ: Polyglutamine

PRAS40: Proline-rich Akt substrate of 40 kDa

PtdIns3K: Phosphatidylinositol 3-kinase

PTM: Post-translational modification

PVDF: Polyvinylidene difluoride

RFP: Red fluorescent protein

ROS: Reactive oxygen species

RNA: Ribonucleic acid

SDS-PAGE: Sodium dodecyl sulphate–polyacrylamide gel electrophoresis

SIM: SUMO-interacting motif

siRNA: small interfering RNA

SNARE: Soluble N-ethylmaleimide-sensitive factor activating protein receptor

SPOP: Speckle-type POZ protein

SUMO: Small ubiquitin-like modifier

SQSTM1: Sequestosome 1

TBS: Tris-buffered saline

TORC1: Target of rapamycin complex 1

TRAF6: TNF Receptor Associated Factor 6

TRAIL: Tumour necrosis factor-related apoptosis-inducing ligand

TRIM16: Tripartite motif protein family 16

TRIM21: Tripartite motif-containing protein 21

UBA: Ubiquitin-associated

ULK: Unc-51 Like autophagy activating kinase

UPS: Ubiquitin-Proteasome System

WT: Wild-type

Y2H: Yeast two-hybrid

Publications associated with this work

Yang, Y., Willis, T. L., Button, R. W., Strang, C. J., Fu, Y., Wen, X., Grayson, P. R. C., Evans, T., Sipthorpe, R. J., Roberts, S. L., Hu, B., Zhang, J., Lu, B., & Luo, S. (2019). Cytoplasmic DAXX drives SQSTM1/p62 phase condensation to activate Nrf2-mediated stress response. Nat Commun, 10(1), 3759. doi:10.1038/s41467-019-11671-2

Yang, Y., Valionyte, E., Kelly, J., & Luo, S. (2020). Histone H3F3/H3.3 chaperone DAXX converts to modulate SQSTM1 phase condensation for NFE2L2 activation. Autophagy, 16(1), 171-172. doi:10.1080/15548627.2019.1677323

1 Introduction

1.1 An overview of protein degradation pathways

1.1.1 The ubiquitin-proteasome system (UPS)

There are two main routes for intracellular protein degradation that have been described in eukaryotic cells, the Ubiquitin-Proteasome System (UPS) and the autophagy-lysosome pathway [1]. The UPS is responsible for 80-90% of proteins degradation, including short-lived proteins, insoluble misfolded proteins and polypeptides [2-4]. Through the UPS, targeted proteins are modified by the attachment of ubiquitin chains which are synthesised via a set of enzymes in an adenosine triphosphate (ATP)-dependent manner. Initially, ubiquitin forms ubiquitin adenylate in an ATP-requiring step and the C-terminal glycine residue of ubiquitin is attached to a cysteine residue of a specific activating enzyme, E1, with the release of adenosine monophosphate (AMP). The activated ubiquitin is transferred to the ubiquitin-conjugating enzyme, E2, and then linked to the targeted protein, catalysed by ubiquitin ligase enzyme, E3 (**Figure 1**) [3, 5]. Polyubiquitinated targets are then recognised and digested to short peptides by 26S proteasomes [6, 7]. To prevent cytoplasmic proteins from being degraded spuriously, targeted proteins are delivered into the proteasome core particle through a narrow channel. Therefore, the UPS substrate proteins must be unfolded before they can reach the active site. This also increases efficient hydrolysis of substrates.

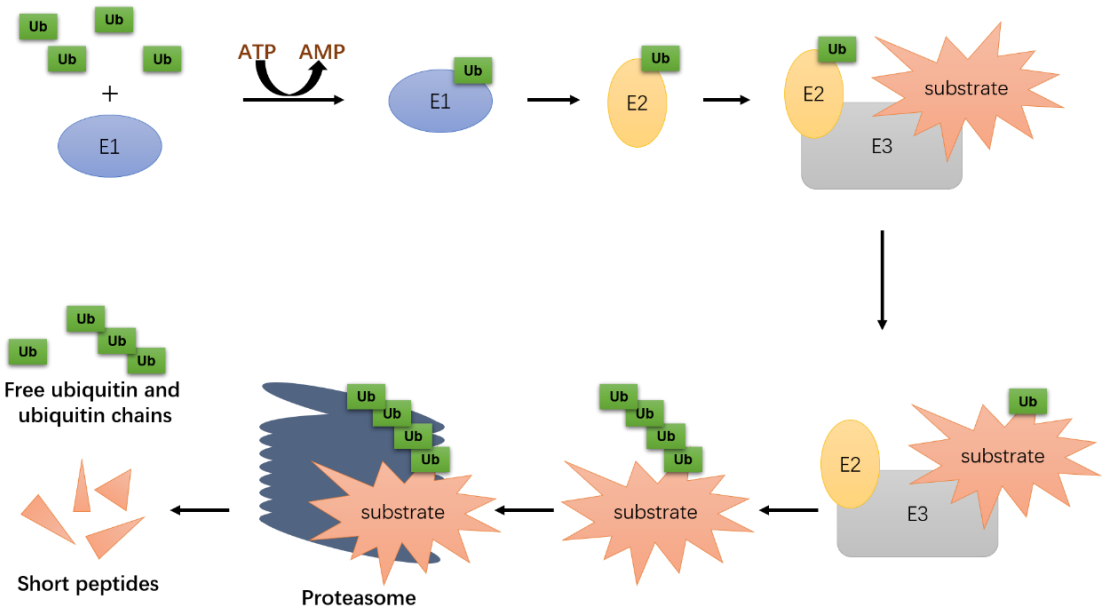

Figure 1 The ubiquitin-proteasome system.

The ubiquitin-proteasome system is the major cytosolic proteolytic system in eukaryotes. Through the ubiquitin-proteasome system, substrates are modified by ubiquitination, a covalent post-translational modification. Initially, ubiquitin is attached to a ubiquitin-activating enzyme (E1) in an ATP-dependent manner. The activated ubiquitin is then transferred to a cysteine of a ubiquitin-conjugating enzyme (E2). Then, E2 teams up with a ubiquitin-ligase (E3) to ubiquitinate the substrate. Substrates can be modified with a single ubiquitin or ubiquitin chains. Ubiquitinated substrates are recognised and degraded by the proteasome. In this way, short peptides and ubiquitin are released into the cytoplasm for recycling. Image adapted from [3, 8].

1.1.2 Different types of autophagy

Autophagy is involved in protein and organelle degradation and represents a single cell's adaption to starvation—when lack of food in the surroundings, a cell would break down part of itself for nutrient supply to stay alive [9, 10]. Hence, basal levels of autophagy are critical for maintaining cellular homeostasis. The term 'autophagy' refers to the 'self-eating' process in eukaryotes, coming from the Greek words that 'auto' means self while 'phagy' means eating [11]. Delivery of contents for degradation can occur in different ways. In higher eukaryotes, three major types of autophagy have been investigated in the past several

decades, microautophagy, chaperone-mediated autophagy (CMA) and macroautophagy (**Figure 2)** [12]. Microautophagy was first described by de Duve and Wattiaux in 1966, and studies were conducted mainly in yeast in the past two decades because of the lack of specific approaches [13, 14]. In microautophagy, the lysosomal membrane undergoes rearrangement to engulf cargoes and portions of cytoplasm, and resembles the formation of multivesicular bodies [15]. Studies of microautophagy on mammalian cells have been developed in recent years, mostly performed on rat hepatocytes or cardiac muscle cells. Recent studies have shown that endosomal microautophagy responds rapidly during starvation, eliciting rapid degradation of specific proteins [16, 17].

Chaperone-mediated autophagy (CMA) is a more selective process depending on the recognition of a chaperone, the heat shock-cognate protein of 70 KDa (HSC70), on cytosolic substrate proteins with a pentapeptide motif [18, 19]. The HSC70/cytosolic substrate complex binds to the lysosome membrane receptor protein, lysosome-associated membrane protein type 2A (LAMP-2A), then the substrate proteins undergo unfolding and translocating into lysosomes for degradation [20, 21]. This feature makes CMA distinctive from microautophagy and macroautophagy in that no vesicle formation occurs, and substrate proteins seem to cross the lysosomal membrane directly [21, 22].

Macroautophagy, by-far the most well-understood process of the three, will be focused on in this thesis. This is a process where double-membrane vesicles sequester parts of the cytoplasm and then fuse with lysosomes, transferring contents for degradation. The resulting contents are released back to the cytoplasm, contributing to future protein synthesis [23]. While CMA only degrades soluble proteins, macroautophagy has the capacity of delivering large structures

or even entire organelles for degradation. In this thesis, macroautophagy is referred to simply as 'autophagy', while microautophagy and CMA will be designated when appropriate.

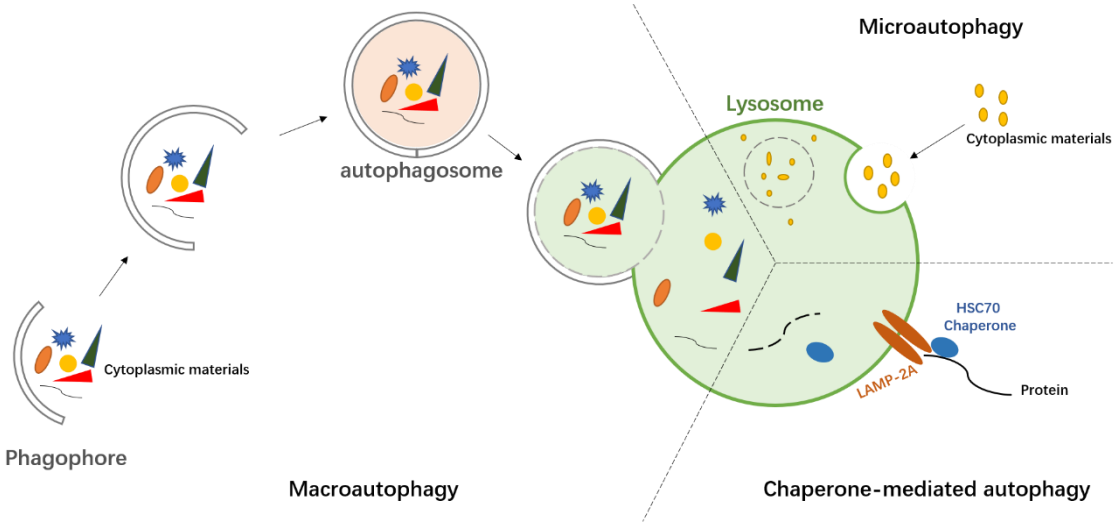

Figure 2: Different types of autophagy.

Three major pathways of autophagy, microautophagy, macroautophagy and chaperone-mediated autophagy, have been characterised. In microautophagy, substrates are engulfed directly in vesicles formed from lysosomal membranes. Macroautophagy is normally referred to as autophagy, and the hallmark is the presence of double-membrane autophagosomes engulfing substrates. Autophagosomes then fuse with lysosomes to form autolysosomes where the engulfed substrates are degraded. In chaperone-mediated autophagy, chaperone proteins, like the HSC70, target specific cytosolic substrates to the lysosome, and the HSC70/cytosolic substrate complex is recognised by lysosomal LAMP-2A and translocated into the lysosome. Substrates in these three types of autophagy are degraded in the lysosome. Image adapted from the Novus online source (https://www.novusbio.com/research-areas/autophagy).

1.2 Macroautophagy (Autophagy)

Autophagy is one of the major degradative pathways in eukaryotic cells, conserved from yeast to mammals [24]. It is a lysosome-dependent degradation system that mediates intracellular clearance of unwanted components, acting as a protein quality control mechanism during toxic macromolecules damage and as

a nutrient supply during cell starvation [25-27]. Autophagy has important roles in programmed cell death, tumour suppression, immune defence, cell development and prevention of neuron degeneration [28, 29].

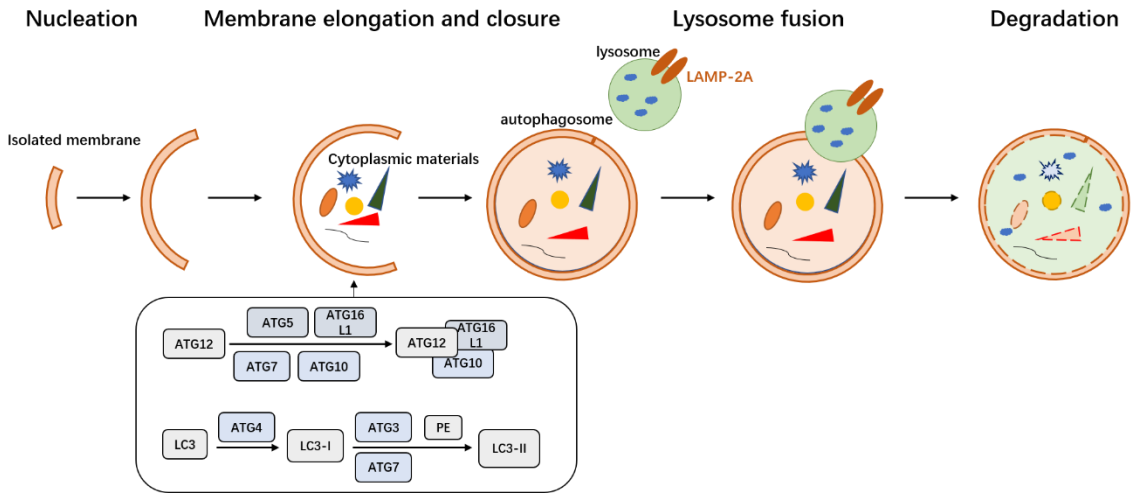

Figure 3: Brief overview of autophagy flux.

In mammalian cells, the process of autophagy initiates with the formation of crescent-shaped isolated membranes. Isolated membranes elongate and wrap substrates inside. Elongation of the isolated membranes depends on two ubiquitin-like conjugation systems. In the Atg12-Atg5-Atg16L1 system, Atg7 and Atg10 act as E1-like and E2-like enzymes, respectively, to conjugate Atg12 to Atg5 for Atg16L1 non-covalent binding. LC3 is cleaved by Atg4 to form LC3-I, which then conjugates to phosphatidylethanolamine (PE) and binds to autophagosomal membranes. The conjugation of LC3 to PE is believed to drive the expansion of autophagosomes. Following closure, autophagosomes are transported to late endosomes or lysosomes, forming autolysosomes. The sequestered substrates are then degraded by lysosomal hydrolases. Building blocks (e.g., amino acids from degraded proteins) are delivered back to the cytosol for reuse. Image adapted from [3].

During autophagy, induction, cargo recognition, autophagosome nucleation, autophagosome expansion and completion, autophagosome fusion with the vacuole/lysosome and breakdown, and nutrient recycling make up the process (**Figure 3**) [30]. A family of autophagy-related (Atg) proteins have been identified in yeast that have different functions during this process, and many of them have

orthologues in other eukaryotes [29-32]. Among these Atg proteins, Atg1-10, 12-14, 16 and 18 are referred to as ‘core Atg proteins’ that are required for autophagosome formation and are highly conserved in mammals, acting in a similar hierarchical manner [33, 34].

In mammalian cells, autophagy occurs at a basal level, and a mechanism for sensing the stress to induce autophagy is needed. One of the major nutrient and energy sensors is the mechanistic target of rapamycin (mTOR) which inhibits autophagy under basal condition. mTOR is a serine/threonine kinase that constitutes the complex 1, mTORC1, through the association with Raptor, DEP domain-containing mTOR-interacting protein (DEPTOR), the proline-rich Akt substrate of 40 kDa (PRAS40) and mammalian lethal with SEC13 protein 8 (mLST8), suppressing the Unc-51 Like autophagy activating kinase (ULK) complex under nutrient-rich conditions, and is sensitive to rapamycin [35]. Upon starvation, autophagy induction initiates by inactivation of mTORC1 and activation of ULK complex which is composed of the Atg1 homolog Unc-51-like kinase 1 or 2 (ULK1 or ULK2), Atg13, focal adhesion kinase (FAK)-family-interacting protein of 200 KD (FIP200) and Atg13-binding protein, Atg101 [36]. Starvation also causes a lack of glucose or accumulation of AMP that activates AMP-activated protein kinase (AMPK) and subsequently inactivates mTORC1 and activates the ULK1 complex [37]. Activation of ULK1 facilitates the capacity of autophagosome formation.

Then, the nucleation starts with the recruitment of Atg proteins to the isolated membrane, and the activation of the phosphatidylinositol 3-kinase (PtdIns3K) complex is essential. The nucleation of the isolated membrane is regulated by the Class III PtdIns3K complex (composed of beclin1, Vps34 and Vps15) that

functions as a positive regulator of autophagy [38]. Beclin 1, the ortholog of yeast Atg6, interacts with Class III PtdIns3K to mediate the localisation of autophagy proteins to the isolated membrane [39]. Class III PtdIns3K complex I contains Atg14, directing the complex to phagophore initiation sites and facilitating elongation [40, 41]. Atg9L1 (a mammalian Atg9 homologue), the only known transmembrane core Atg protein, is also required for autophagosome formation [42]. Atg9 was identified in yeast and it is believed to be essential for autophagosome formation. Atg9L1 is the orthologue of Atg9 in mammal, which is required for both the initiation and the expansion of the autophagosome. Recruitment of Atg9L1 to the autophagosomal membrane is dynamic and transient. It localises to autophagic structures, omegasomes, endosomes and trans-Golgi network, and shuttles among these organelles, delivering membranes to the expanding isolated membrane under regulations of p38 mitogen-activated protein kinase (MAPK)-binding protein, p38IP, and Beclin 1-binding protein, Bif-1 [43-45].

The origin of autophagic membranes remains a matter of debate, but plasma membrane, endoplasmic reticulum (ER), mitochondria, ER-Golgi intermediate compartment (ERGIC) are all considered possible sources [46]. Two ubiquitin-like (UBL) conjugation systems are involved in mammalian autophagic vesicle expansion and completion: Atg12-Atg5-Atg16L1 and microtubule-associated protein 1A/1B-light chain 3 (LC3)-phosphatidylethanolamine (PE). In the first, Atg12 is conjugated to Atg5, with Atg7 functions as an E1 enzyme and Atg10 functions as the E2 enzyme, then the conjugate interacts with Atg16L1. LC3 is cleaved by Atg4 and then activated by Atg7 (E1 enzyme), followed by transferring to Atg3 (E2 enzyme) and conjugating to PE, a major component of various

biological membranes [47]. The cleaved LC3, with an exposed glycine, is defined as form I (LC3-I). Then, the glycine residue conjugates to PE to form LC3-II, which is tightly bound to autophagosomal membranes. The conjugation of LC3 to PE is suggested to drive the expansion of autophagosomes [48, 49]. Though these two conjugates play essential roles in elongation and closure of the isolation membrane, the Atg12-Atg5 conjugate also acts as an E3 ligase assisting E2-like enzyme, Atg3, and enhance its activity in the LC3-PE system [50]. The Atg12-Atg5-Atg16 complex determines the site of LC3-PE production [51]. While LC3-II presents on both sides of the isolation membrane and part of the conjugates are left inside the autophagosome for degradation, Atg12-Atg5-Atg16 preferentially localises on the outer membrane and dissociates from the intact autophagosome [52, 53].

Upon maturation, autophagosomes fuse with endosomes or lysosomes to acquire lytic capacity and form autolysosomes, leading to the degradation of cargoes by hydrolases. In mammalian cells, LAMP-2, soluble N-ethylmaleimide-sensitive factor activating protein receptor (SNARE) proteins like Syntaxin 17 and Vesicle-associated membrane protein 8 (VAMP8) are required for this fusion step [54]. Syntaxin 17 localises to the outer membrane of completed autophagosomes but not to the unclosed intermediate autophagic structures, acting as a fusion signal with lysosomes [55].

Following fusion, substrates that are engulfed inside autophagosomes and the inner membrane of the autophagosomes are degraded by hydrolases. The molecular building blocks like amino acids and fatty acids produced by the cargoes are subsequently recycled back into the cytoplasm for reuse [56, 57].

1.3 Selective autophagy and p62

Autophagy used to be described as a ‘bulk’ process for protein degradation, in which cytosolic components are indiscriminately engulfed by phagophores for recycling during nutrient deprivation and cellular stress [58, 59]. However, mounting evidence has reviewed that autophagy is a more selective process responsible for specifically removing certain components, such as misfolded proteins and impaired organelles [60]. In non-selective autophagy, the phagophore grows out from ER, and the inner surface of the phagophore is not connected to any specific cargo, enabling a more random engulfment of cytoplasmic materials [61]. However, in selective autophagy, cytoplasmic components are selected before being sequestered into autophagic membranes, and these cargoes are tagged, often with ubiquitin, to increase the recognition by autophagy receptors [61]. According to the cytoplasmic materials that autophagosomes carry, selective autophagy can be classified into aggrephagy (aggregate-prone or misfolded proteins) [52-54], pexophagy (peroxisomes) [55, 56], mitophagy (mitochondria) [57-62], xenophagy (bacteria and virus) [63-65], reticulophagy (surplus ERs) [66] and ribophagy (ribosomes) [67], as shown in **Figure 4** [68-70].

Both bulk autophagy and selective autophagy share the same core autophagy machinery, but selective autophagy involves specific components that do not participate in bulk autophagy [27]. In selective autophagy, autophagy receptors are needed to connect selected substrates with lipidated Atg8 family proteins to the inner surface of the phagophore. The selected substrates are labelled before recognition by autophagy receptors, and many of them are labelled with ubiquitin.

It is also suggested that autophagy receptors and cargoes need to 'co-aggregate' to form a large enough structure to enable phagophore formation [61].

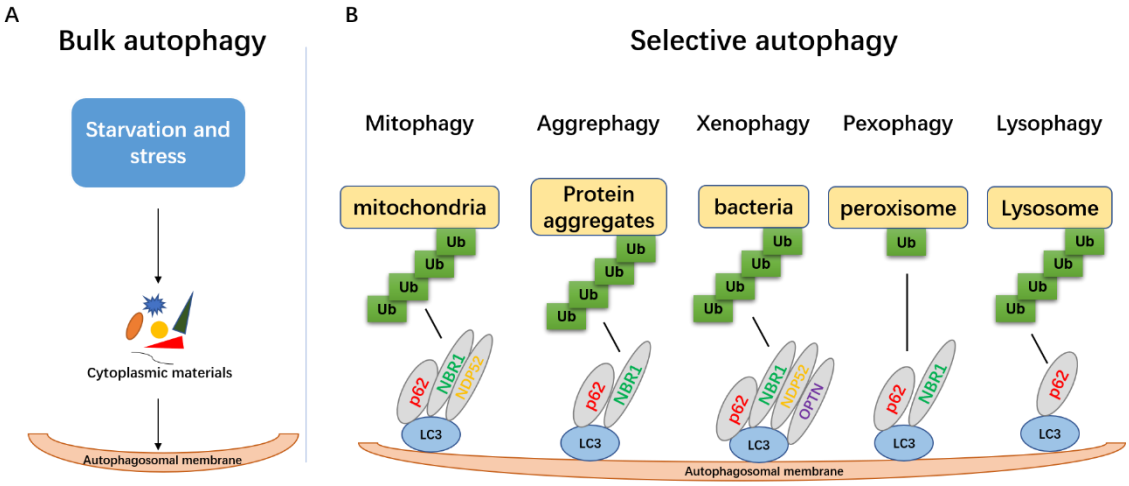

Figure 4: Bulk autophagy and selective autophagy.

A. Bulk autophagy serves to recycle building blocks in response to lack of nutrients and is thought to be non-selective towards its substrates. During bulk autophagy, cytoplasmic cargoes are sequestered into autophagosomes indiscriminately. **B.** Selective autophagy results in a more specific removal of damaged or harmful cellular components. The selectivity of autophagy is conferred by cargo receptors/autophagy receptors, such as p62, NBR1 and OPTN, that tether cargoes to autophagosomal membranes by binding cargoes and ATG8-family proteins simultaneously. In ubiquitin-dependent selective autophagy, the polyubiquitin chain in a ubiquitinated protein serves as a marker for cargo recognition by autophagy receptors via their ubiquitin-associated (UBA) domains. Selective autophagy is classified into a variety of types depending on the cargos that autophagosomes carry, such as mitophagy (mitochondria), aggrephagy (protein aggregates), xenophagy (bacteria), pexophagy (peroxisome) and lysophagy (lysosome). Image adapted from [62, 63].

1.3.1 Selective autophagy receptor p62

The recognition and isolation of specific types of cargoes are achieved by the action of autophagy receptors, such as sequestosome 1 (SQSTM1)/p62, that connect the cargoes to autophagic membranes. p62 is the first identified autophagy receptor, and after the discovery of p62, a set of autophagy receptors

are identified, such as the neighbour of Brca1 gene 1 (NBR1), nuclear domain 10 protein 52 (NDP52) and Optineurin [64-67]. These receptors can form aggregates in cells, interact with Atg8 family proteins and ubiquitin, and are selectively degraded with their cargoes [61, 65, 68, 69]. They participate in selective autophagy of different intracellular substrates. While p62 is implicated in the degradation of misfolded proteins, damaged organelles and intracellular bacteria, other autophagy receptors have more substrate specificity, like Nip3-like protein X (NIX) for degradation of mitochondria, nuclear receptor coactivator 4 (NCO4A) for degradation of ferritin, tripartite motif protein family 16 (TRIM16) for the degradation of lysosomes and FAM134B for the degradation of ER [70-73].

Among autophagy receptors, p62 is the most studied and described. The human p62 is 440 amino acids long. It harbours an N-terminal Phox1 and Bem1p (PB1) domain, a ZZ-type zinc (ZZ) finger domain, two nuclear localisation signals (NLSs), a TRAF6-binding domain (TB), a nuclear export signal (NES), an LC3-interacting region (LIR), a Kelch-like ECH-associated protein 1 (Keap1)-interacting region (KIR) and a C-terminal ubiquitin-associated (UBA) domain (**Figure 5**) [63, 74]. The protein-protein interaction domain PB1 enables p62 to interact with other PB1-containing proteins, such as NBR1, and complete its self-oligomerisation, allowing it to bind to ubiquitin-positive cargoes and isolated membranes with high avidity [75, 76]. The NLSs and NES allow p62 to shuttle between the nucleus and the cytoplasm, and in this way, p62 is found not only in the cytoplasm but also in the nucleus [77]. The C-terminal UBA domain binds to both monoubiquitin and polyubiquitin, leading to p62 accumulation in ubiquitin-positive inclusions [78, 79]. The KIR is involved in regulating the activation of the oxidative stress response transcription factor, nuclear factor erythroid 2–related

factor 2 (Nrf2) [80]. p62 binds to PE-conjugated autophagosomal LC3-II via its LIR domain, recruiting ubiquitinated proteins as well as itself for autophagic degradation [68].

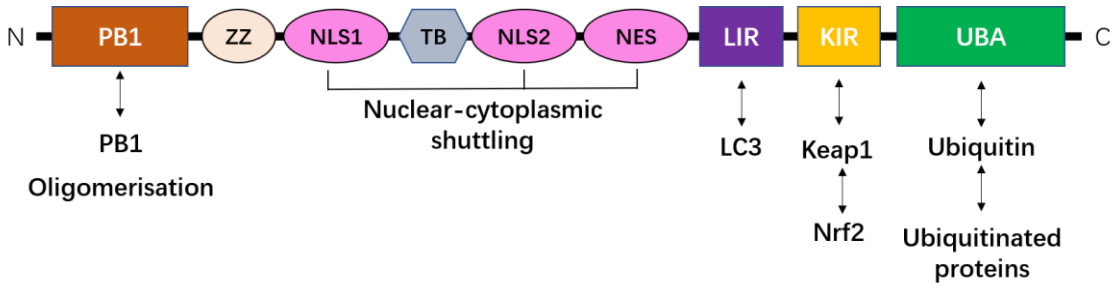

Figure 5: The domain architecture of p62.

p62 harbours several functional domains. The N-terminal Phox1 and Bem1p (PB1) domain is responsible for its self-oligomerisation. The ZZ zinc-finger (ZZ) domain binds to receptor-interacting proteins. Two nuclear localisation signals (NLSs) and a nuclear export signal (NES) allow p62 to shuttle between the nucleus and the cytoplasm. The TRAF6 binding (TB) domain binds to TRAF6, and the LC3-interacting region (LIR) interacts with LC3. The Kelch-like ECH-associated protein 1 (Keap1) interacting region (KIR) interacts with Keap1, participating in the regulation of Nuclear factor erythroid 2-related factor 2 (Nrf2) in oxidative stress. The ubiquitin-associated (UBA) domain regulates the interaction of p62 with polyubiquitinated proteins. Image adapted from [81].

1.3.2 Regulation of selective autophagy

Selective autophagy is a tightly regulated process regulating cellular homeostasis in cooperating with other intracellular quality control systems, and the dysfunction of selective autophagy is associated with ageing and other aggregate-prone protein-based diseases like Alzheimer's disease and Parkinson's disease [82]. Selective autophagy initiates locally at the sites where selected substrates accumulate [83].

The roles of p62 in selective autophagy are widely established. The regulation of p62 in selective autophagy is at the transcription level to increase the amount of p62 and at the post-translational level to facilitate co-aggregation of p62 with cargoes. It acts as a scaffold for the formation of protein aggregates as well as a receptor between ubiquitinated proteins and LC3, linking ubiquitin-tagged protein cargoes to autophagosomes for degradation [84, 85]. The selection and labelling of damaged cytoplasmic materials is an important step, and the recruitment of autophagy receptors to their cargoes triggers the process.

Autophagic clearance of polyubiquitinated proteins requires p62 to recruit them into inclusion bodies, mediated by its UBA domain and PB1 domain that facilitates homo-oligomerisation [84, 86]. The oligomerisation of p62 serves different roles, for example, sequestering ubiquitinated proteins into inclusions and forming filamentous structures that may serve as a site for phagophore membrane development [87]. During selective autophagy, p62 forms long PB1-linked helical filaments inducing autophagosome nucleation when recognised and bound by autophagosomal marker LC3 [86]. Then ubiquitinated proteins are recruited to these filaments, fragmented into shorter forms and engulfed by the nascent autophagosomal membrane [84, 86]. Finally, the structures are degraded through autophagy.

Transcriptional regulation of p62

The level of p62 is maintained low by continuous degradation under normal conditions; however, when cells are under oxidative stress, p62 is strongly up-regulated by transfection factor Nrf2 for cellular oxidative stress responses [88]. The Keap1-Nrf2 pathway is one of the major cell defence mechanisms against oxidative stress, and Nrf2 is degraded via a Keap1-Cullin-3-dependent

mechanism by the UPS pathway under quiescent conditions (**Figure 6**) [89]. p62 is able to competitively interact with the Nrf2-binding domain on Keap1, inhibiting the Keap1-Nrf2 interaction. In response to oxidative stress, Keap1 is recruited to p62 via KIR and degraded together with p62, resulting in Nrf2 detaches from Keap1 and enters the nucleus for activation of oxidative stress response genes [80]. The transcription of p62 enhances the capacity of selective autophagy. In this way, a positive feedback loop created by p62 and Nrf2 in response to oxidative stress, and when removal of oxidative stress, p62 is degraded and the loop is turned off [88]. In addition to responding to oxidative stress, p62 is associated with other stress conditions, for example, the pro-inflammatory nuclear factor kappa B (NF-κB) pathway [63]. p62 interacts with atypical protein kinase C (aPKC) via PB1 domain, and the p62-aPKC complexes act as signal-organising centres where p62 interacts with E3 ligase, TNF Receptor Associated Factor 6 (TRAF6), activating the transcription factor NF-κB [90, 91]. NF-κB also induces transcription of p62 and constitutes a positive p62- NF-κB feedback loop in cancers [92]. TRAF6 also activates nuclear factor-kappa-B essential modulator (NEMO), and both NEMO and p62 act in the NF-κB signalling pathway, promoting inflammatory and prosurvival pathways [93].

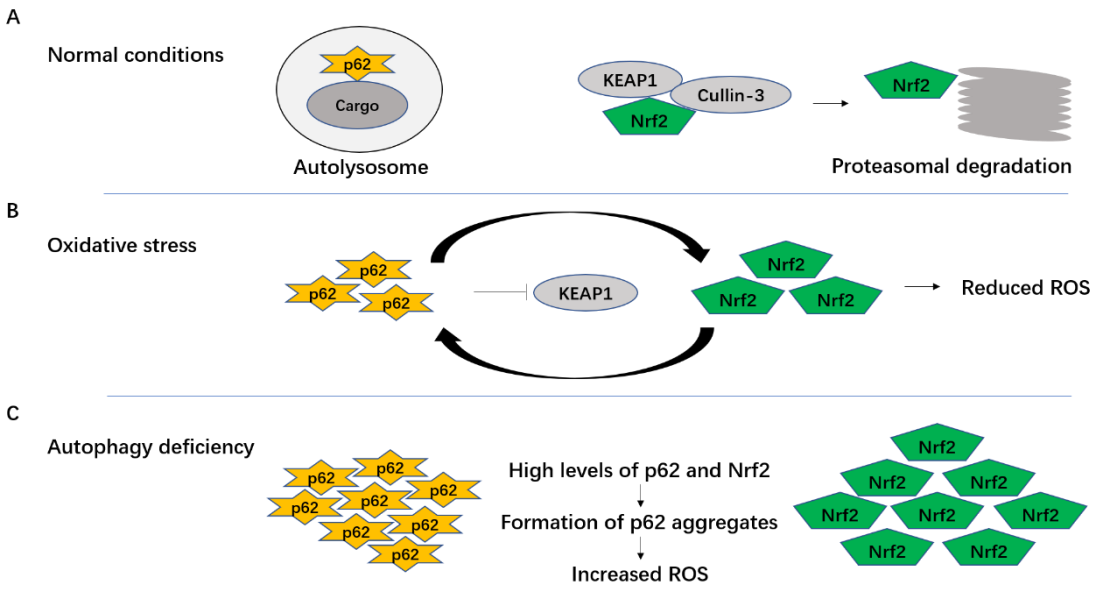

Figure 6: p62 and Nrf2 in oxidative stress response.

A. Under normal conditions, p62 is degraded with cargoes in the autolysosome by autophagy, and Nrf2 is degraded with Keap1 by the proteasome. **B.** Under oxidative stress, elevated p62 recruits Keap1 and allows Nrf2 to enter the nucleus, activating the transcription of stress-response enzymes. A feedback loop is formed between p62 and Nrf2 where Nrf2 induces p62 expression and p62 inhibits Keap1-mediated Nrf2 degradation. This results in the induction of intracellular antioxidant response. **C.** Autophagy deficiency leads to high levels of p62 and Nrf2. The accumulation of excess p62 and Nrf2 potentially induces ROS production. Image adapted from [63, 94].

Regulation of p62 by post-translational modifications

Post-translational modifications (PTMs) of proteins are crucial in determining protein structure, activity, function and destination. For example, phosphorylation regulates protein-protein interaction, glycosylation regulates protein folding, and ubiquitination regulates protein degradation [95-98]. Post-translational modifications are normally tightly regulated but can occur non-specifically during increased cellular stress. In this way, the activity of autophagy receptors is regulated by PTMs to control their interactions with cellular components.

For p62, its ability to interact with ubiquitinated substrates is also induced by PTMs. When not required as an autophagy receptor, p62 is inactivated through homodimerisation of its UBA, preventing its interaction with ubiquitin [99]. Phosphorylation of p62 within UBA enhances its association with ubiquitinated proteins, promoting its sequestering activity. Precisely, phosphorylation on serine residue 407 via ULK1 facilitates UBA transition from dimer to monomer, liberating the UBA domain [100]. Then phosphorylation of p62 on serine residue 403 increases its affinity and enhances its binding with ubiquitin chains [101]. Serine 349, conserved across vertebrate species, is another essential phosphorylation site in p62. It locates in p62's KIR motif, and serine 349-phosphorylated p62 has a higher affinity for Keap1, in a mTORC1-dependent manner. This process participates in a cytoprotective mechanism in response to bacterial infection (xenophagy), and phosphorylation of p62 activates the Keap1-Nrf2 pathway, inducing expression of cytoprotective Nrf2 targets [102, 103].

In addition to phosphorylation, ubiquitination of p62 also plays an important role in blocking the UBA homodimerisation and increasing ubiquitin binding. Endogenous p62 is found to increase ubiquitination upon stress such as heat shock via interacting with E2 ubiquitin-conjugating enzymes, UBE2D2 and UBE2D3, catalysing ubiquitination on lysine residue 420 [104]. This may change p62 conformation and switch on the recognition of polyubiquitin chains. Lysine 420 of p62 can be ubiquitinated by the Keap1/Cul3 E3 ligase complex, enhancing sequestration activity and degradation [105]. Ubiquitination of p62 also occurs in the PB1 domain. Tripartite motif-containing protein 21 (TRIM21) ubiquitinates p62 at lysine 7, abrogating p62 oligomerisation, thus inhibiting p62's sequestration activity [106].

1.3.3 Multifunction of p62

In addition to being a cargo receptor in selective autophagy, p62 plays pivotal roles in diverse cellular events, including cell survival and death, amino acid sensing and oxidative stress response. p62 recruits polyubiquitinated caspase-8 for the caspase activation in tumour necrosis factor-related apoptosis-inducing ligand (TRAIL) stimulation, positively control apoptosis signalling pathway, which can be used in examining cell death [107, 108]. p62 binding to TRAF6 is required for the sustained activation of NF-κB that is necessary for cell survival, and loss of p62 enhances cell death in embryo fibroblasts [109]. p62 interacts with Raptor, the mTORC1 components, and activates mTORC1 in response to amino acids [110]. In oxidative stress conditions, p62 recruits Keap1 from the cytoplasmic Keap1-Nrf2 complex, contributing to the expression of anti-oxidant and anti-inflammatory enzymes [80].

p62 and the Keap1-Nrf2 pathway

Reactive oxygen species (ROS), such as hydrogen peroxide (H_2O_2), are more active than molecular oxygen, and high levels of intracellular ROS can oxidise biological molecules, constantly damage cells in an oxygen-rich environment [111-113]. H_2O_2-induced Deoxyribonucleic acid (DNA) double-strand breaks and chromosomal aberration are considered to be a primary cause of cancer, and these breaks are repaired more slowly than those induced by irradiation [114-116]. ROS have essential roles in cell growth and differentiation [117], gene expression [118, 119] and signalling pathways [120]. However, while high ROS levels are accompanied by actions that harm cell survival, low ROS levels activate signalling pathways to initiate biological processes [121]. It is critical to maintain a balance in ROS, and oxidative stress occurs once this balance is

disturbed [113, 118, 122]. Many assays measure ROS, and 2′-7′-Dichlorodihydrofluorescein diacetate ($DCFH_2$-DA) is one of the most widely used fluorescent probes for detection by flow cytometry [123-125]. When crossing the cell membrane, the colourless and reduced $DCFH_2$-DA is deacetylated into non-fluorescent and cell-impermeable 2′,7′-dichlorodihydrofluorescein ($DCFH_2$) by intracellular esterases. $DCFH_2$ is then oxidised into 2′,7′-dichlorofluorescein (DCF) that is fluorescent and can be detected by flow cytometry, excited at 485 nm and measured at 530 nm [124, 126, 127].

The Keap1-Nrf2 system is a cellular defence mechanism against oxidative and electrophilic stresses, acting as a cytoplasmic sensor for oxidative stress and ROS response [128-130]. Transcription factor Nrf2 is found to bind the antioxidant response elements (ARE) with high affinity and regulate the expression of detoxifying enzymes, such as glutathione S-transferase Mu 1 (GSTM1) and NAD(P)H: quinone oxidoreductase 1 (NQO1) [131-134]. Under basal conditions, Nrf2 is retained in the cytosol and degraded by proteasomes rapidly. Nrf2 maintains a low protein level in cells, and Keap1 suppresses Nrf2 transcription activity by interacting with its highly conserved amino-terminal region [135-138]. Under oxidative stress conditions, ROS inactivates Keap1, and Nrf2 translocates to the nucleus and initiates the transcription of detoxifying enzymes to protect the cell from oxidative damage [139].

It is reported that autophagy substrates such as p62, p53-regulated p21 and Bcl-XL-interacting protein, phosphoglycerate mutase 5 (PGAM5), disrupt the Keap1-Nrf2 pathway by competitively binding to Keap1, resulting in persistent activation of Nrf2 [88, 140-142]. p62 binds to Keap1 through its KIR motif. Oxidative stress is well recognised in neurodegenerative pathology, and Nrf2 is confirmed to have

a protective role against neurodegenerative diseases that provides new avenues for drug development, disease prevention and therapy [143-146].

1.4 Liquid-liquid phase separation (LLPS)

Over the past few years, a series of intracellular body structures have been described as non-membrane-bound liquid compartments, including Cajal bodies, nucleoli, P granules and promyelocytic leukaemia (PML) bodies [147, 148]. Cajal bodies were described as ‘semifluid spheres suspended in semifluid nucleoplasm’ in 2005. P granules are ribonucleic acid (RNA) and protein-containing bodies in embryos of *Caenorhabditis elegans* formed by phase separation, which was confirmed to have liquid-like properties [147, 149, 150]. Later, nucleoli were observed as similar structures [151]. Such non-membrane structures were evident from their appearance, deformability and dynamic exchanges of components, and evidence has suggested that these non-membrane structures are formed through liquid-liquid phase separation (LLPS) [152, 153]. LLPS is a physical process that a homogeneous solution separates into two distinct phases, with one phase is enriched for the macromolecules components and another is depleted the same. When proteins or nucleic acids undergo LLPS, they condense into a dense phase, behaving like liquid droplets and co-existing with a dilute phase [154]. These non-membrane structures, acting as biomolecular condensates, are able to concentrate biomolecules and subsequently increase the local concentration of biomolecules, having function consequences such as sequestering molecules and buffering molecule concentration [155]. In this way, LLPS defines distinct compartments to efficiently organise cellular processes, without interfering with each other in the complex and heterogeneous environment [156]. LLPS is mediated by weak and transient interactions between

molecules with multivalent domains or intrinsically disordered regions (IDRs) [157]. The states of condensates transit from liquid-like into gel-like or solid-like during phase separation, in which weak and transient interactions become strong and stable interactions. Thus, the condensates exhibit reduced mobility [158]. The properties of condensates are critical for their function.

LLPS of proteins and RNA drives the formation of RNA granules, such as stress granules, Cajal bodies and nucleoli [155]. The non-membrane feature allows these organelles quick assembly and disassembly, reflecting various cellular conditions. This process is highly regulated in the complex intracellular environment, and unregulated RNA granules have been observed in disease, for example, the transition of stress granules into ‘aggregate-like’ inclusions is believed to be a significant cause in neurodegenerative diseases such as amyotrophic lateral sclerosis (ALS) and frontotemporal dementia (FTD) [159]. Also, changes in numbers and shapes of nucleoli in most cancer cells indicate that a cancer-specific nuclear environment may be related to the assembly and disassembly of these condensates [156].

1.4.1 LLPS plays roles in autophagy

LLPS is involved in different steps of autophagy, contributing to the assembly of autophagosome formation sites, the regulation of the activity of TORC1 kinase, and the degradation of protein cargoes. Phase separation and transition can be modulated by stress condition or pathological insults, resulting in the failure of protein condensates degradation by autophagy.

LLPS mediates the assembly of autophagosome formation sites

LLPS organises the preautophagosomal structure in yeast. In yeast, autophagosome initiates from a single site, the preautophagosomal structure (PAS) on the vacuolar membrane, and fuses with vacuole directly upon closure. The yeast Atg1 complex, which consists of Atg1, Atg13, Atg17, Atg29 and Atg31, has a central role in autophagy initiation [160]. The multivalent interaction of the scaffold protein Atg17 and the intrinsically disordered protein Atg13 dimers induces Atg1 complex phase separation. PAS organisation is regulated by TORC1. Under normal conditions, Atg13 is hyperphosphorylated by TORC1, inhibiting the formation of the ATG1 complex; upon autophagy induction, Atg13 is dephosphorylated and the ATG1 complex is formed [161]. The condensates are tethered to the vacuolar membrane, moving rapidly and forming a large condensate, the early PAS [162]. Atg proteins are recruited to the early PAS in a hierarchical order and form the PAS. The PAS has the property of high liquidity, which allows dynamic exchanges of materials in the cytoplasm to enhance autophagosome generation [161, 163]. Further studies are needed to investigate if LLPS of ULK1 complex triggers autophagosome formation site in multicellular organisms.

LLPS mediates TORC1 activity

TORC1 regulates various steps of autophagy [164]. TORC1 activity is modulated by stress-induced phase separation products, and the sequestration of TORC1 into stress granules is an adaptive response. Under heat stress, TORC1 is recruited to stress granules; TORC1 is reactivated through stress granules disassembly upon heat stress recovery [165]. Moreover, yeast polyA binding protein-binding protein 1, Pbp1, induces autophagy by inhibiting TORC1 signalling [166]. Pbp1 binds to TORC1 via a C-terminal low-complexity region.

The phase separation of this low-complexity region forms reversible assemblies under respiratory stress and is required for inhibition of TORC1. Together, stress-induced LLPS is involved in TORC1 activity.

LLPS specifies protein cargoes for degradation

LLPS also identifies protein cargoes for selective autophagic degradation. Recently, studies have discovered that autophagy selectively degrades proteins in a state of liquid droplet that is formed through LLPS but does poorly with protein aggregates [167]. The vacuolar enzyme aminopeptidase I (Ape1) in yeast is a target of selective autophagy, participating in the cytoplasm-to-vacuole targeting (Cvt) pathway [168]. Ape1 undergoes LLPS to form the semi-liquid droplet, the Ape1 complex, which has gel-like properties. The Ape1-specific receptor protein Atg19 interacts with Atg8 and Atg11, functioning in the generation and expansion of the isolated membrane to sequester the Ape1 complex into the Cvt vesicle [169]. However, the Pro-to-Leu mutation at residue 22 (P22L) in Ape1 forms condensates with almost no mobility which fail to be selectively sequestered by isolated membranes. Taken together, the gel-like property of protein cargoes is crucial for selectively autophagic clearance of biomolecular condensates.

1.4.2 LLPS and p62

p62 recognition and selection of cargo materials is an essential step allowing cargoes to be isolated by autophagic membranes. In the previous study, p62 is observed in several types of cytoplasm inclusions and associated with protein aggregates in several aggregation diseases [170, 171]. These p62 bodies were described to co-localise with ubiquitin under fluorescence microscopy, thus been thought that p62 achieves cargo recognition by forming protein aggregates [79, 84]. However, it is found that in cultured cells, endogenous p62 forms inclusion

bodies containing polyubiquitin chains, and these spherical p62 bodies seems to grow by fusion, which makes it not a classical ‘aggregate’ [84].

When cells suffer from proteotoxic stress, ubiquitin-positive proteins are concentrated into condensates, which is largely dependent on p62 [84]. Autophagic cargoes are tethered through p62 filaments, followed by phase separation into larger condensates and link to autophagic membranes [8]. The PB1 domain and UBA domain of p62 are required for this activity, and the presence of ubiquitin chains containing three or more ubiquitins is essential. Recent studies demonstrate that p62 bodies are also formed via phase separation, and recombinant p62 undergoes liquid-liquid phase separation *in vitro* [148, 172]. These findings showed that the structures formed by p62 have liquid-like properties and undergo phase separation. Unlike protein aggregates that are considered to lack mobility and are unlikely to have biochemical reactions, p62 liquid-like droplets can maintain their conformation and activity, exchanging components including ubiquitin and LC3, with the surrounding environment [148]. Besides that, p62-ubiquitin condensates are believed as substrates for selective autophagy.

LLPS represents a biophysical process with roles in neurodegenerative diseases. For example, LLPS of phosphorylated Tau is confirmed as the initial step toward tau aggregation, causing long-term toxicity through ER stress and further neuronal death [173]. It occurs in Alzheimer disease brains, with hyperphosphorylated tau undergoing LLPS.

For p62, as phase separation is required for p62 body formation, which is essential for its cargo recruitment and subsequent degradation, understanding

the initial and progressive LLPS of p62 may support the development of study on p62 functions.

1.4.3 *In vitro* LLPS assays

Numerous studies have shown that cellular non-membrane organelles and compartments are assembled by LLPS, and this tightly controlled assembly is a key mechanism for cells to spatiotemporally coordinate intracellular biochemical reactions [152, 155]. By converting a homogeneous liquid phase into a dense inhomogeneous phase, LLPS offers these non-membrane compartments defined boundaries as well as the capacity to remain dynamic, exchanging materials with surroundings, at the same time [174]. Phase separation/condensation/transition is regulated by parameters, such as protein concentration, microenvironmental temperature and ionic strength, the presence of other molecules (such as another protein or RNA), and also the tag on recombinant proteins [175-178].

Different assays are used to investigate LLPS step-by-step, from expression and purification of recombinant proteins as well as induction of LLPS to studies of the biophysical properties of the liquid droplets formed by LLPS. *In vitro* phase separation assays of purified recombinant proteins have become the standard way to test whether the proteins have the ability of phase separation or liquid condensates formation. Since many phase-separating proteins harbour a complex domain organisation and are highly aggregation-prone, expression and purification should be carried out carefully, and recombinant proteins should be heterologously overexpressed. BL21 (DE3) competent *E.coli* strain is often sufficient for efficient recombinant protein expression. Other expression systems, like yeast or insect cells, are available to reduce the aggregation propensity and offer post-translational modifications and can be used for optimisation [179].

Besides, multi-step affinity chromatography with low-binding resins, like Ni-NTA (Nickel-charged affinity resin crosslinks with chelating ligand nitrilotriacetic acid), is preferred for the purification of sticky proteins. Salt concentration and pH of phase separating buffers and stocking buffers, and stocking temperature also affect the properties of proteins, and conditions should be optimised for each specific protein. After purification, protein samples should always be adjusted to sodium dodecyl sulphate–polyacrylamide gel electrophoresis (SDS-PAGE) to test the purity and integrity before applied to phase separation assay.

Microscopic detection of LLPS is often used when detecting LLPS, and among which, light microscopy is the most common way [154]. Initially, macromolecules have no apparent assemblies at starting condition. With a change in conditions, such as changes in pH, temperature or ion strength, followed by a fixed incubation time, the presence of liquid droplets can be observed and imaged microscopically. Fluorescence recovery after photobleaching (FRAP) is an assessment of droplets' liquidity because different components vary in the rate of recovery due to different mobilities. It can be carried out on a confocal microscope equipped with a necessary laser, and is useful for assessing material states or changes in the state through time. The fluorescence recovery is quicker in liquid-like droplets than in gel-like droplets, and the fluorescence signals fail to recover in protein aggregates. It can also be used as a half-FRAP when the structure is large enough [147]. The rearrangement of fluorescence from the unbleached area to the bleached area gives direct information on the mobility of macromolecules within one droplet. Other methods, like fluorescence correlation spectroscopy and polarised fluorescence microscopy, may be used for more accurate estimates and detections of the droplets [180, 181]. In addition,

proteinase K digestion can be used to examine the density of protein aggregates/bodies because highly dense protein bodies resist proteinase K digestion [182]. Wetting assay and sedimentation assay are also used for confirmation of LLPS.

1.4.4 LLPS and diseases

There are maybe dangers buried in the cytoplasm. The molecular interactions that are important for driving the assembly of non-membrane organelles may also lead to the formation of physiological structures in healthy cells. Those same interactions could go awry and cause problems in cells. The RNA-binding protein with a polyQ-expansion called Whi3 separates into liquid droplets, but over time those liquid droplets can form solid inclusions, suggesting that the liquid state has the potential to transit to more stable and toxic fibrous states [183]. The ALS related RNA binding protein, heterogeneous nuclear ribonucleoproteins A1 (hnRNPA1), also forms pathological solid fibrillar deposits [184]. Aberrant liquid-solid phase transition leads to the formation of solid aggregates with strong interactions of components; for example, the disease-linked solid phase of ALS-associated protein, FUS, even exhibits crystal-like structures [185]. Apart from neurodegenerative diseases, aberrant LLPS is also associated with cancers and other human diseases [186]. These studies are yet at a very early stage. Several key signalling transduction proteins, which are essential for tumour proliferation, have been found to form condensates, suggesting that LLPS may be crucial for maintaining the highly proliferative state of tumour cells [187].

1.5 DAXX

Death domain-associated protein 6 (DAXX) is first described as a signalling protein that binds to cell surface death receptor, Fas, to induce Fas-mediated apoptosis and activate the Jun N-terminal kinase (JNK) pathway [188]. DAXX is ubiquitously expressed in various human tissues, and its orthologs are only found in animals, termed DLP in *drosophila* [189]. Structurally, human DAXX is 740 amino acids long with several domains; the 4-helix bundle (4HB), 55-144 amino acids of DAXX, is the major binding site for proteins that interact with N-terminal DAXX, while the small ubiquitin-like modifier (SUMO)-interacting motif (SIM) is for protein interactions with C-terminal DAXX (**Figure 7**). The central part of DAXX is a highly conserved region containing six α-helices that can fold into a defined structure [190]. The crucial structure of this core domain is the histone-binding domain (HBD) that forms a complex with histone H3.3-H4. As a histone chaperone, DAXX directly and specifically binds to one of the histone variants, H3.3, expressed in the cell cycle continuously, and can assemble H3.3-containing nucleosomes [191, 192]. This nucleosome turnover is crucial in epigenome maintenance, and the assembly of chromosomal DNA acts as a constitutive way in eukaryotic chromatins [193-195].

Apart from being a histone chaperone, DAXX is a multifunctional protein in both the cytoplasm and the nucleus, regulating several processes such as cell death and cell survival, apoptosis, transcriptional regulation and DNA damage response. Loss of DAXX causes embryonic lethality in early mouse development, indicating the role in embryogenesis [197]. DAXX overexpression is commonly observed in diverse cancers, correlating with tumorigenesis, disease progression and treatment resistance. Increased expression of DAXX is seen in several cancers

compared with corresponding controls, and DAXX levels are further increased markedly in metastases in breast, prostate and colon cancers, compared with primary tumours, supporting the oncogenic role of DAXX [196]. Indeed, DAXX overexpression enhances tumorigenesis and metastasis in ovarian cancer cells [198]. DAXX is also involved in DNA damage response by dissociating from mouse double minute 2 homolog (Mdm2), an E3 ligase that increases tumour suppressor p53 degradation, and contributing to p53 activation [199].

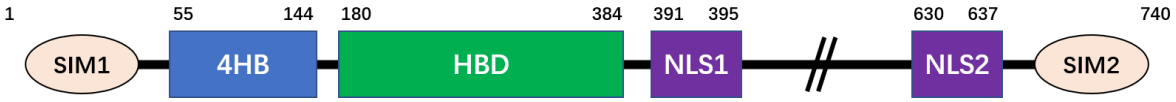

Figure 7: The domain architecture of DAXX.

DAXX is a scaffold protein that interacts with proteins with diverse roles. DAXX harbours a 4-helix bundle (4HB) and two nuclear localisation signals (NLS1 and NLS2). The central part of DAXX is a highly conserved region, the histone binding domain (HBD), forming a complex with a histone H3.3/H4 dimer. The N- and C-terminal SUMO-interacting motifs (SIMs) bind to SUMOs. Image adapted from [196].

In the nucleus, DAXX localises to PML bodies, interacts with tumour suppressor PML and functions in transcription regulation and apoptosis [200-202]. PML bodies are highly organised membraneless bodies existing in a liquid-like phase that is separated from their surroundings. In addition to PML bodies, DAXX forms a phase-separated nuclear body with tumour suppressor Speckle-type POZ protein (SPOP), and SPOP promotes DAXX degradation in phases-separated droplets [203]. This suggests that phase separation may occur in principle favour of DAXX's interaction with a specific partner.

1.6 Methods in autophagy research

Autophagy has been involved in many aspects of cell functions, as well as physiological and pathological processes. As autophagic processes are dynamic and complicated, precise study approaches are necessary [204]. As a multi-step process, autophagy is described as a ‘flux’ other than just the formation of autophagosomes or the fusion with lysosomes. The term ‘autophagy flux’ is used to represent a complete process of autophagy, which highlights its dynamic property, including autophagosome biogenesis, autophagosome maturation, fusion with the lysosome and substrates breakdown inside the autolysosome.

Research in autophagy has faced historical challenges for decades, such as capturing a dynamic process by static measurements, bringing inherent limitations and giving misleading results. For example, it is hard to determine the accumulation of early intermediates in neurodegenerative diseases is the result of increased autophagy or a block in the later stages of autophagy [205]. Also, as a common feature in dying cells, autophagy was erroneously presumed to lead to cell death. In contrast, it is now approved that autophagy fights to keep cells alive under stressful conditions [206]. Therefore high demands for methods in autophagy research have increased, and new techniques have been developed to monitor this dynamic process.

1.6.1 Monitoring cellular autophagic activity

A common misconception exists for a long time is that increased numbers of double-membrane autophagosomes in cells represent the increased cellular autophagic activity. However, being included in a multi-step process, the autophagosome is an intermediate structure, and the number of autophagosomes depends on the rate between autophagosome formation and

autophagosome degradation. In other words, autophagosome accumulation may result from autophagy induction as well as the suppression of autophagosomes fusion with lysosomes. Measuring the number of autophagosomes give a direct vision when compared with the basal levels of autophagy, but it is insufficient to estimate autophagy activity only by the number of autophagosomes. Rather, monitoring of autophagosome numbers and autophagic flux is critical when assessing autophagic activity.

1.6.2 Monitoring the number of autophagosomes

Electron microscopy (EM)

The first transmission electron microscope was constructed by Ernst Ruska in 1933, and after that, it was utilised widely by cell biologists observing native cellular ultrastructures [207]. The biological reality hiding behind the subcellular structures is also focused on autophagy research. According to the record, Johannes Rhodin could be the first to describe autophagy in 1954, when he observed mitochondria engulfed in membrane-bounded bodies [208]. In 1957, the first picture of mitochondria inside an electron-dense membrane-bounded body in mouse kidney epithelium was published by Sam Clark; unfortunately, the membrane appeared to be discontinuous so that the observation was overlooked [209]. In 1959, Alex Novikoff observed similar structures and inferred that these bodies could associate with lysosomes for cellular autolysis, and later defined them as cytolysomes [210, 211]. Massive ultrastructural evidence had been observed in the next following years, and the autophagosome was defined as a double-membraned structure containing cytoplasmic contents. With a high resolution in the nanometer range that allows the clear recognition of subcellular components, electron microscopy is needed and indispensable in analysing the

ultrastructural details of organelles and other autophagy-related structures when autophagy being studied [212]. However, when it comes to imaging, the observation is normally more complicated than the theory because autophagy is a dynamic process and autophagic vacuoles are highly morphological heterogeneous. It is important for biologists to identify autophagic vacuoles in each step of autophagy, for example autolysosomes have only single membrane, and to exclude the false recognition of swollen mitochondria or endocytosed apoptotic bodies [213, 214]. Therefore, special attentions should be paid to identify all these compartments. Being a powerful tool in autophagy study and harbouring the resolution power advantage over that of the light microscope, the application of EM will continue in the future.

Fluorescence microscopy

After the discovery of ATG genes, the approach of fluorescence microscopy, together with molecular genetic techniques, has become widely used for the assessment of autophagosome numbers. Unlike EM that requires skilled expertise and expensive equipment, fluorescence microscopy has the advantage of bringing results faster and requiring lower investment in the microscope. In mammalian cells, LC3 is a marker of autophagosomes, and endogenous LC3 or green fluorescent protein (GFP)-LC3 exists as a diffused cytoplasmic pool or as punctate structures that represent autophagosomes. The detection of LC3 or GFP-LC3 can be used to monitor autophagy by fluorescence microscopy [53]. Using LC3 antibodies for immunocytochemistry or immunohistochemistry make it possible to detect the endogenous proteins. Co-transfection of GFP-LC3 and the protein of interest can be used to visually investigate the role of the protein of

interest in autophagosome formation. Also, GFP-LC3 is used for *in vivo* studies in transgenic organisms such as *Caenorhabditis elegans* and mice [215, 216].

This method also has limitations; for example, overexpressed GFP-LC3 could form protein aggregates as well as lead to nuclear localisation; the level of endogenous LC3 is below the level of detection so that signals could be too weak to be detected, that all could bring the possibility of false-positive or false-negative results [217]. Besides, the increased number of LC3-positive puncta is insufficient to represent either the induction of autophagy or the inhibition of autophagosome clearance. Therefore, at critical points, fluorescence microscopy still needs the support of other approaches to investigate autophagy.

Biochemical assays

LC3 is involved during autophagy since the isolation membrane has formed and remains on the inner membrane after intact autophagosome has formed so that LC3 is also useful in biochemical assays. Upon activation of autophagy, LC3 is cleaved at C terminus by Atg4 and become LC3-I, then the cytosolic LC3-I is lipidated to form LC3-II that is specifically recruited to phagophore membrane. During autophagosome maturation, LC3-II moves from the outer membrane to the inner membrane so that the level of it could represent the autophagosome number (or, more accurately, the amount of autophagic membrane labelled with LC3-II) [53, 218]. The conversion from LC3-I to LC3-II can be detected by immunoblotting.

1.6.3 Monitoring autophagic flux

As mentioned above, autophagy is a highly dynamic and multi-step process that makes it impossible to identify if the accumulation of autophagosomes results

from increased autophagosome generation or a block of autolysosome maturation. Therefore, the detection of autophagosome numbers or the presence of LC3 is insufficient to evaluate the process. The term ‘autophagic flux’ represents the whole dynamic process of autophagy, including autophagosome formation and maturation, fusion with the lysosome, subsequent degradation and release into the cytosol [219]. Several methods are currently used for monitoring autophagic flux.

LC3 turnover assay

LC3-II is degraded after autophagosomes fusion with lysosomes, but the increased level of LC3-II is not sufficient to conclude autophagy induction or blockade [220]. Autophagy flux is often measured by western blot based on LC3-II turnover in the presence and absence of lysosomal degradation inhibitors [221, 222]. The level of LC3-II will be increased when lysosome functions are affected by lysosomal inhibitors, such as chloroquine and bafilomycin A1, because the degradation of LC3-II through the autophagic pathway will be blocked [221]. Therefore, the difference of LC3-II amount in the presence and absence of lysosomal inhibitors reflects the transit of LC3-II through the autophagic pathway [223]. This method requires complete inhibition of lysosomal degradation when testing compounds that block the fusion step to avoid misleading results of increased autophagosome synthesis. Therefore, pretests of proper inhibitor concentrations and incubation time are necessary [224].

Degradation of selective substrate p62

p62 is primarily degraded through selective autophagy, thus measuring its levels has been used to monitor autophagic flux [225]. Harbouring a ubiquitin-binding

domain that binds to ubiquitin and an LC3-interacting region associated with LC3, p62 can link ubiquitinated proteins to autophagic membranes and enable them to be degraded in the autolysosome [226, 227]. In this way, p62 is engulfed together with ubiquitinated proteins in the intact autophagosome and then degraded in the autolysosome, and the amount of p62 is considered to correlate with autophagic activity [227]. However, it should be noted that p62 is a multifunctional protein working in different cellular pathways, and it can be transcriptionally upregulated in some situations, such as the activation of Raf/MEK (Mitogen-activated protein kinase (MAPK)/extracellular signal-regulated kinase (ERK) kinase)/ERK pathway [228]. Also, there is a crosstalk between autophagy and the UPS, and p62 play roles between them. This makes p62 take part in proteasomal degradation, and the level of it could be increased when the proteasomal activity is inhibited. Besides that, p62 also serves as a shuttling factor for delivery of polyubiquitinated proteins for proteasomal degradation [1, 229-231].

As p62 is a multifunctional scaffolding protein that participates in diverse processes, the level of p62 may be affected by homeostatic regulation independently of autophagy. For this reason, additional assays may be important to validate changes in autophagic flux.

Delivery of mRFP-GFP-LC3 to the lysosome

Another assay is based on the difference between the characteristics of GFP and red fluorescent protein (RFP). GFP is quenched by low pH inside lysosomes, resulting in undetectable GFP-LC3 signals co-localisation with lysosomes, while RFP is more stable and can be detected inside autolysosomes [53, 232]. GFP-RFP-LC3 is a useful reporter to quantify autophagic flux in individual cells by fluorescence microscopy or flow cytometry, with autophagosomes and

autolysosomes labelled with yellow and red signals, respectively [233, 234]. When autophagic flux increased, both yellow and red puncta increased; but only yellow puncta are increased when the fusion of autophagosome and lysosomes is blocked. Of note, this method is highly dependent on lysosomes, and the acidification and degradation capacity of lysosomes could affect the observation of signals; for example, autolysosomes might be observed yellow when GFP signals were quenched slowly because of the low activity of lysosomal enzymes [205]. Thus, data collection and quantification with flow cytometry may provide more reliable results on autophagic flux using the ratio of RFP to GFP.

Long-lived protein degradation

As autophagy seems to be the only way for long-lived protein degradation, specific assays can be used to measure this process, which makes the measurement of bulk degradation of long-lived proteins a traditional method for monitoring the autophagic flux [235]. In this assay, cells are cultured with isotope-labelled amino acids, normally [^{14}C]- or [^{3}H]-valine or leucine, for a relatively long period of time (several hours to several days) to label long-lived proteins as autophagic substrates. Then cells are cultured without isotope-labelled amino acids to wash out short-lived proteins (the proteasome substrates) and treated with autophagy-inducing stimulus [236]. Trichloroacetic acid-soluble radioactivity is measured, and the cellular release of degraded proteins in culture supernatant is quantified, giving a precise numerical result. The rate of degradation of long-lived proteins is calculated from the ratio of the acid-soluble radioactivity in the supernatant to that in the cell pellet. It is recommended to compare degradation rates between samples with or without an autophagy inhibitor to exclude any potential pathways that might contribute to long-lived protein degradation [219].

1.6.4 Inhibition and activation of autophagic activity

As a multi-step process, autophagy can be modulated both positively and negatively at each step [237]. The level of autophagy is low at the baseline range, and the flux through the system is constant at a baseline level; therefore, interests have grown in activating autophagy as a potential therapeutic treatment (**Figure 8**).

There are numerous methods to activate autophagy, such as serum starvation, amino acid deprivation, hypoxia, exposure to various chemicals. The most potent way to induce autophagy is serum starvation or amino acids starvation, and the upregulation of autophagy can be observed as soon as 1 hour after amino acid withdrawal. Autophagy can be pharmacologically induced by inhibiting negative regulators, such as mTOR with rapamycin or antiapoptotic proteins, B-cell lymphoma 2 (Bcl-2) and B-cell lymphoma-extra large (Bcl-xL), that bind to Beclin1, with ABT-737 [238, 239]. mTOR regulates different cellular processes, and its activity inhibits autophagy. As mTOR inhibitors, rapamycin and its analogue CCI-779 can be used to induce autophagy even under nutrient-rich conditions. However, starvation and mTOR inhibition lead to not only autophagy induction but also other cellular responses and should be used carefully. Trehalose is a natural disaccharide, widely found in several organisms, which has been approved to be neuroprotective and is used as a treatment in neurodegenerative diseases. It may work as an autophagy enhancer in an mTOR-independent manner [240, 241]. Apart from targeting autophagy steps, disrupting the proteasome-regulated degradation by proteasome inhibitor MG132 was reported to lead to accumulation of LC3B-II and accumulation of autophagic vacuoles in several cell lines, indicating the induction of autophagy [242].

The non-toxic compound 3-methyladenine (3-MA) is an effective and selective autophagy inhibitor, with the capacity that 5-10 mM 3-MA can completely block autophagic sequestration in mammalian cells, acting as an inhibitor of class III phosphatidylinositol (PtdIns) 3-kinases and inhibiting autophagic protein degradation with no detectable effects on other proteolytic pathways [243-245]. Other PtdIns 3-kinase inhibitors also inhibit autophagy, like wortmannin and LY294002, but they are less specific than 3-MA due to their capacity of inhibiting class I PtdIns 3-kinase strongly [245]. While 3-MA inhibits the autophagosome formation step, autophagy can also be pharmacologically inhibited by targeting the step of autophagosomes fusion with lysosomes, using inhibitors of the lysosomal proton pump such as Bafilomycin A1, which inhibits the vacuolar ATPase, blocks the fusion of autophagosomes with lysosomes and leads to an accumulation of autophagosomes [246]. Also, the accumulation of LC3-II can be induced by interfering with the autophagosome and lysosome fusion step by inhibiting the V-ATPase with bafilomycin A1 or raising the lysosomal pH with chloroquine [247]. Chloroquine (CQ), an acidotropic drug that impairs lysosomal acidification leading to the accumulation of autophagy substrates, is also widely used as an autophagy inhibitor [248]. Besides, lysosomal protease inhibitors E64d and pepstatin A are shown to affect the final degradation of autophagic substrates inside autolysosomes [221].

Genetic knockouts and knockdowns are also available for the inhibition of autophagy. As ATG genes are essential for autophagy, knockouts or knockdowns of these genes offer more specific inhibition than pharmacological agents. However, losing essential autophagy genes lead to death in targeted mutant mice, like neonatal lethality in Atg5 or Atg7 deficient mice and embryonic lethality in

Beclin 1-deficient mice [9, 249, 250]. Blocking protein expression with small interfering RNA (siRNA) targeting ATG genes, like ATG5, Beclin 1, ATG10 and ATG12, is implemented in mammalian cells and confirmed efficient suppression of autophagy [251]. Most ATG gene knockdowns or knockouts block the initiation of autophagosome formation, further affect the whole autophagy process, and studies that focused on later steps of autophagy may not be appropriate for this method. Another consideration is that some ATG genes, like ATG5, function normally in autophagy even when expressed at a very low level so that the siRNA-mediated silencing efficiency may need to be measured precisely to confirm the knockdown.

A common way to switch on autophagy is changing the cell culture medium (containing serum and high levels of amino acid) to a nutrient-poor medium. However, several pathways may be altered at the same time, such as PtdIns 3-kinase class I dependent autophagy-suppressive pathway will be inhibited when lacking serum growth factors.

These methods detect different stages of autophagy and should be used coordinately with each other to determine whether an increase in intermediates, like autophagosomes, represents an increase in autophagic degradation or, instead, a block in the completion of the process. There is no single ‘gold standard’ to determine autophagic activity currently, and in most cases, it is worth considering combining multiple approaches together for autophagy detection. [223]

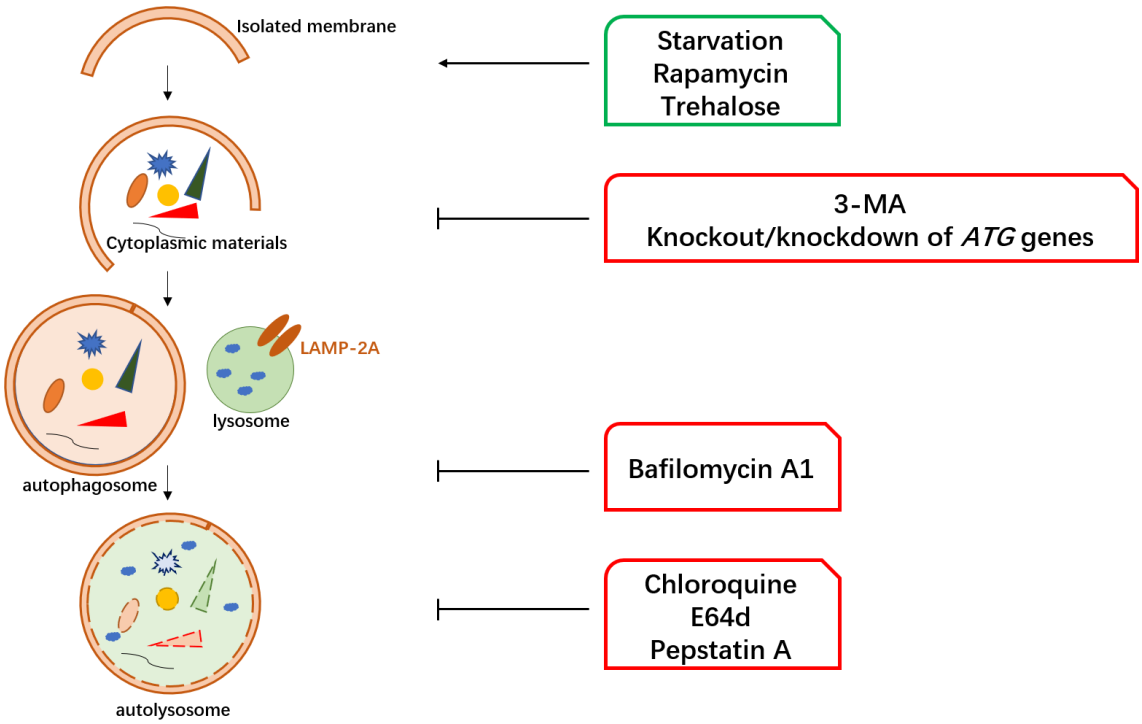

Figure 8: A list of treatments and reagents that modulate autophagy.

The level of basal autophagy is low, and the autophagy flux remains constant. Autophagy can be induced or inhibited at each step. Nutrient deprivation and inhibition of mTORC1 can activate the initiation of autophagy. Inhibitors of class III phosphatidylinositol (PtdIns) 3-kinases, such as 3-MA, can block autophagosome formation. In the later step of the autophagic process, Bafilomycin A1 blocks the fusion of autophagosomes and lysosomes, leading to the accumulation of autophagosomes. Chloroquine inhibits lysosome acidification. E46d and pepstatin A are lysosomal protease inhibitors that inhibit the final degradation of autophagic substrates in autolysosomes.

1.7 Autophagy and neurodegeneration

Although in yeast, autophagy is primarily in response to starvation, it is involved in a wider range of physiological and pathological processes in mammal. As a critical protective mechanism for cellular homeostasis, autophagy is tightly regulated, induced when needed otherwise maintained at a basal level [32]. Dysfunction of autophagy results in accumulations of protein aggregates which

seems to be correlated with toxicity [252]. Indeed, early studies have shown that autophagosome accumulation is commonly observed in the brains of patients with neurodegenerative diseases such as Huntington disease, Parkinson's disease and Alzheimer's disease, underlying the pathophysiologies of many diseases [239, 253]. This section will focus on the background and progress of autophagy in these three neurodegenerative disorders.

1.7.1 Huntington disease (HD)

HD is a dominantly inherited neurodegenerative disorder with characteristic cognitive and motor features as well as variable psychiatric disturbances [254]. Pathologically, HD usually presents in adulthood for the duration of decades, with brain atrophy and neurodegeneration [255]. The primary affected site is the medium spiny neurons of the caudate-putamen, but the affected regions expand as the severity of pathology gets worse.

Huntington disease is caused by a CAG (cysteine, adenine and guanine) repeat expansion in the coding region of the *HD* gene, resulting in long stretches of polyglutamine (polyQ) in its encoded protein, huntingtin (Htt) [256]. Htt is expressed ubiquitously across cell types (most highly in neurons) and has essential roles in functions, such as transcriptional regulation, nucleo-cytoplasmic shuttling, mitochondrial dynamics and anti-apoptotic activity, and the elimination of HD gene expression results in embryonic lethality [257]. In healthy individuals, the number of CAG repeats varies from 6 to 35, while more than 36 repeats results in HD onset. Mutant Htt has a notable feature that its propensity to accumulate and aggregate, forming intranuclear and intracytoplasmic inclusions and causing toxicity [258]. Since studies have shown that abolishing the expression of mHtt can lower the level of aggregation in HD mouse brains, and

adult neurons are able to eliminate proteinaceous inclusions, therapeutic approaches of inclusion elimination have been investigated to combat HD [259, 260].

Lysosome-mediated degradation pathway, autophagy, plays critical roles in aggregated protein clearance. Studies have shown that mutant huntingtin aggregates can be degraded by autophagy, suggesting that there might be a crosslink between autophagy and HD [84, 261]. In 2010, Zeitlin and colleagues published that the loss of polyQ stretch appeared to increase autophagic capacity in neurons [262]. Recent studies have implicated that Htt functions in selective autophagy. It acts as a scaffold by mediating the binding between p62 and ULK1, increasing cargo recognition and autophagy initiation so that autophagy deficit might contribute to HD pathogenesis [263]. Phosphorylation of p62 at S409 increases the binding affinity for ubiquitin and enhances degradation of aggregated proteins, including those with expanded polyQ, indicating that autophagy is crucial in response to mHtt expression [100].

1.7.2 Parkinson's disease (PD)

Parkinson's disease is a common neurodegenerative disorder with the symptoms of slow movements, inflexible muscles and tremor. At the cellular level, the presence of intracytoplasmic inclusions, Lewy bodies, is a pathological hallmark [264]. Lewy bodies, containing α-synuclein, neurofilament, ubiquitin and other proteins, are observed in neurons of the substantia nigra pars compacta (SNc) and other regions in the central and peripheral nervous system. Lewy bodies are thought of as aggresomes in response to excess unwanted and potentially toxic proteins to protect cells from proteolytic stress. As a degradation pathway for misfolded proteins, autophagy is essential for neuronal survival, but its

dysfunction correlates to the accumulation of aggregates and, subsequently, cellular toxicity and PD onset [264]. Back in 1997, autophagic vacuoles accumulation was found in PD patients [265]. Also, autophagy-deficient mouse models have been observed developing neurodegenerative phenotypes, for example, progressive deficits in motor function that accompanied by the accumulation of cytoplasmic inclusion bodies in neurons [266, 267]. These findings suggest that autophagy may provide protection against neurodegeneration.

Both increased production and impaired clearance can lead to protein accumulation that occurs in PD. Indeed, it is reported that the dysfunction of autophagy occurs in the brains of PD patients and PD animal models, indicating that autophagy has participated in this disease. Studies have shown the involvement of α-synuclein and leucine-rich repeat kinase 2 (LRRK2) genetically linked to autosomal dominant PD in the autophagy pathway, while PTEN-induced putative kinase 1 (PINK1) and Parkin participate in mitophagy [268-270].

α-synuclein localises to the presynaptic terminals in the central nervous system and is mainly degraded by chaperone-mediated autophagy via binding to HSC70 and then LAMP-2A [271]. The pathogenic A53T and A30P α-synuclein mutants bind more strongly to LAMP-2A but failed to be transported across lysosomal membrane, preventing other CMA targets from binding and leading to the block of CMA [271, 272]. This leads to a high degree of toxicity.

Mitochondria provide >90% of energy in eukaryotic cells, but at the same time, they are also the primary source of cellular ROS [273]. In mitochondrial respiratory defect, excessive ROS causes damage to cellular components, including mitochondria, and accumulation of this damage has been linked to PD

[274, 275]. Among different types of selective autophagy, mitophagy, selective autophagic degradation of mitochondria, has been implicated in PD through the PINK1-Parkin mediated pathway. Parkin is shown selectively translocated to functionally impaired mitochondria and then eliminated by mitophagy, as a mechanism of the mitochondrial quality control system [276, 277]. Parkin, an E3 ubiquitin ligase, mediating ubiquitination of itself and mitochondria with low membrane potential, is recruited to the mitochondrial outer membrane by PINK1 [278]. Mutations in Parkin and PINK1 are predominant in autosomal recessive cases of PD, interfering with mitophagy and being linked to recessive forms of PD [279, 280].

The Discovery of therapeutic drugs that enhance autophagic activity or maintain mitochondrial homeostasis could potentially slow down PD progression. However, both reduced and excessive autophagy can be detrimental; simply upregulating autophagy is not a practical action and treatment with autophagy-inducing drugs should be undertaken with extreme caution [270].

1.7.3 Alzheimer's disease (AD)

Alzheimer's disease (AD) is a chronic progressive neurodegenerative disease, with unclear pathogenesis and no cure today. AD is the most common cause of dementia and is pathologically characterised by progressive neuronal loss in the cortex and hippocampus, with accumulation and aggregation of extracellular β-amyloid plaques and intracytoplasmic tau occur in AD brains and associate with disease progression [281]. As these protein aggregates accumulate, more and more nerve cells become damaged, leading to AD symptoms [282]. Although drug discovery and development of AD are arduous and high rates of failure occurs in these programs, there are 132 agents in clinical trials for the treatment

by 2019, and 25% of which target cognitive enhancement, neuropsychiatric and behavioural symptoms [283]. More than 70% of agents intend to achieve disease modification on amyloid and tau. In general, these aggregate-prone proteins can be degraded by autophagy, protecting cells from potential toxic accumulations [252]. However, in AD brains, massive neuronal autophagic vacuoles such as autophagosomes, amphisomes and autolysosomes accumulate, indicating that the autophagic process in neurons is stalled [284]. Autophagic vacuoles are filled with undigested or partially digested substrates, even though abundant lysosomes are available around, pointing that disruption of autolysosomal proteolysis may be the principal mechanism underlying autophagy failure in AD [285]. In addition, lysosomal dysfunction affects axonal transport of autophagy-related compartments and leads to cargo accumulation in axonal swellings, promoting neuritic dystrophy in AD [286]. Impairment is also seen in early stages of autophagy in AD patients, as expressions of Beclin 1 decreases in affected brain regions [287]. Deletion of Beclin 1 in amyloid precursor protein (APP) AD mouse model decreases autophagy, increasing β-amyloid accumulation, and this effect can be eliminated when Beclin 1 is overexpressed.

1.7.4 Current outlook

Autophagy, as a major degradation pathway for proteins, is essential for neuron survival. It is exciting to see that studies have described the deficiency of autophagy in several neurodegenerative diseases; therefore, autophagy may be an attractive therapeutic target of disease treatment. Stimulating the induction of autophagy, enhancing selective autophagy, improving lysosome efficiency and preventing or reversing impairments in autolysosomal clearance have been widely considered promising therapeutic approaches [288]. Notably, as a

multistep process, autophagy should be targeted on the specific step that is disrupted in different diseases (cargo recognition in HD, and lysosomal function in PD and AD). Failure in consideration of this may bring the opposite effect; for example, induction of autophagy may exacerbate pathology when lysosomal clearance is impaired in AD models [288].

Gene therapy has shown great potential in treating neurological disorders and has made straightforward progress [289]. Therapeutic genes delivered by viral vectors such as lentiviruses and adeno-associated viruses (AAV) into the brain have exhibited a reduction in β-amyloid levels in mouse models, suggesting a reasonable candidate for gene therapy trials in AD [290, 291]. This platform can achieve gene expression at therapeutic levels for a relatively long time, but safety concerns remain; for example, viral vectors might cause immune or inflammatory reactions [292]. The development of siRNA nanocomplexes, as non-viral vectors, has approved an efficiently approach delivering genes to brains, and the delivery of siRNAs together with peptides for β-amyloid has shown ameliorating AD-associated symptoms, indicating it could be a promising treatment for AD [293].

1.8 Autophagy and cancers

Associations between autophagy and cancers have been investigated in the past decades. Normally, autophagy contributes to adaptation to cellular stress, immunity and longevity, providing a protective function in response to metabolic stress for cell survival. However, when it occurs in tumour cells, autophagy could also be a powerful tool to promote their survival by providing materials to adapt to the increasing need for energy [294, 295].

1.8.1 Autophagy and tumour suppression

Autophagy can prevent cancers in several possible ways.

Autophagy defects are found in many human tumours, and the role of autophagy in tumour suppression was first demonstrated on Beclin1, the mammalian orthologue of yeast Atg6 [296]. Beclin1 is monoallelically deleted in human breast and ovarian cancers and is expressed at reduced levels. Also, mouse models with a monoallelic deletion of Beclin1 (Beclin1$^{+/-}$) suffered from a high incidence of spontaneous tumours such as lymphomas, hepatocellular carcinomas and lung adenocarcinomas, with higher cancer rates, larger tumour sizes and more spectrum of tumour types, compared with wild-type mouse [39, 249]. Other autophagy-related genes are found to play roles in tumour suppression as well. Deletion or knockout of Atg4, Atg5 or Atg7 in murine models have all been reported to accelerate oncogenesis, and mutations of Atg2B, Atg5, Atg9B and Atg12 are commonly observed in gastric and colorectal carcinomas [297-300].

Autophagy also mitigates cellular damage and may suppress tumorigenesis. Autophagy-defective tumour cells fail to deal with p62 accumulation, ER chaperones and protein disulphide isomerases in response to stress, indicating a protein quality control failure. Sustained p62 expression and its accumulation not only lead to excessive oxidative stress but also affect NF-κB regulation and promote tumorigenesis. Thus, the persistence of high levels of p62 caused by defective autophagy is commonly observed in human tumours and contributes directly to tumorigenesis [301]. Consistent with this, p62 deficiency attenuated liver injury in autophagy-deficient mice [79]. The accumulation of p62 and its cargoes elicits cytotoxicity, including activation of DNA damage response, alteration in gene expression, and DNA mutations [301]. In liver and pancreas,

autophagy loss leads to oxidative stress, inflammation and tissue damage, which are all well-known factors to promote tumour initiation. Moreover, autophagy-defective tumour cells also show genome damage, suggesting that autophagy could mitigate damage and is a cell-autonomous mechanism of tumour suppression [302].

Autophagy participates in antioxidant defence. Damaged mitochondria lose membrane potential and trigger activation PINK1 and further the E3 ligase Parkin, providing the signal for recognition and degradation by autophagy. This mitochondrial quality control process is a potential way to reduce ROS and oxidative stress that contributes to tumorigenesis [277, 303]. ROS are also highly genotoxic, and the function that autophagy prevents DNA damage through its cellular housekeeping role in removing sources of oxidative stress also contributes to preventing cancer.

Moreover, autophagy is involved in anticancer immunosurveillance, with the immune system continually removing potential tumorigenic cells before they are developing malignant lesions [304]. Also, malignant transformation can be stimulated by an inflammatory surrounding containing a high amount of ROS and mitogenic cytokines, while decreased autophagy enhances necrosis-dependent inflammation, further promoting tumour development [305].

Taken together, these observations strongly suggest that autophagy deficiency favours tumorigenesis, and in turn, suggests that autophagy may play an important role in human tumour suppression.

1.8.2 Autophagy and tumour progression

As in normal cells, autophagy is activated in tumour cells when they experience increased metabolic stress such as nutrient starvation and oxygen deprivation. In other words, autophagy may be a tool that tumour cells utilise for their own cytoprotection, promoting cell survival from energy and nutrients shortages caused by the high metabolic demand of cell proliferation and altered metabolism [306, 307]. In hypoxic tumour regions, autophagy is induced and supports cell survival, and deletion of essential autophagy genes leads to tumour cell death [306]. Hypoxia universally occurs during tumorigenesis, induces ER stress, and activates autophagy in a hypoxia-inducible factor (HIF)-dependent manner [308, 309]. Besides, autophagy also promotes the survival of cancer cells by targeting damaged organelles for degradation, thereby buffering oxidative stress caused by cancer treatments. In these ways, autophagy improves the resistance of cancer cells to endogenous conditions that usually provoke cell death.

Recent studies suggest that autophagy provides a protective function against tumour necrosis and genome damage in tumour cells and facilitates glycolysis which tumour cells prefer for their growth [310]. Compared with normal cells, many cancer cell lines have high basal levels of autophagy. Moreover, oncogenic Ras that induces tumour growth can upregulate basal autophagy in tumour cells [310, 311]. Cancer stem cells often display an increased autophagic flux, and tumour formation can be abolished by inhibition of Beclin 1 or Atg4a [312, 313]. Tumour cells subjected to autophagy inhibition are less resistant to exogenous stimuli, and autophagy-deficient tumours are often more sensitive to several chemotherapeutic agents and radiation therapy than their autophagy-proficient

counterparts [314-316]. In other words, autophagy offers tumour cells less sensitive to therapy-induced cell death.

Autophagy may sustain the survival of cancer cells by entering a state of dormancy or senescence in response to therapy. Tumour supporting functions of autophagy also include sustaining the survival of cancer cells that enter a state of dormancy. Normally tumour cells are defective in apoptosis, and activated autophagy in response to stress enables them long-term survival, for weeks, in conditions of deprivation [306, 307]. During this period, tumour cells could digest themselves to smaller sizes, suppress cell division and motility to conserve energy, maintaining in a ‘dormant’ state with the capacity to return to the normal state once having normal growth conditions restored [317].

Advanced human tumours show an increase in autophagic flux, associating with tumour cell proliferation, high nuclear grade and poor patient outcome [318, 319]. This reflects that the widespread, active autophagy in malignant tumours acts as a pro-survival mechanism for cancer cells. Pharmacological inhibitors of autophagy may exert antineoplastic effects, at least in some settings.

1.8.3 Autophagy in anticancer therapy

Although autophagy plays a similar role that support cell survival, in tumour cells as it does in normal cells, the dependence on autophagy is different because the inherent stress that tumour cells encounter is heavier. This difference may be useful in cancer therapy. As basal autophagy levels are high in cancer cell lines, these cells have a limited ability to increase autophagy levels in response to stress. This diminished adaptation to stress suggests that oncogene activation may be a stress, and autophagy is needed to maintain homeostasis and cancer cell survival. For example, in Ras-expressing cell models, autophagy deficiency

is confirmed abrogating the tumorigenicity, indicating that Ras activation and autophagy deficiency are synthetically lethal. This could be a method for treatment for Ras-driven cancers [303, 311, 320].

Paradoxically, it is difficult to conclude whether turning autophagy on or off is a good method to kill a tumour cell. While the absence of autophagy increases susceptibility to death when cells suffer stressful conditions, a high level of autophagy can also lead to cell death through excessive self-digestion. On the one hand, autophagy limits tissue damage, inflammation and genome instability that can promote tumorigenesis, suggesting that stimulating autophagy may help cancer prevention. Induction of autophagy by inhibitors of mTORC1 is a possible antitumour mechanism, and related drugs such as Temsirolimus and Everolimus are registered for the treatment of renal cell carcinoma [321, 322]. Everolimus is also confirmed inducing autophagy and reducing tumour sizes in mouse models of acute lymphoblastic leukaemia, suggesting mTOR inhibitors may be a part of the chemotherapy. Besides, proteasome inhibitors, histone deacetylases (HDAC) inhibitors, and some monoclonal antibodies show the capability to induce autophagy and further tumour cell death to some extent [296]. On the other hand, autophagy is a survival strategy for tumour cells, great interests in inhibiting autophagy for cancer therapy has developed.

Studies found that combined inhibition of both autophagy and proteasome caused more cell death than either of them alone, and *in vivo* experiment confirmed that proteasome inhibitor showed an enhanced antitumour effect in autophagy-deficient mouse models [301, 323]. However, a small amount of remaining tumour cells is sufficient for tumours to reoccur, even years later, accompanied by the deadly consequences. Thus, tumour cell dormancy and

regeneration mechanisms need to be established precisely, and therapeutic targeting of autophagy to impair dormancy and regeneration is worthwhile [295].

Complexity in autophagic pathways implies that selective targeting of individual autophagy pathways may be more effective than the application of non-specific autophagy inhibitors. For example, two separate autophagic pathways, marked by differential requirements for LC3B and LC3C separately, play tumour-promoting and tumour-suppressing roles in renal cancer [324]. Thus, small-molecules that selectively target LC3B-dependent autophagy could be an effective method for renal cancer therapy.

However, autophagy inhibition might have intrinsic oncogenic potential, and only a part of the links between autophagy and cancer have been investigated. Pharmaceutical treatment of autophagy modulators should be tested carefully [325]. Future studies of the relationship between autophagy and cancer are urgently awaited to shed additional light on cancer therapy.

1.9 Project aims

The primary hypothesis of this project is that DAXX promotes p62 body formation and phase condensation, increasing p62 recruitment of polyubiquitinated proteins. It is also hypothesised that DAXX, participating in the p62-Keap1-Nrf2 pathway, has a regulatory role on the maintenance of cellular redox homeostasis.

The overall aim of this project is to identify that cytoplasmic DAXX regulates p62 phase condensation and its receptor activity in selective autophagy. Selective autophagy mediates the degradation of cytoplasmic materials to maintain intracellular homeostasis. The cargo specificity is achieved by autophagic cargo receptors such as p62. For effective degradation by selective autophagy, cargoes

should be concentrated and segregated into autophagosomes. The formation of p62 non-membrane-bound liquid condensates is critical for its function as a cargo receptor and its autophagic degradation. p62 condensates are formed via Liquid-liquid phase separation, with spherical-like shapes and are able to fuse with each other. While hundreds of proteins are gathered in phase-separated condensates, only a few proteins can promote the formation of liquid condensates. p62 oligomerisation plays a crucial role in binding polyubiquitinated proteins and LC3 simultaneously, and is predicted to be dynamically regulated to meet its diverse functions for cellular homeostasis. This project aims to find a p62 interacting partner that could function as a chaperone to regulate the dynamics of its oligomerisation and phase condensation.

Specific objectives are therefore as follows:

1.9.1 Determination of DAXX as a p62 interaction protein

Initially, the interaction of p62 and DAXX will be investigated by observing the protein co-localisation using immunocytochemistry and microscopy, and the direct interaction will be examined by immunoprecipitation. The regions for their interaction will be figured out by co-transfection of p62 variants and DAXX variants. Different cell models will be used to confirm that the interaction is not affected by transfection efficiency. Given that p62 oligomerisation is essential for its function of recruiting ubiquitinated proteins, immunohistochemistry of DAXX knockdown or DAXX knockout tissues will be applied to test if DAXX induces p62 oligomerisation.

1.9.2 Investigation of DAXX-induced p62 phase separation

Next, whether DAXX modulates p62 phase separation will be investigated. Unlike protein aggregates that lack mobility, p62 bodies have been confirmed to maintain their activity, undergo fusion and exchange molecules with the surrounding environment. As non-membrane p62 bodies are formed as liquid droplets, it is worth asking if DAXX regulates p62 phase assembly or drives p62 phase condensation. Fluorescence Recovery After Photobleaching (FRAP) assay will be used to determine the dynamic mobility of p62 bodies in living cells, and proteinase K digestion will be used to detect the condensation of p62 condensates. Then, recombinant proteins will be purified and subjected to *in vitro* assays. Factors such as the concentration of DAXX that could modulate p62 phase condensation will be tested. Whether DAXX-induced p62 condensates would undergo fusion will be examined. The sedimentation assay will be used to confirm that DAXX promotes p62 phase condensation.

1.9.3 Investigation into the role of DAXX in the modulation of cellular redox homeostasis

Since p62 oligomerisation is important for its recruitment of ubiquitinated proteins, I will investigate if DAXX mediates the interaction between p62 and polyubiquitinated proteins. Different cell models and tissues will be used, and co-localisation of p62 and ubiquitin will be quantified. Given that p62 recruits keap1 during oxidative stress and induces the expression of Nrf2-mediated antioxidant enzymes, this project will examine if DAXX plays a role in this process. ROS assay and the dual-luciferase assay will be used. Ultimately, I aim to examine whether DAXX would modulate redox homeostasis via the p62-DAXX interaction.

2: Materials and methods

2.1 Antibodies, reagents and cell lines

Antibodies

Rabbit polyclonal antibodies: anti-actin (1:1000) (Sigma, A2066); anti-ATG5(1;1000) (Sigma, A0731); anti-DAXX (1:500) (Santa Cruz, sc-7152); anti-Flag (1:1000) (CST, #14793); anti-GFP (1:1000) (Abcam, ab6556); anti-Glutathione-S-Transferase (GST) (1:10,000) (Sigma, G7781); anti-Lamin B1 (1:1000) (Abcam, ab16048); anti-LC3 (1:3000) (CST, #12741); anti-Myc (1:1000) (Sigma, C3956); anti-Nrf2 (1:1000)(MBL, PM069); anti-p62 (1:3000) (MBL,PM045)

Mouse monoclonal antibodies: anti-Flag (M2) (1:3000) (Sigma, F3165); anti-Glyceraldehyde-3-phosphate dehydrogenase (GAPDH) (1:5000) (Ambion, AM4300); anti-GSTM1 (1:100) (DSHB, CPTC-GSTMu1-1); anti- hemagglutinin (HA) (1:1000) (Biolegend,901501); anti-Keap1 (1:2000) (Origene, TA501989); anti-Myc (9E10) (1:1000) (Sigma, M4439); anti-NQO1 (1:1000) (CST, #3187); anti-p62 (1:1000) (BD, #610833); anti-tubulin (1:5000)(Sigma, T5168); anti-ubiquitin (1:500) (CST, #3936);

Guinea pig polyclonal antibodies: anti-p62 (1:2000) (Progen, GP62-C) (Immunostaining)

Reagents

Chloroquine (CQ) (C6628), cycloheximide (CHX) (C4859) and Hygromycin B (H3274) were from Sigma-Aldrich. Geneticin (G418) (11811023) and Doxycycline

Hydrochloride (#10592-12-9) was from Fisher Scientific. Puromycin (#53-79-2) was purchased from Santa Cruz.

Cell lines

Hela (ATCC, #CCL-2), human embryonic kidney (HEK) 293T (ECACC, 12022001), Atg5 wild-type and knockout mouse embryonic fibroblast cells (MEFs) (kindly provided by Dr N. Mizushima) and Atg7 wild-type and knockout MEFs (kindly provided by Dr M. Komatsu) were cultured in Dulbecco's modified Eagle's medium (DMEM, D6046) supplemented with 10% fetal bovine serum (FBS) (12133C, Sigma). DAXX knockout and control HAP1 (generated by Horizon Discovery) were cultured in Iscove's Modified Dulbecco's Medium (IMDM) with 10% FBS. HAP1 is a human near-haploid cell line derived from the chronic myelogenous leukaemia cell line, having a single copy of almost every human chromosome. Hela Tet-on p62-GFP stable cells were cultured in DMEM containing 10% FBS, 100 μg/ml G418 and 50 μg/ml Hygromycin B. Expression of p62-GFP was induced by 250 ng/ml Doxycycline (Dox) for 20 hours. Where applicable, cells were treated with 10 μg/ml puromycin or 20 μM chloroquine for the indicated times.

Generation of Hela Tet-on p62-GFP cells: pTRE-2Hyg-p62-GFP plasmid was transfected into Hela Tet-on cells. 300 μg/ml Hygromycin B and 500 μg/ml G418 were used to select stably transfected cells for 2 weeks. Stable cells were then diluted and plated into 96-well plates at the density of 0.8 cell/well. After 4 weeks, single colonies were expanded and induced by 250 ng/ml Doxycycline (Dox). 20 hours later, positive colonies were assessed by microscopy for GFP expression, and then cells were collected for Western blot. Colonies were then expanded and

maintained in DMEM containing 10% FBS, 100 μg/ml G418 and 50 μg/ml Hygromycin B for later experimental uses.

Generation of DAXX knockout MEFs: For lentivirus production, HEK 293T cells were split into a 10 cm dish and transfected with the total amount of 5 μg DNA per well, with 10 μl TransIT-2020 (Mirus). DNAs and the ratio were: pCMV-VSVg: psPAX2: pLentiCRISPRv2-DAXXgRNA = 1: 3: 4 (Plasmids were described in [326] in **Supplementary Table 1**). pCMV-VSVg and psPAX2 are lentiviral packaging plasmids. Viruses were harvested at 24, 48, 72 hours after transfection by medium collection, followed by filtering through a 0.45 μm filter. MEFs were infected with viral supernatant (DAXX knockout or control element) with 5 μg/ml polybrene. Polybrene is a cationic polymer that can enhance lentiviral infection efficiency to the mammalian cells by neutralising the charge repulsion between virions and the cell surface. Three days after infection, cells were split into the selection medium (containing 10 μg/ml puromycin). After 4 weeks, single colonies were expanded and analysed. Western blot was used to confirm the DAXX knockout efficiency. Positive colonies were expanded and maintained in DMEM containing 10% FBS and 5 μg/ml puromycin.

Transfection

Cells were split one day before transfection to 50~70% confluency. DNA and siRNAs were transfected with Lipofectamine 2000 (Invitrogen) for Hela cells and TransIT-2020 (Mirus) for MEFs and HAP1 cells, according to the manufacturer's instructions.

DNA transfections: Plasmids were prepped with Qiagen Plasmid Kits, and concentrations of plasmids were measured by NanoDrop™ 2000 (Thermo

Scientific™). The total amount of plasmids was 0.2-0.4 μg per well in a 6-well plate. The medium was changed 4 hours after transfection, with cells fixed/collected between 24-48 hours after transfection. Plasmid vector was used as a negative control.

Plasmid details: Flag-DAXX (#27974), pMXs-puro-GFP-p62 K7A D69A (#38281) (kindly provided by Dr N. Mizushima) and LentiCRISPRv2 (#52961) were from Addgene. HA-DAXX was kindly gifted from Dr Hsiu-Ming Shih.

siRNA transfection: The final concentration of siRNAs was 50 nM. The medium was changed after overnight incubation, with cells fixed/collected 48-72 hours after transfection. Scramble siRNA was used as a negative control.

Human siRNA sequences:

control siRNA-1 (Eurofins): 5′-CGUACGCGGAAUACUUCGA-3′

DAXX siRNA (Eurofins): 5′-GGAGUUGGAUCUCUCAGAA-3′

Atg5 siRNA (CST: #6345): 5′- GCCUGUAUGUACUGCUUUA-3′

Beclin 1 siRNA (CST: #6222): 5′-GGUCUAAGACGUCCAACAA-3′

Atg10 siRNA (Invitrogen): 5′-CCAUGGGACACUAUUACGC-3′

p62 siRNA (Eurofins): 5-GCATTGAAGTTGATATCGAT-3′

Smartpool Atg16L1 siRNAs (Dharmacon, L-021033-01): 5′-UGUGGAUGAUUAUCGAUUA-3′ (Set 1); 5′-GGCACACACUCACGGGACA-3′ (Set 2); 5′-GCAUUGGAUUAACGGAAAC-3′ (Set 3); 5′-GUUAUUGAUCUCCGAACAA-3′ (Set 4)

2.2 Immunofluorescence

Cells: Cells that were split on coverslips were fixed with 4% paraformaldehyde (PFA) for 10 minutes, followed by three washes with phosphate-buffered saline (PBS). Cells were then permeabilised with PBST (PBS containing 0.5% Triton) for 10 minutes then washed three times with PBS. Following blocked in PBS containing 1% bovine serum albumin (BSA) and 1% heat-inactivated goat serum for 30 minutes, cells were incubated with primary antibodies for 16-20 hours at 4°C. After three 5-minute washes with PBS, cells were incubated with secondary antibodies for 30 minutes at room temperature. After further washes, slides were mounted with mounting buffer (50% PBS and 50% glycerol containing 1 μg/ml 4′,6-diamidino-2-phenylindole (DAPI)).

Mouse thymus: DAXX conditional knockout and control mice were produced and maintained at Thomas Jefferson University, as described previously [330]. Briefly, mice carrying the conditional knockout allele of DAXX (DAXXf/f) were crossed with LckCre transgenic mice. The resulting heterozygous DAXX+/f LckCre mice were intercrossed to obtain DAXXf/f LckCre mice, which are T cell-specific DAXX-deficient. DAXXf/f LckCre mice were subsequently crossed with DAXXf/f mice to produce DAXXf/f LckCre (50%) mutant and DAXXf/f (50%) control mice. DNA was extracted from the mouse tail to determine the genotype. Wild-type and conditional DAXX knockout alleles were genotyped by PCR using primers 5′-AGCAGTAACTCCGGTAGTAGGAAG-3′ and 5′-AGGAACGGAACCACCTCAG-3′. The LckCre transgene was genotyped by PCR using primers 5′-CGAAATTGCCAGGATCAGG-3′ and 5′-CTTACCTGTAGCCATTGCAGCTAG-3′. Animal work performed in UK complied with UK Home Office legislation: the UK Animals (Scientific Procedures) Act with appropriate Home Office Project and

Personal animal licences and with local Ethics Committee approval. The procedures using mice in Thomas Jefferson University were approved by the institutional animal care and use committee (IACUC) at Thomas Jefferson University.

Tissues were fixed in 4% PFA, mounted in optimal cutting temperature (O.C.T) embedding compound (Tissue-Tek), frozen at -196°C and stored at -80°C. Before sectioning, tissues were left at -20°C for at least 2 hours. Tissues were cut into 10 µm thickness using a cryostat. Frozen slides were left at room temperature for 15 minutes and then blocked with 10% goat serum in TBST (tris-buffered saline (TBS) containing 0.1% Triton-X) for 1 hour before incubating with primary antibodies overnight at 4°C. Tissues were washed 3 times with TBST for 10 minutes each. Secondary antibodies were applied to the tissue for 30 minutes and then washed away with TBST for 10 minutes, 3 times. Tissues were mounted with mounting buffer (50% PBS and 50% glycerol containing 1 µg/ml DAPI).

Drosophila brains: Dissected *Drosophila* brains were fixed in 4% PFA for 20 minutes followed by 3 washes in PBS, then permeabilised in PBST (PBS containing 0.5% Triton-X) for 16-20 hours at 4°C. After 3 washes in PBS, brains were blocked with blocking buffer (PBS containing 5% BSA) for 2 hours and incubated with primary antibodies overnight at 4°C. Brains were washed 3 times with PBST for 10 minutes each. Secondary antibodies were applied to the tissue for 30 minutes and then washed away with TBST for 10 minutes, 3 times. Tissues were mounted with mounting buffer (50% PBS and 50% glycerol containing 1 µg/ml DAPI).

2.3 protein analysis

Immunoblot

Cells were harvested 24-48 hours after transfection and lysed with 1x Laemmli buffer. Cell lysates were boiled at 100°C for 10 minutes then fast spun for 5 seconds. Supernatants and protein marker were loaded onto protein gels and run at 135 V for 1.5 hours. Proteins were then transferred to polyvinylidene difluoride (PVDF) membranes for 90 minutes, and membranes were then blocked in the blocking buffer (5% skimmed milk in TBS-0.05% Tween 20) for 30 minutes. Primary antibodies were diluted in the blocking buffer, and membranes were incubated at 4°C overnight. Membranes were washed in 1x TBST (3 times, 5 minutes each) and incubated with appropriate conjugated secondary antibodies for 30 minutes. After 3 washes (5 minutes each), membranes were incubated with enhanced chemiluminescence, Pierce ECL Western Blotting Substrate (Fisher, 32106), and then blots were developed.

Native PAGE

Cells were harvested 24-48 hours after transfection and lysed in 100 µl Buffer A containing 0.5% nonyl phenoxypolyethoxylethanol (NP)-40 and protease inhibitor cocktail for 15 minutes. Cell lysates were centrifuged at 12,000 x *g* for 10 minutes. The supernatant of cell lysates was diluted (1:1) in Native Sample Buffer (Bio-Rad #1610738) and then subjected to 10% or 12% native PAGE (Bio-Rad) and immunoblotted with indicated antibodies.

Nuclear fractionation

HeLa cells were transfected with siRNAs for 48 hours. Cells in a 35-mm dish were washed with PBS and lysed in 300 µl Buffer A (20 mM Tris-HCl, pH 7.4, 2 mM

$MgCl_2$, 150 mM NaCl, 5 mM NaF, 1 mM Na_3VO_4, 0.5% NP-40, protease inhibitor cocktail (Roche)) and scraped thoroughly. Pipetting and incubating on ice for 15 minutes. The cell lysates were centrifuged at 720 x *g* for 5 minutes. The supernatants containing cytoplasmic fraction were collected. The pellets containing nuclear fraction were washed with 300 µl Buffer A and centrifuged at 720 x *g* for 5 minutes. The pellets were collected. The total cell lysates, cytoplasmic fractions and nuclear fractions were used for immunoblot.

2.4 *In vitro* experiments

Protein expression and purification

6x His-tagged p62 or DAXX was cloned into pET-28a (Novagen) for protein expression. Plasmids were transformed into BL21 (DE3), and 0.2 mM isopropyl β-d-1-thiogalactopyranoside (IPTG) was added into the LB medium to induce protein expression. Bacteria were centrifuged at 5500 x *g*, 4°C, for 15 minutes, and then pellets were resuspended in binding buffer (0.5 M NaCl, 20 mM Tris, 5 mM imidazole, pH 7.9) containing protease inhibitor cocktail and 0.1 mg/ml PMSF. All procedures were performed on ice. The bacteria were then lysed with BugBuster 1× protein extraction reagent (Millipore) and 50 U/ml benzonase (Thermo), followed by centrifugation at 16,000 x *g* for 20 minutes. The supernatants were applied to Amicon® Pro Affinity Concentration Kit (Merck Millipore) according to the supplier's instructions. Briefly, supernatants were applied to 6x His-affinity resins, then resins were washed with washing buffer (0.5M NaCl, 20mM Tris, 60mM imidazole, pH 7.9), and proteins were eluted with elution buffer (0.5M NaCl, 20mM Tris, 1M imidazole, pH 7.9).

To purify and concentrate the proteins, eluted samples were subjected to size exclusive chromatography with Superose 6 Increase 10/300 GL (GE Healthcare).

The purified proteins were concentrated to at least 10 μM using Amicon Ultra-0.5mL Centrifugal Filters in the desired stock buffer as described below.

Stock buffer of p62: 40 mM Tris-HCl pH 7.4, 300 mM NaCl, 1 mM dithiothreitol (DTT), 10% glycerol, or 40 mM Tris-HCl pH 7.4, 1 mM DTT, 10% glycerol.

Stock buffer of DAXX: 40mM Tris-HCl pH 7.4, 150 mM NaCl, 1 mM DTT.

***In vitro* phase separation assays**

Purified recombinant p62 or DAXX was centrifugated at 16,000 x g for 5 minutes before phase separation assay to remove any potential protein aggregates. Phase separation assay was carried out in a 0.2 ml microcentrifuge tube at room temperature in the buffer containing 40mM Tris-HCl pH 7.4, 150 mM NaCl, 1mM DTT. Imaging was performed in a 384-well optical bottom plate (Thermo Scientific Nunc) or a glass slide. Images were acquired with Leica DMi8 microscopy or Leica confocal microscopy SP8.

***In vitro* sedimentation assays**

To remove potential protein aggregates, purified recombinant p62 or DAXX was centrifugated at 16,000 x *g* for 5 minutes before sedimentation assay. A mixture of p62 (15 μl, 10 μM) and DAXX (15 μl, 10 μM), or p62 and buffer were subjected to *in vitro* sedimentation assay at room temperature for 1 hour, followed by centrifugation at 12000 x *g* for 5 minutes. The supernatant was subjected to immunoblot directly, and the pellet was washed once with the phase separation buffer before immunoblot.

2.5 Protein phase condensation assays

Fluorescence recovery after photobleaching (FRAP)

Hela cells and Atg7 wild-type/knockout MEFs were transfected with GFP-p62 or GFP-p62/mCherry-DAXX. 24 hours after transfection, live imaging and FRAP analysis were carried out using x 40 oil immersion objective on Leica confocal microscopy SP8. GFP-p62 puncta were bleached 11.8 seconds (8 × 1.477 seconds) with a 100% laser intensity of 488 nm. Fluorescence recovery was recorded for the indicated times, and the recovery intensity was exported by LAS X software.

Proteinase K digestion

After transfected with GFP-p62/vector or GFP-p62/mCherry DAXX for 20 hours, HeLa cells were fixed in 4% PFA for 10 minutes, followed by three 5-minute washes with PBS. Cells were then treated with 50 μg/ml proteinase K in PBS at 37°C for 30 minutes. After three 5-minute washes with PBS, cells were mounted and images were acquired with Leica DMi8 microscopy.

Cell fraction of NP-40 and urea

HeLa cells were transfected for 20 hours, trypsinised and resuspended in 100 μl Buffer A (20mM Tris-HCl, pH 7.4, 2 mM MgCl2, 0.5% NP-40, protease inhibitor cocktail (Roche)) on ice for 15 min. The cell lysates were centrifuged at 17,000 x *g* for 10 min. The supernatants were kept as NP-40 fractions. The pellets were dissolved in 8 M urea-containing Buffer A on ice for 20 minutes. The NP-40 fractions and urea fractions were used for SDS-PAGE and immunoblot.

2.6 Proteasome activity assays

Hela cells were transfected with siRNA for 48 hours or DNA for 24 hours. Proteasome activity assays were carried out according to the manufacturer's instruction (Abcam). Briefly, cells were harvested and washed once with cold PBS.

The cells were resuspended in 0.5% NP-40 (~4 volumes) and homogenised quickly by pipetting up and down. Cell lysates were centrifuged at 4°C, 13000 rpm for 10 minutes. The supernatants were collected into a clean tube. Add 1 µl Proteasome substrate to 50 µl cell lysates, mix well and incubate for 30 minutes at 37°C protected from light. The samples were measured with a fluorescent microplate reader with the filter Ex/Em = 350/440 nm.

2.7 Redox assays

ROS assay by flow cytometry

Cells were treated with or without 300 µM H_2O_2 for 16 hours and washed twice with PBS. $DCFH_2$-DA was diluted in PBS with the concentration of 5 µM, where cells were incubated for 20 minutes at 37°C. Cells were trypsinised, washed twice with PBS containing 2% FBS, and resuspended in PBS. Samples were loaded through Becton-Dickinson (BD) FACSAria II flow cytometer. Data were collected with accompanying software and analysed with FlowJo software. The unstained sample was used as negative control.

Nrf2 luciferase reporter assay

The Nrf2 antioxidant response pathway functions in cellular antioxidant defense. Under basal conditions, Nrf2 is retained in the cytosol by binding to Keap1; upon exposure to oxidative stress, Nrf2 is released from Keap1 and translocates to the nucleus, where it binds to the antioxidant response element (ARE) region of the gene promoter and induces the expression of antioxidant enzymes.

The dual-luciferase reporter assay is an efficient method to examine transcriptional activity. Two-type luciferases are needed for the assay. Firefly

luciferase is used as a reporter for transcriptional regulation assays, and constitutively expressing-*Renilla* luciferase is used as a control. The process of the dual-luciferase assay is shown in **Figure 9**.

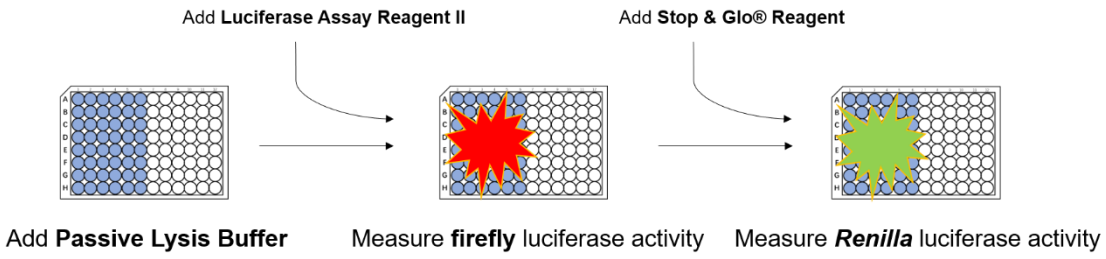

Figure 9: The dual-luciferase reporter assay.

The dual-luciferase assay can be performed in a 96-well plate. The following procedures are conducted to complete the assay. 1. Growth medium is removed, and cultured cells are rinsed in 1x PBS; 2. After removal of the rinse solution, 20 µl of passive lysis buffer is added into a well, and the plate is gently shaken for 20 minutes at room temperature; 3. 100 µl of Luciferase Assay Reagent II is added to each well, and firefly luciferase activity is measured with a luminometer; 4. 100 µl of Stop & Glo® Reagent is added into each well, and the *Renilla* luciferase activity is measured with a luminometer. Image adapted from https://www.promega.co.uk/products/luciferase-assays/reporter-assays/dual_luciferase-reporter-assay-system/?catNum=E1910

HeLa cells were transfected with control siRNA, p62 siRNA, DAXX siRNA and DAXX+p62 siRNAs before Luciferase assay. After 20 h, the cells were split into a 96-well luminometer plate. ARE firefly luciferase reporter vector and constitutively expressing *Renilla* luciferase vector, and negative control vector (BPS Bioscience, #60514) were transfected into pre-knockdown HeLa cells. After 20 hours, the dual-luciferase assay was performed with Dual-Luciferase® Reporter Assay System (Promega, E1910) according to the supplier's instruction. Briefly, the growth medium was removed from cells, and the cells were washed once with PBS, followed by lysed in 1x Passive Lysis Buffer for 20 minutes, on a

gentle orbital shaker. Then 100 µl of Luciferase Assay Reagent II was added to each well, and the firefly luciferase activity was measured by a luminometer. Next, 100 µl of Stop & Glo® Reagent was added to each well, and the *Renilla* luciferase activity was measured. Data were analysed and normalised with control.

2.8 Polymerase Chain Reaction (PCR)

Real-Time Quantitative Reverse Transcription PCR (RT-qPCR) analysis

RNAs were isolated with the RNeasy (Qiagen) according to the manufacturer's instructions. The quality and the quantity of RNAs were measured with NanoDrop^{TM} 2000 to guarantee that RNAs with 260/280 ratio >1.8 and 260/230 ratio >2.0 were used for RT-qPCR. 1 µg RNA was reverse transcribed with High-Capacity cDNA Reverse Transcription Mix (Applied Biosystems) using cycles of 25°C (10 minutes), 37°C (120 minutes) and 85°C (5 minutes). cDNA templates were used for RT-qPCR with LightCycler 480 DNA SYBR Green I Master kit (Roche) in LightCycler 480 II system (Roche). Primers were from Sigma and used at 0.5 µM. RT-qPCR was performed in triplicate for each sample, and a relative quantification approach was performed using the $2^{-\Delta\Delta Ct}$ method. Human actin was used as a control.

Primer sequence:

Human actin: 5′-ACTGGCATCGTGATGGACTC-3′ (forward) and 5′-TCAGGCAGCTCGTAGCTCTT-3′ (reverse);

Human NQO1: 5′-AAAGGACCCTTCCGGAGTAA-3′ (forward) and 5′-CTTGGAAGCCACAGAAATGC-3′ (reverse);

Human GSTM1: 5′-TGTCCTTGACCTCCACCGTA-3′ (forward) and 5′-GAACACAGGTCTTGGGAGGA-3′ (reverse).

2.9 Yeast two-hybrid screening

Yeast two-hybrid (Y2H) screening was applied with Clontech Matchmaker Gold Yeast Two-Hybrid System. Briefly, p62 1-300aa was cloned into pGBKT7 as a bait and then transformed into the yeast strain, Y2HGold. The Y2HGold was mated with yeast Y187 that was pre-transformed with pGADT7 and harboured human cDNA library (Mate & Plate Human Heart Library, #630417). This mating allows four reporters to detect protein-protein interactions, namely Aureobasidin A (Aba) resistance, histidine (His) minus resistance, adenine (Ade) minus resistance and blue colour with X-alpha-Gal. In addition, pGBKT7 plasmid confers leucine (Leu) minus resistance, and pGADT7 confers tryptone (Trp) minus resistance. Therefore, media with Leu-, Trp- and His-, Ade- along with Aba resistance and blue colour were used to select positive yeast clones. Plasmids were purified from the positive clone and cDNAs were recovered by transforming into E.coli. DNA sequencing and gene basic local alignment search tool (BLAST) were performed successively. To confirm the direct interaction between p62 1-300aa and DAXX 1-370aa in yeast, pGBKT7-p62 1-300aa-Y2HGold and pGADT7 1-370aa-Y187 were mated and cultured in media with Aba, X-alpha-Gal, His minus and Ade minus.

2.10 Statistical analysis

Statistical analysis was performed primarily with Graphpad Prism.

The unpaired two-tailed t-tests were conducted for the comparison between two groups; one-way or two-way analysis of variance (ANOVA) was used for the

comparison among multiple groups: one-way ANOVA for variables influenced by a single factor; two-way ANOVA for variables influence by two or more factors (***: $P < 0.001$, **: $P < 0.01$, *: $P < 0.05$, ns: not significant).

3 Results

3.1 DAXX is a p62 interaction protein

3.1.1 Direct p62-DAXX interaction

In the previous study, our group performed an unbiased Yeast two-hybrid (Y2H) screening with p62 (1-300aa) as a bait to identify proteins interacting with p62. 38 potential p62 binding proteins were found, which were listed in **Supplementary Table 2** in the reference [326]. Among 38 potential p62 binding proteins, DAXX was pulled out, suggesting that DAXX might be a candidate in binding p62. I initially confirmed the potential interaction between p62 and DAXX by co-transforming p62 and DAXX into yeasts (**Figure 10A**).

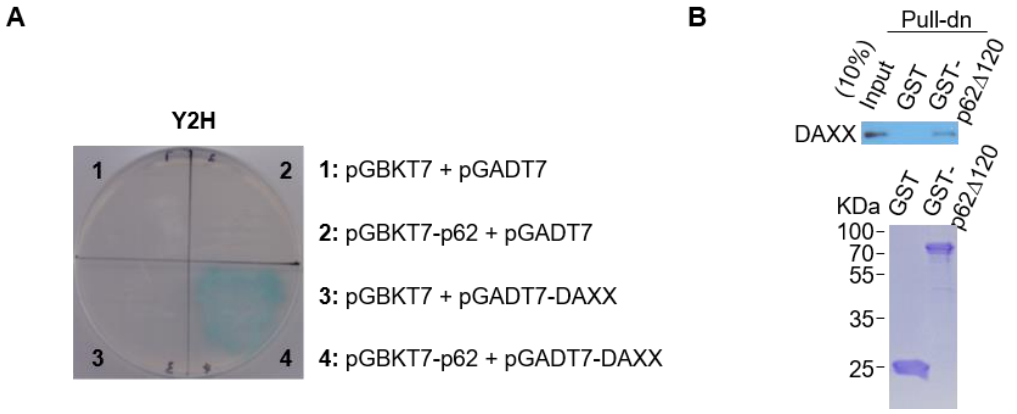

Figure 10: p62-DAXX interaction in yeast and *in vitro*.

A. Confirmation of p62-DAXX interaction in yeasts. Co-transformation of p62 and DAXX into yeasts. Survival of yeasts in nutrient-deficient medium indicates p62-DAXX interaction in yeasts. **B.** Confirmation of *in vitro* p62-DAXX interaction. 5 µl of *in vitro* expressed DAXX was incubated with GST or GST-p62Δ120 overnight. The pull-down (Pull-dn) samples were subjected to SDS-PAGE and probed with DAXX antibody. SDS-PAGE analysis (Coomassie brilliant blue staining) was carried out to confirm the expression of GST or GST-p62Δ120.

To further test the direct interaction between p62 and DAXX, bacterially expressed GST-p62 with 1-120 amino acid deletion (GST-p62Δ120) was incubated with DAXX and pulled down with GST proteins. **Figure 10B** suggests

that DAXX was pulled down by GST-p62Δ120, indicating the direct interaction between p62Δ120 and DAXX. The p62-DAXX interaction was further tested in HeLa cells and 8-week mouse striata. **Figure 11A** and **Figure 11B** confirmed the endogenous p62-DAXX interaction in HeLa cells by either immunoprecipitation p62 or *vice versa*. **Figure 11C** confirmed the p62-DAXX interaction in mouse striata.

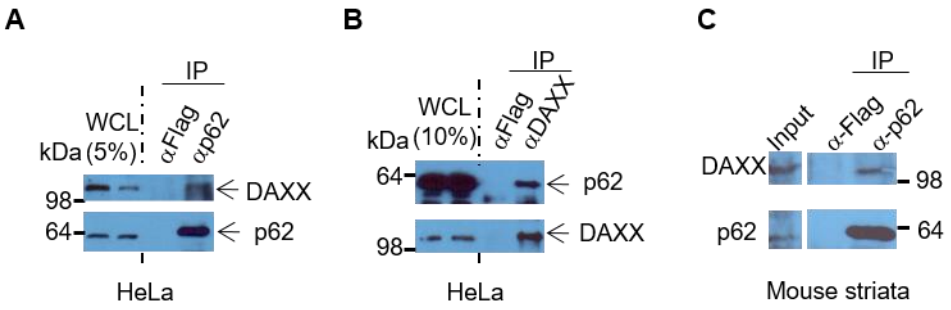

Figure 11: Endogenous p62-DAXX interaction in HeLa cells and Mouse striata.

A. Endogenous p62-DAXX interaction (p62 antibody pull-down). HeLa cell lysates were subjected to Flag antibody and p62 antibody immunoprecipitation (IP). Flag antibody was used for IP control. The whole cell lysates (WCL) and the immunoprecipitates were probed with DAXX antibody and p62 antibody. The dot line separates the WCL and IP samples. **B.** Endogenous p62-DAXX interaction (DAXX antibody pull-down). HeLa cell lysates were subjected to Flag antibody and DAXX antibody immunoprecipitation (IP). Flag antibody was used for IP control. The WCL and the immunoprecipitates were probed with p62 antibody and DAXX antibody. The dot line separates the WCL and IP samples. **C.** Mouse striata lysates were subjected to Flag antibody and p62 antibody immunoprecipitation (IP). Flag antibody was used for IP control.

3.1.2 Interaction regions in DAXX and p62

Then, the regions in p62 and DAXX that contribute to their interaction needed to be investigated. To identify the region of p62 that binds DAXX, a series of p62 variants were generated. From the immunoprecipitation results, neither p62 1-120aa nor p62 1-180aa were enough for the binding (**Figure 12A**), and the

binding region on p62 might locate between 246-300aa (**Figure 12B**). This indicated that the PB1 domain on p62 might not be necessary for p62-DAXX binding.

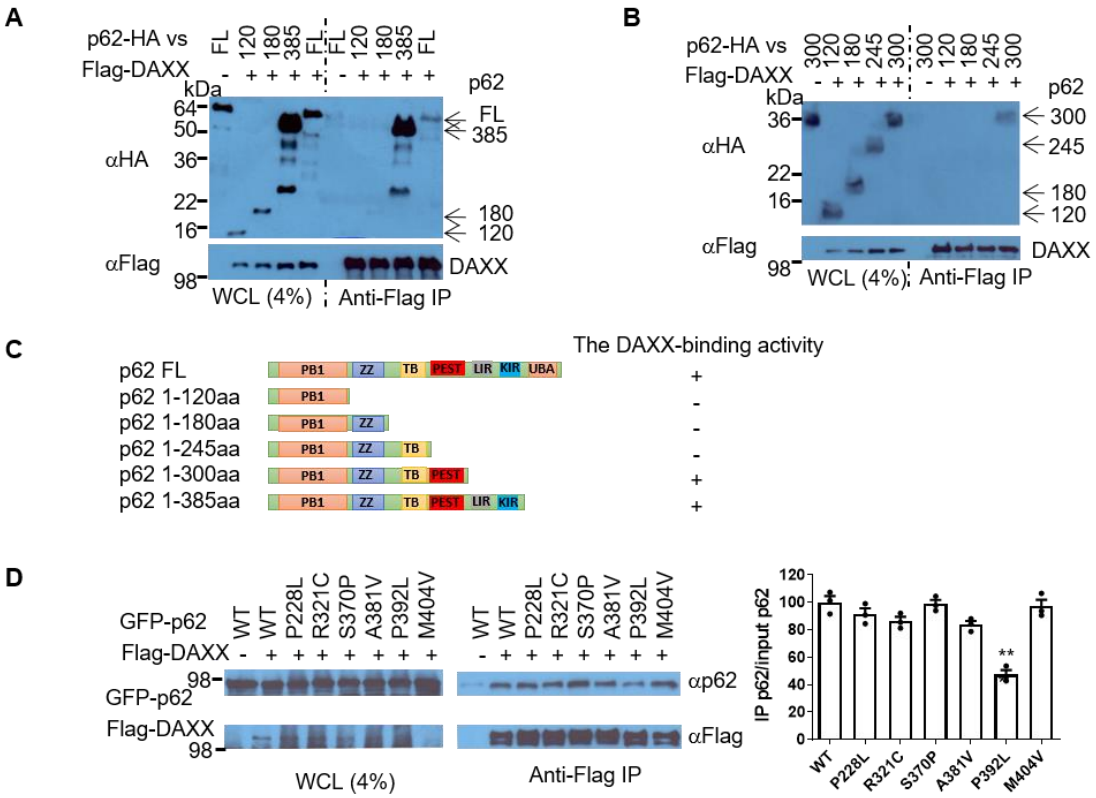

Figure 12: p62 regions required for p62-DAXX interaction.

A. p62 1-180aa is not required for p62-DAXX interaction. p62-HA/empty vector (control), p62 1-120aa-HA/Flag-DAXX, p62 1-180aa-HA/Flag-DAXX, p62 1-385aa-HA/Flag-DAXX and p62-HA/Flag-DAXX were co-transfected into HeLa cells. After 20 hours, cells were harvested for immunoprecipitation (IP) with Flag antibody. The whole cell lysates (WCL) and the immunoprecipitates were probed with HA antibody (mouse) and Flag antibody (rabbit). The dot line separates the WCL and IP samples. **B.** p62 246-300aa is required for p62-DAXX interaction. p62 1-300aa-HA/empty vector (control), p62 1-120aa-HA/Flag-DAXX, p62 1-180aa-HA/Flag-DAXX, p62 1-245aa-HA/Flag-DAXX and p62 1-300aa-HA/Flag-DAXX were co-transfected into HeLa cells. After 20 hours, cells were harvested for immunoprecipitation (IP) with Flag antibody. The whole cell lysates (WCL) and the immunoprecipitates were probed with HA antibody (mouse) and Flag antibody (rabbit). The dot line separates the WCL and IP samples. **C.** Schematic diagrams of deletion constructs of p62 with functional domains and their DAXX-binding activities. **D.** P392L mutation in p62 reduces the p62-DAXX interaction. GFP-p62/empty vector (control), GFP-p62/Flag-DAXX and GFP-p62 mutants/Flag-DAXX were co-transfected into HeLa cells. After 20 hours, cells were harvested for immunoprecipitation (IP) with Flag antibody. The whole cell lysates (WCL) and the immunoprecipitates were probed with GFP antibody and Flag antibody. The ratios of immunoprecipitated p62 and input p62 were quantified. n=3 independent experiments. Statistical analysis was performed with one way ANOVA. Tukey's test was used for comparison. ***: P<0.0001. Data are shown as mean±sem.

Figure 12C summarised deletions of p62 used for DAXX binding assays and their DAXX-binding activities. It is reported that p62 mutations were associated with diseases, such as Paget's disease of bone (PDB) [327] and amyotrophic lateral sclerosis (ALS) [328, 329], and I was wondering if these mutations affect the p62-DAXX binding. Among six p62 mutations p62 P228L, R321C, S370P, A381V, P392L, and M404V, p62 P392L reduced the p62-DAXX interaction significantly, suggesting that C-terminal of p62 might also contribute to its binding to DAXX (**Figure 12D**).

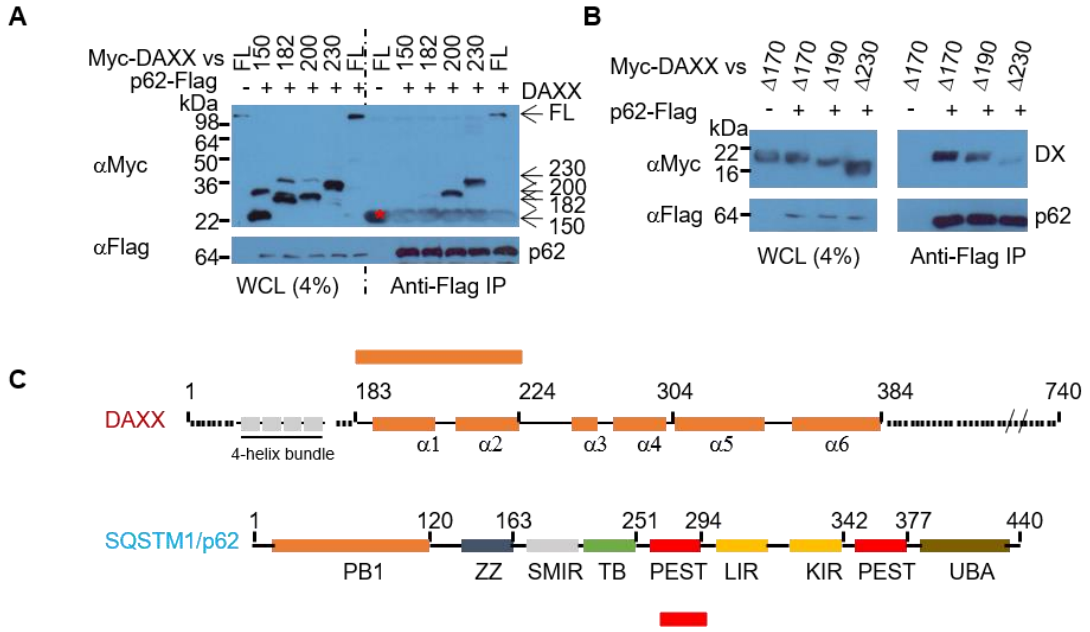

Figure 13: DAXX regions required for p62-DAXX interaction.

A. DAXX 1-182aa is not required for p62-DAXX interaction. Myc-DAXX full-length (FL)/empty vector, Myc-DAXX 1-150aa/p62-Flag, Myc-DAXX 1-182aa/p62-Flag, Myc-DAXX 1-200aa/p62-Flag, Myc-DAXX 1-230aa/p62-Flag, and Myc-DAXX-FL/p62-Flag was co-transfected into HeLa cells. After 20 hours, cells were harvested for immunoprecipitation (IP) with Flag antibody. The whole cell lysates (WCL) and the immunoprecipitates were probed with Myc antibody (rabbit) and Flag antibody (rabbit). The dot line separates the WCL and IP samples. * represents antibody light chain. **B.** DAXX 170-230aa is required for p62-DAXX interaction. Myc-DAXX 171-370aa (1-170 deletion, Δ170)/empty vector vector, Myc-DAXX 171-370aa (Δ170)/p62-Flag, Myc-DAXX 190-370aa (Δ190)/p62-Flag, or Myc-DAXX 231-370aa (Δ230)/p62 Flag was co-transfected into HeLa cells. After 20 hours, cells were harvested for immunoprecipitation (IP) with Flag antibody. The whole cell lysates (WCL) and the immunoprecipitates were probed with Myc antibody (rabbit) and Flag antibody (rabbit). The dot line separates the WCL and IP samples. DX: DAXX. **C.** Schematic architectures of DAXX and p62.

Next, DAXX variants were generated to identify the region of DAXX that interacted with p62. **Figure 13A** and **Figure 13B** shows that DAXX 1-182aa was not required for p62-DAXX interaction, but DAXX 182-230aa was needed. By far, the domain architectures of DAXX and p62 was mapped (**Figure 13C**). It is concluded that p62 246-300aa and DAXX 182-230aa are essential for their interaction.

3.1.3 DAXX and p62 co-localisation in cells and mouse striata

It was observed that endogenous DAXX bodies and p62 bodies were always co-localised together in HeLa cells (**Figure 14A**) and mouse striata (**Figure 14B**), and DAXX bodies were always associated with p62 bodies that had stronger signals and bigger sizes, but not all DAXX bodies with stronger signals and bigger sizes were positive for p62. This could indicate that cytoplasmic DAXX might have other roles except for interacting with p62.

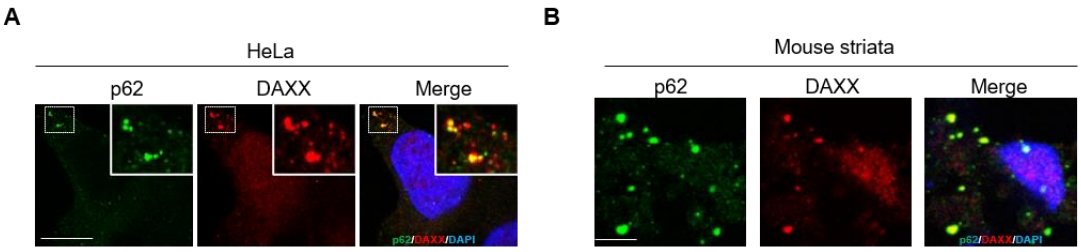

Figure 14: p62 and DAXX co-localisation in HeLa cells and Mouse striata.

A. Endogenous p62 and DAXX co-localisation in HeLa cells. HeLa cells were fixed and stained with p62 antibody and DAXX antibody. Images were acquired by Leica confocal microscopy. Bar: 10 μm. Bar (inset): 2 μm. **B.** Mouse striatal sections were stained with p62 antibody and DAXX antibody. Images were acquired by Leica confocal microscopy. Bar: 10 μm.

Both p62 and DAXX are widely expressed in mammalian cells, including neuronal cells and glial cells. The types of stained cells in the mouse striata were not

defined. However, the co-localisation data support the p62-DAXX interaction, which is predicted to be a general phenomenon in various cell types.

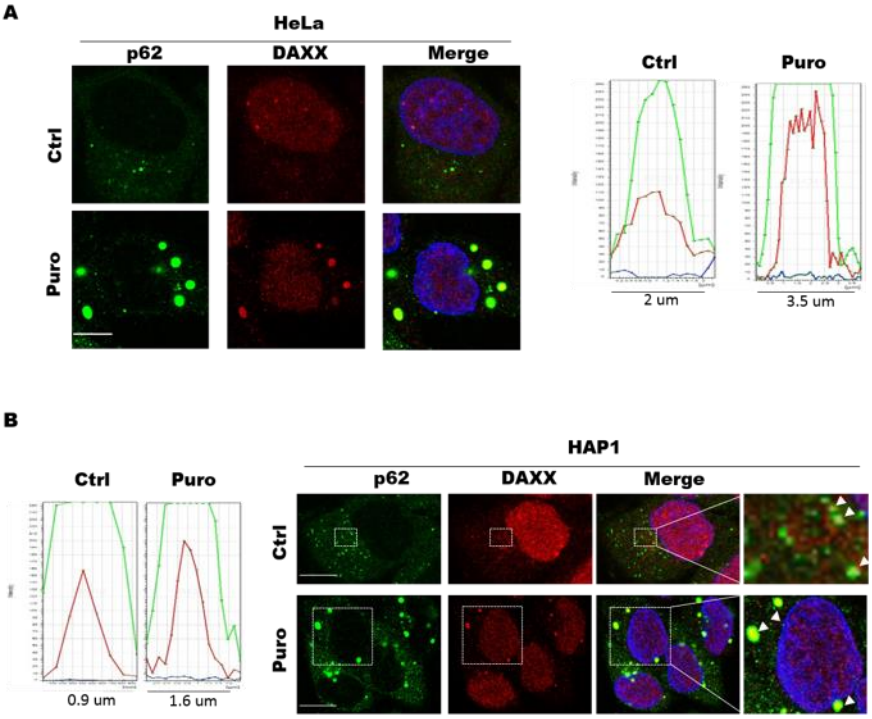

Figure 15: p62 and DAXX co-localisation is enhanced after puromycin treatment.

A. Co-localisation of endogenous DAXX and p62 in HeLa cells. Cells were treated with 10 µg/ml puromycin for 5 hours, stained with p62 antibody (guinea pig) and DAXX antibody (rabbit). Images were acquired by Leica confocal microscopy. Bar: 10 µm. Line profiles were done by LAS AF Lite. **B.** Co-localisation of endogenous DAXX and p62 in HAP1 cells. Cells were treated with10 µg/ml puromycin for 5 hours, stained with p62 antibody (guinea pig) and DAXX antibody (rabbit). Images were acquired by Leica confocal microscopy. Bar: 10 µm. Line profiles were done by LAS AF Lite.

It is also observed that while endogenous p62 and DAXX co-localised under resting conditions, both of them formed larger puncta after treatment with puromycin, a proteotoxin causing protein misfolding by inducing the premature release of polypeptide chains from ribosomes. After puromycin treatment, the co-localisation of p62 and DAXX was markedly enhanced in HeLa cells (**Figure 15A**).

Similar results were observed in HAP1 cells (**Figure 15B**). The p62-DAXX co-localisation appeared dependent on the interaction of these two proteins.

Former results showed that p62 mainly interacted with 182-230aa of DAXX, and consistently, **Figure 16A** illustrates that p62 had strong interactions with full-length DAXX (DAXX-FL) and amino-terminal DAXX (DAXX-N), but less interaction with carboxyl-terminal DAXX (DAXX-C). Indeed, the immunostaining results show that the p62 also co-localised with DAXX-FL and DAXX-N, but not DAXX-C (**Figure 16B**).

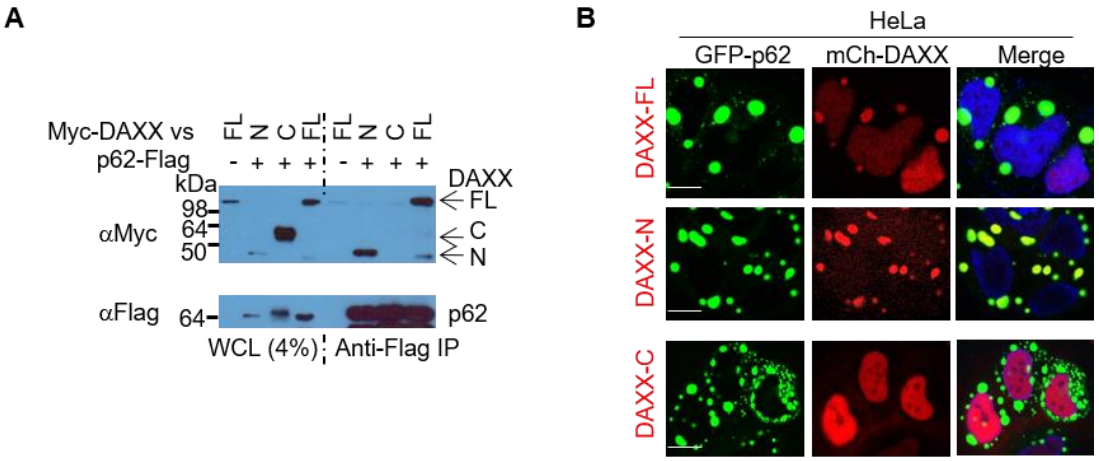

Figure 16: p62 interacts with full-length and amino-terminal DAXX.

A. p62 has no visible interaction with carboxyl-terminal DAXX. Myc-DAXX full-length (FL)/vector (negative control), Myc-DAXX-N (1-370aa)/p62-Flag, Myc-DAXX-C (371-740aa)/p62-Flag and Myc-DAXX-FL/p62-Flag were co-transfected into HeLa cells. After 20 hours, cells were harvested for immunoprecipitation (IP) with Flag antibody. The whole cell lysates (WCL) and the immunoprecipitates were probed with Myc antibody (rabbit) and Flag antibody (rabbit). The dot lines separate the WCL and IP samples. **B.** p62 has no visible co-localisation with carboxyl-terminal DAXX in HeLa cells. GFP-p62 was co-transfected into HeLa cells with mCherry-DAXX-FL, mCherry-DAXX-N and mCherry-DAXX-C. After 20 hours, cells were fixed. Images were acquired by Leica confocal microscopy. Bar: 10 μm. mCh: mCherry. N: amino-terminal. C: carboxyl-terminal.

3.2 DAXX promotes the formation of p62 bodies

3.2.1 DAXX promotes the size of p62 bodies

The functional consequences of the interaction between p62 and DAXX were further tested. Interestingly, the sizes of GFP-p62 bodies were largely increased in DAXX overexpressed cells (**Figure 17**). The size of the largest puncta in each cell, the number of puncta over a certain size in each cell and the percentage of cells with puncta over certain size can reliably reflect the size extent of the puncta in the cell population; hence these criteria were used to quantify the p62 bodies. As shown in **Figure 17**, DAXX enhanced the size of the largest puncta in each cell and the percentage of cells with larger puncta markedly.

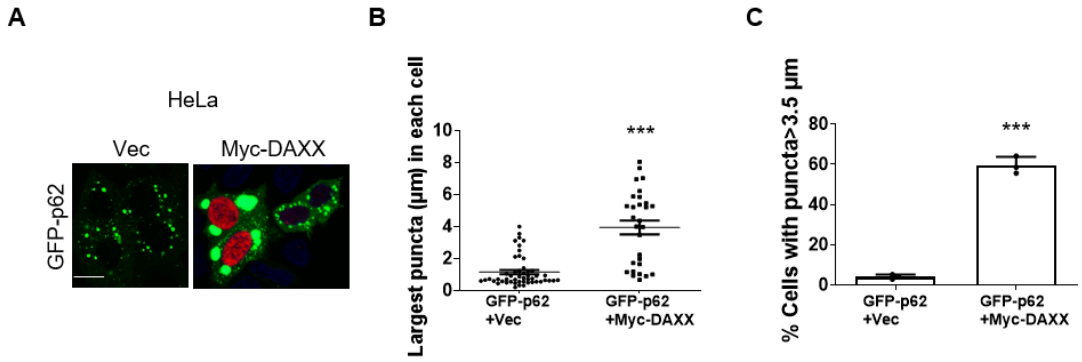

Figure 17: Overexpressed DAXX promotes GFP-p62 body formation in HeLa cells.

GFP-p62 was co-transfected into HeLa cells with vector and Myc-DAXX. After 20 hours, cells were fixed and stained with Myc antibody (rabbit). **A.** Images were acquired by Leica confocal microscopy. Bar: 10 μm. **B.** The size (diameter) of the largest GFP-p62 puncta (μm) in each cell was measured with LAS AF Lite. Data are shown as mean ± sem. ***: P<0.0001. **C.** The percentage of the cells with puncta >3.5 μm was measured with LAS AF Lite. Data are shown as mean±sem. ***: P<0.0001.

The following experiment was intended to exclude the possibility that the variation in transfection efficiency could lead to the differences in p62 body sizes.

Tet-on-inducible p62 stably expressing HeLa cells were generated in which p62-GFP expression was induced by an additional supplement of doxycycline into the medium. Remarkably, in the cells stably expressing p62-GFP, DAXX expression significantly increased p62-GFP puncta formation and decreased the diffused p62-GFP (**Figure 18**).

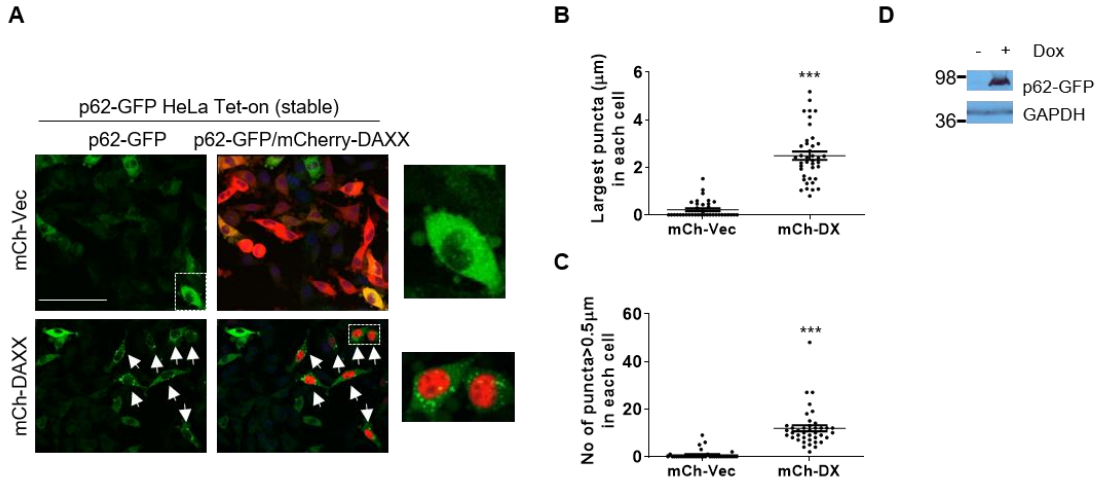

Figure 18: Overexpressed DAXX promotes stably-expressed p62 body formation.

mCherry-vector (mCh-Vec) or mCherry-DAXX (mCh-DX) was transfected into p62-GFP stably expressing HeLa cells (p62-GFP HeLa Tet-on). 3 hours after transfection, doxycycline was supplemented into medium to induce the expression of p62-GFP. **A.** Images were acquired by Leica confocal microscopy. Bar: 50 μm. **B.** The size (diameter) of the largest p62-GFP puncta (μm) in each cell was measured with LAS AF Lite. Data are shown as mean ± sem. ***: P<0.0001. **C.** The number of p62-GFP puncta >0.5 μm was measured with ImageJ. Data are shown as mean ± sem. ***: P<0.0001. **D.** Immunoblot shows p62-GFP expression. Dox: doxycycline.

Further, the DAXX histone H3.3-binding domain (DAXX 178-417aa) was tested and confirmed that this fragment also had a similar effect of improving p62 body formation (**Figure 19**).

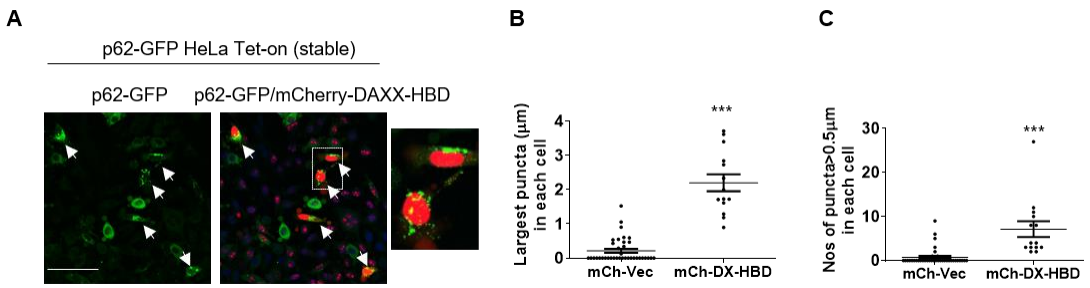

Figure 19: DAXX histone 3.3-binding domain promotes stably-expressed p62 body formation.

mCherry-vector (mCh-Vec) or mCherry-DAXX H3.3-binding domain (mCh-DX-HBD) was transfected into p62-GFP stably expressing HeLa cells (p62-GFP HeLa Tet-on). 3 hours after transfection, doxycycline was supplemented into the medium to induce the expression of p62-GFP. **A.** After 20 hours, cells were fixed and images were acquired with Leica confocal microscopy. Bar: 50 μm. **B.** The size (diameter) of the largest p62-GFP puncta (μm) in each cell was measured with LAS AF Lite. Data are shown as mean ± sem. ***: P<0.0001. **C.** The number of p62-GFP puncta >0.5 μm was measured with ImageJ. Data are shown as mean ± sem. ***: P<0.0001.

To exclude any potential effect of DAXX on p62-GFP expression in the Tet-on cells, which could affect p62 body formation, I first induced p62-GFP expression in these stable cells and then turned the expression off by replacing doxycycline and then transfecting DAXX into the cells. Notably, DAXX expression also increased p62 body formation in HeLa Tet-on cells where p62 expression was pre-induced but then turned off before DAXX was transfected (**Figure 20**).

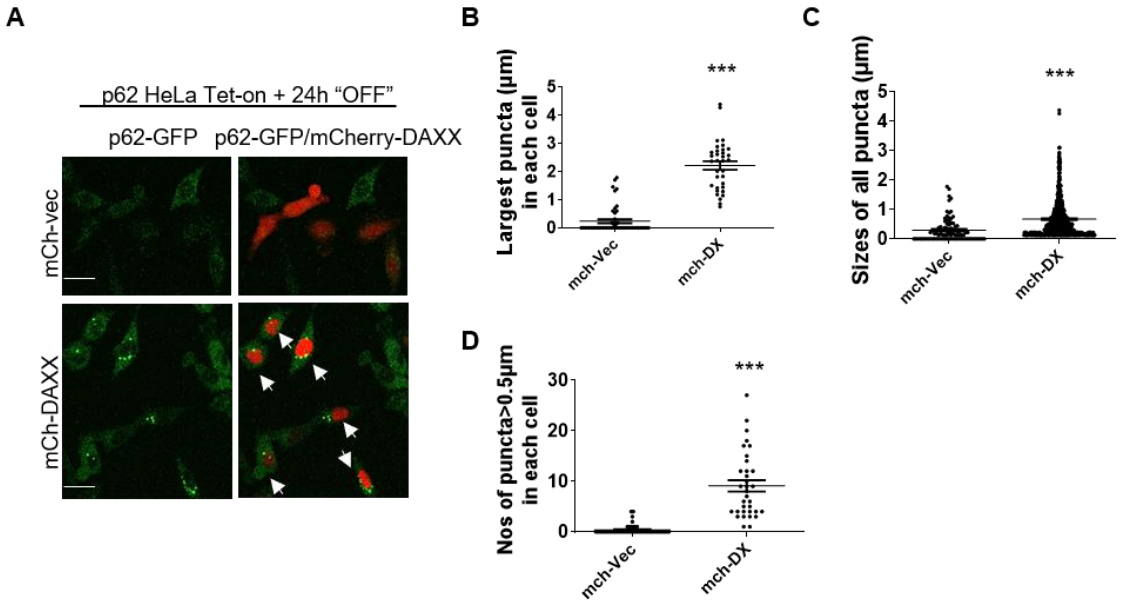

Figure 20: Overexpressed DAXX promotes stably-expressed p62 body formation in Tet-ON/OFF conditions.

Doxycycline was supplemented in medium to induce p62-GFP expression in p62-GFP stably expressing HeLa cells for 24 hours and then removed, followed by transfection of mCherry-vector (mCh-Vec) or mCherry-DAXX (mCh-DX). **A.** After 20 hours, cells were fixed. Images were acquired with Leica confocal microscopy. Bar: 20 μm. **B.** The size (diameter) of the largest p62-GFP puncta (μm) in each cell was measured with LAS AF Lite. Data are shown as mean ± sem. ***: P<0.0001. All p62-GFP puncta (**C**) and the number of p62-GFP puncta >0.5 μm (**D**) was measured with ImageJ. Data are shown as mean ± sem. ***: P<0.0001. mCh: mcherry.

These two experiments allow me to conclude that the effect of DAXX on p62 body formation is independent of p62 expression.

Also, Tet-on-inducible DAXX stably expressing HeLa cells was generated, and consistently, **Figure 21** showed that p62 formed more and bigger puncta when DAXX was overexpressed.

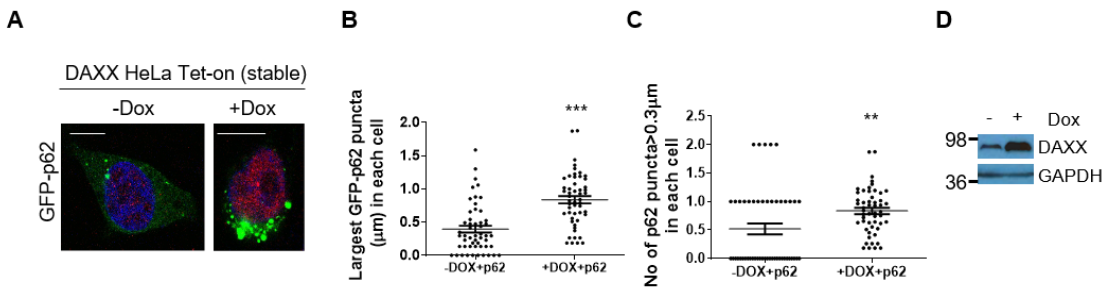

Figure 21: GFP-p62 forms bigger bodies when DAXX expression is induced.

GFP-p62 was transfected into DAXX stably expressing HeLa cells. Doxycycline was added 3 hours after transfection. After 24 hours, cells were fixed and stained with DAXX antibody. **A.** Images were acquired with Leica confocal microscopy. Bar: 10 μm. The size (diameter) of the largest GFP-p62 puncta (μm) (**B**) and the number of p62-GFP puncta >0.3 μm (**C**) in each cell was measured with LAS AF Lite. n=52 cells. Statistical analysis was performed with T-tests. ***: P<0.0001. **D.** Immunoblot shows DAXX expression.

3.2.2 DAXX promotes p62 body sizes in p62 overexpressed cells

Based on the physical experiment results that p62 had strong interactions with full-length DAXX (DAXX-FL) and amino-terminal DAXX (DAXX-N), the next experiment further tested if this effect resulted in p62 body formation. **Figure 22** indicated that, compared with carboxyl-terminal DAXX, full-length DAXX and amino-terminal DAXX, which have apparent physical interactions, helped promote the sizes of p62 bodies and increase the numbers of bigger puncta, suggesting that the physical interaction between p62 and DAXX is required for the effect of DAXX on promoting p62 body formation.

In **Figure 12C**, the p62 mutant, p62 P392L, had less physical interaction with DAXX. Also, **Figure 23** showed that the effect of DAXX on p62 P392L body formation was reduced, compared with that on wild-type (WT) p62. These results indicate that the physical interaction between p62 and DAXX is critical for the effect of DAXX in promoting p62 body formation.

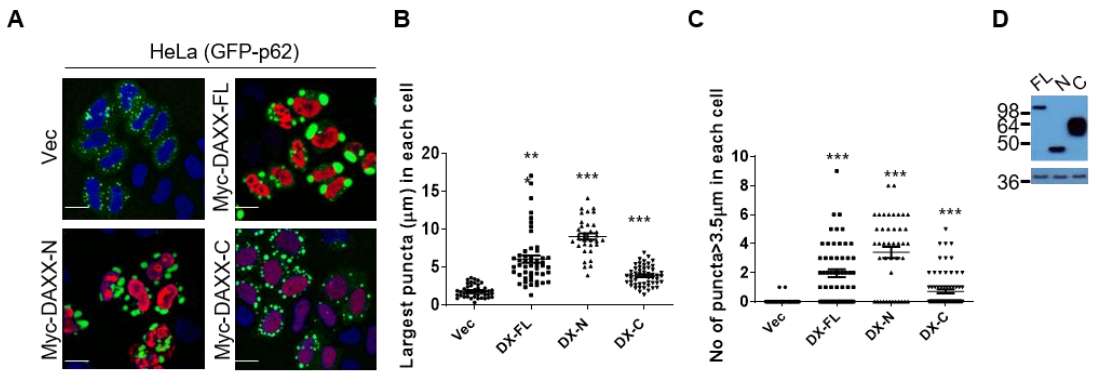

Figure 22: GFP-p62 forms bigger bodies when co-transfected with full-length DAXX and amino-terminal DAXX, compared with carboxyl-terminal DAXX.

GFP-p62 was co-transfected with vector, Myc-DAXX, Myc-DAXX-N (1-379aa) or Myc-DAXX-C (371-700aa). After 20 hours, cells were fixed and stained with Myc antibody. **A.** Images were acquired with Leica confocal microscopy. Bar: 20 μm. The size (diameter) of the largest GFP-p62 puncta (μm) in each cell (**B**) and the number of GFP-p62 puncta > 3.5 μm in each cell (**C**) were measured with LAS AF Lite. Statistical analysis was performed by one-way ANOVA (Tukey's test). Data are shown as mean ± sem. ***P < 0.0001. **D.** Immunoblot shows DAXX expression.

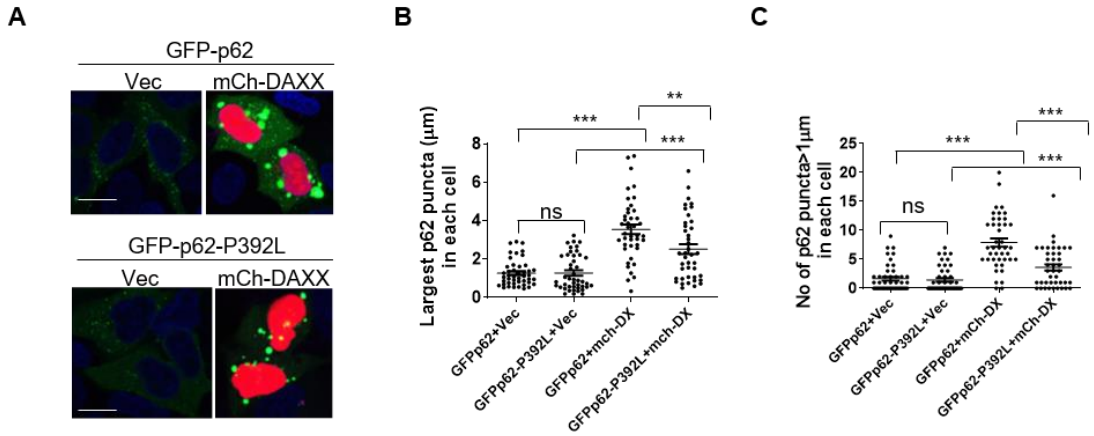

Figure 23: Reduced effect of DAXX on p62 P392L body formation.

GFP-p62 and GFP-p62-P392L were transfected into HeLa cells with empty vector or mCherry-DAXX. **A.** After 20 hours, cells were fixed. Images were acquired with Leica confocal microscopy. Bar: 20 μm. The size (diameter) of the largest GFP-p62 puncta (μm) in each cell (**B**) and the number of GFP-p62 puncta > 1 μm in each cell (**C**) were measured with ImageJ. Statistical analysis was performed with T-tests. ***: P<0.0001; **: P=0.0051; ns: P=0.9491 (left); ns: P=0.6549 (right). mCh: mCherry. DX: DAXX.

To further confirm the effect of DAXX on p62 body formation, WT and DAXX knockout (DXKO) HAP1 cells were tested. Consistently, fewer and smaller p62 bodies were formed in HAP1 DXKO cells, compared with those in HAP1 WT cells (**Figure 24**).

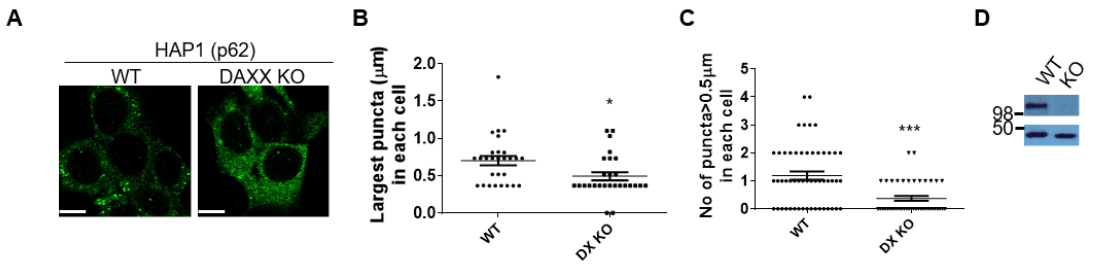

Figure 24: p62 forms smaller puncta in DAXX knockout HAP1 cells.

HAP1 WT and DAXX KO cells were fixed and stained with p62 antibody. **A.** Images were acquired with Leica confocal microscopy. Bar: 10 μm. The size (diameter) of the largest p62 puncta (μm) in each cell (**B**) and the number of p62 puncta > 0.5 μm in each cell (**C**) were measured with LAS AF Lite. Statistical analysis was performed with unpaired/two-tailed T-tests. Data are shown as mean ± sem. *: P = 0.0136; ***: P < 0.0001. **D.** Immunoblot shows DAXX expression. DX: DAXX. WT: wild-type. KO: knockout.

Then DAXX knockout MEFs were generated using the CRISPR/CAS9 system. In DAXX knockout MEFs, fewer and smaller p62 bodies were formed, as shown in DAXX knockout HAP1 cells (**Figure 25**). This effect was enhanced in the presence of puromycin.

It is reported that DAXX knockout resulted in embryonic lethality in mice [197]. DAXX conditional knockout mice [330] were used to test the *in vivo* effect of DAXX on p62 body formation. The transgenic strain expresses Cre under the control of Lck (lymphocyte protein tyrosine kinase) promoter, enabling thymocyte-specific knockout. The expression of Cre is initiated in pro/pre T cells. In this mouse model, DAXX was conditionally knocked out in T cells in the thymus. I attempted to stain both DAXX and CD3 (a T cell marker) in thymus sections,

however the immunofluorescence staining failed to give convincing CD3 signals (Data not shown). As such, I focused on DAXX staining in the tissues. **Figure 26** showed that p62 puncta in DAXX conditional knockout (cKO) thymus were smaller and fewer than those in WT thymus.

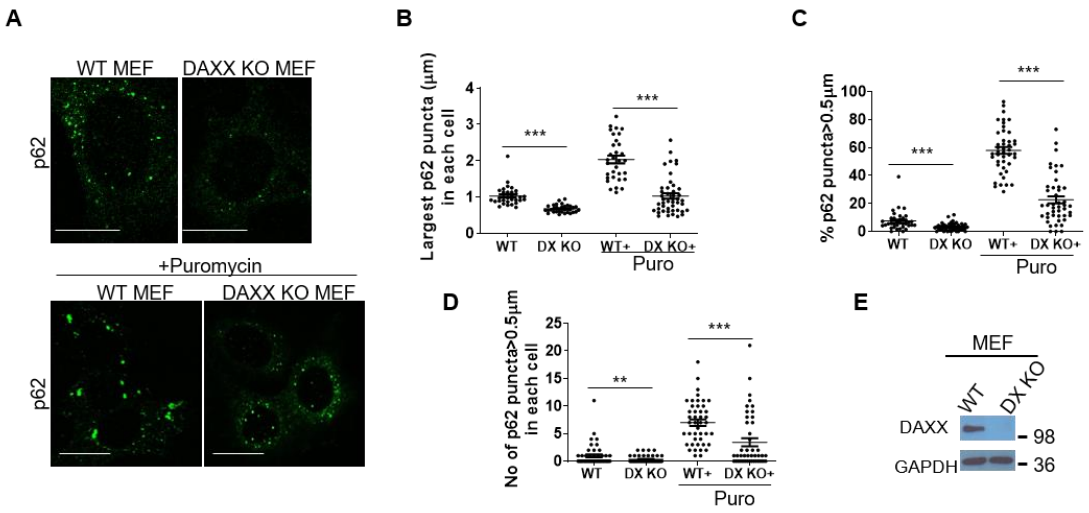

Figure 25: p62 forms smaller puncta in DAXX knockout MEFs.

WT and DAXX KO MEFs were treated with or without 10 μg/ml puromycin for 6 hours. Cells were fixed and stained with p62 antibody. **A.** Images were acquired with Leica confocal microscopy. Bar: 10 μm. The size (diameter) of largest p62 puncta (μm) in each cell (**B**), the number of p62 puncta > 0.5 μm in each cell (**C**) and the percentage of p62 puncta >0.5 μm (**D**) were measured with ImageJ. Statistical analysis was performed with T-tests. Data are shown as mean±sem. **: P=0.0041. ***: P=0.0003. **E.** Immunoblot shows the expression of DAXX. DX: DAXX. WT: wild-type. KO: knockout.

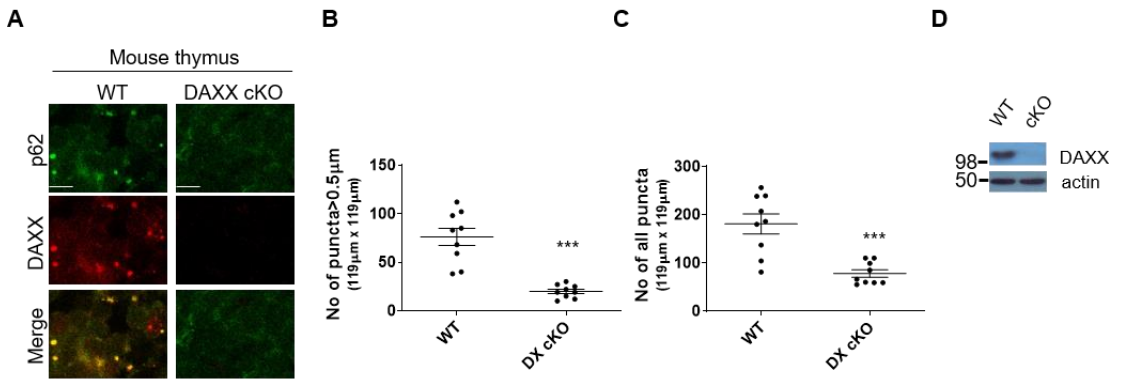

Figure 26: p62 forms smaller puncta in DAXX conditional knockout mouse thymus.

Thymus from WT and DAXX conditional knockout (cKO) mice were stained with p62 and DAXX antibodies. **A.** Images were acquired with Leica confocal microscopy. Bar: 10 μm. The number of p62 puncta > 0.5 μm in each image (119 μm × 119 μm) (**B**) and the number of all p62 puncta in each image (**C**) were measured with ImageJ. Statistical analysis was performed with unpaired/two-tailed T-tests. Data are shown as mean ± sem. ***: P < 0.0001 (left); ***: P= 0.0003 (right). **D.** Immunoblot shows DAXX expression. WT: wild-type.

3.2.3 DAXX does not significantly affect p62 expression

One of the main routes of degrading intracellular proteins is the ubiquitin-proteasome pathway, and it is reported that p62 deficiency promotes proteasomal activity [1, 91]. Considering that the effect of DAXX on p62 body formation could result from DAXX affecting proteasome activity, leading to p62 accumulation, DAXX was knocked down or overexpressed in HeLa cells, and the cells were subjected to proteasome activity assay. **Figure 27A, B** confirmed that either DAXX knockdown or overexpression had no significant effect on proteasome activity. Protein levels of p62 were then tested in DAXX knockdown or overexpressed conditions. Cycloheximide is commonly used to inhibit protein synthesis. **Figure 27C, D** showed that DAXX knockdown or overexpression did not significantly change p62 turnover.

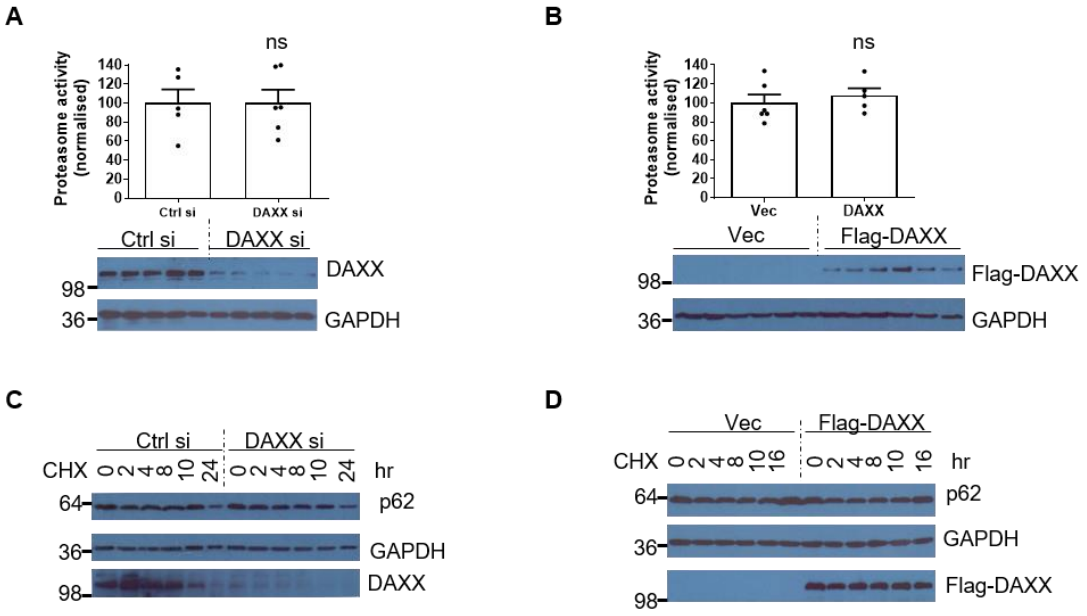

Figure 27: DAXX does not significantly affect p62 protein levels.

A. DAXX knockdown does not change proteasomal activity. Control siRNA and DAXX siRNA were transfected into HeLa cells for 48 hours. Cells were subjected to proteasome activity assay. Immunoblot was used to confirm DAXX knockdown efficiency. ns: P=0.9703. n=5. **B.** DAXX overexpression does not change proteasomal activity. Vector and Flag-DAXX were transfected into HeLa cells for 24 hours. Cells were subjected to proteasome activity assay. Immunoblot was used to confirm DAXX knockdown efficiency. Data are shown as mean ± sem. ns: P=0.5165. n=6. **C.** DAXX knockdown does not change p62 turnover. HeLa cells were transfected with control siRNA or DAXX siRNA, and treated with cycloheximide (50 μg/ml) for the indicated time. 48 hours after transfection, cells were harvested and subjected to immunoblot with p62, DAXX and GAPDH antibodies. **D.** DAXX overexpression does not change p62 turnover. HeLa cells were transfected with Vector or Flag-DAXX, and treated with cycloheximide (50 μg/ml) for the indicated time. 48 hours after transfection, cells were harvested and subjected to immunoblot with p62, Flag and GAPDH antibodies.

Results from RT-qPCR confirmed that DAXX overexpression did not significantly increase p62 mRNA levels, and DAXX knockdown did not significantly decrease p62 mRNA levels (**Figure 28**), indicating that DAXX did not alter p62 protein expression. In this experiment, DAXX was constructed in pRK5 plasmid, and pRK5-Flag was thus used as a control plasmid. Consequently, these data suggest that DAXX can positively modulate the formation of p62 bodies.

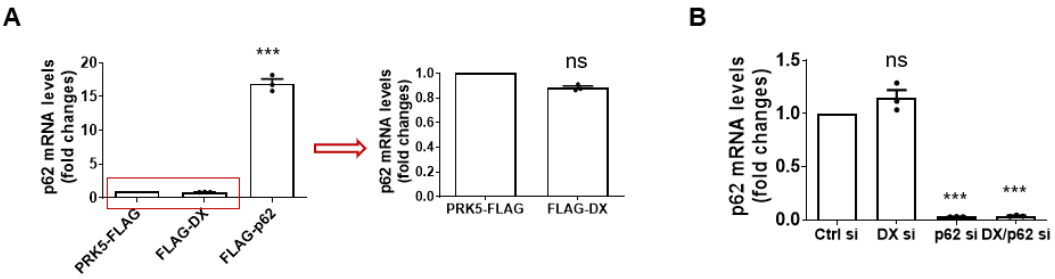

Figure 28: DAXX does not affect p62 mRNA levels.

A. DAXX overexpression does not change p62 mRNA level. HeLa cells were transfected with PRK5-Flag (control), Flag-DAXX and Flag-p62 (positive control). After 24 hours, cells were subjected to RNA purification. RNAs were then subjected to reverse transcription-PCR and RT-qPCR. Three replicates were used for each RNA. Close-up view on the p62 mRNA levels of the boxed samples. Statistical analysis was performed by one-way ANOVA. Tukey's test was used for the comparison. ***: P<0.0001; ns: not significant. **B.** DAXX knockdown does not change p62 mRNA level. HeLa cells were transfected with control siRNA, DAXX siRNA, p62 siRNA and p62 siRNA +DAXX siRNA. After 48 hours, cells were subjected to RNA purification. RNAs were then subjected to reverse transcription-PCR and RT-qPCR. Three replicates were used for each RNA. Statistical analysis was performed by one-way ANOVA. Tukey's test was used for the comparison. ***: P<0.0001; ns: not significant. Data are mean ± sem in the figure. DX: DAXX

3.3 DAXX promotes p62 body formation independently of autophagy

Previously DAXX was proposed as a transcriptional repressor to negatively regulate the transcription of a set of autophagy genes and autophagy. It is possible that DAXX promotes the formation of p62 bodies by inhibiting autophagy and leads to p62 accumulation. To test this possibility, lysosome functions were inhibited and p62 body sizes were measured. **Figure 29A** shows that chloroquine treatment did not abolish the effect of DAXX on promoting p62 body formation. DAXX, however, increased GFP-p62 body sizes in both CQ treatment and non-CQ treatment conditions. Autophagy-competent WT MEFs and autophagy-defective Atg5 KO MEFs were used to test the possibility that DAXX promotes p62 body formation in autophagy-deficient conditions. As shown in **Figure 29B**,

DAXX significantly increased the sizes of p62 bodies in both WT MEFs and Atg5 KO MEFs, suggesting that the effect of DAXX on p62 sizes appeared independent of autophagy.

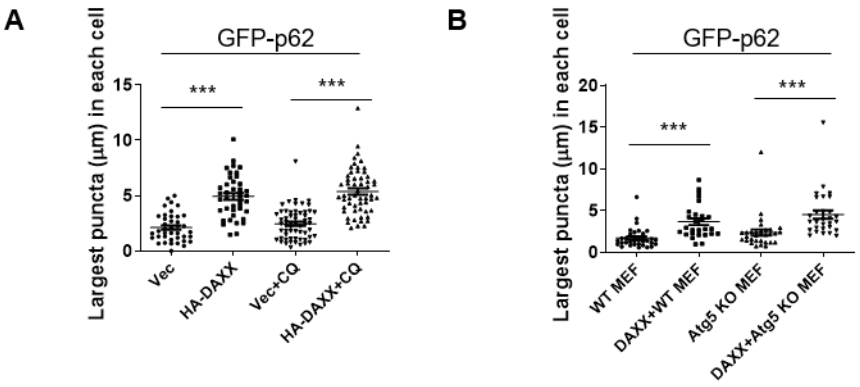

Figure 29: DAXX promotes GFP-p62 body sizes in autophagy-deficient conditions.

A. DAXX promotes GFP-p62 body size in the chloroquine treatment condition. GFP-p62/vector or GFP-p62/HA-DAXX was co-transfected into HeLa cells. 3 hours after transfection, cells were treated with or without 20 μM Chloroquine (CQ). After 20 hours, cells were fixed and images were acquired with Leica confocal microscopy. The size (diameter) of the largest p62 puncta (μm) in each cell was measured with LAS AF Lite. Statistical analyses were performed by T-tests. ***: P<0.0001. **B.** DAXX promotes GFP-p62 body size in ATG5 knockout cells. GFP-p62 was transfected into WT and ATG5 KO MEFs with vector or Myc-DAXX. After 20 hours, cells were fixed and stained with Myc antibody. Images were acquired with Leica confocal microscopy. The size (diameter) of the largest p62 puncta (μm) in each cell was measured with LAS AF Lite. Statistical analyses were performed by T-tests. ***: P<0.0001 (left); ***: P=0.0008 (right).

Previous results of p62 stably expressing HeLa cells showed that DAXX modulated p62 body formation independently of variation in p62 transfection efficiency. As autophagy is regulated by the Atg family, ablation of ATG gene expression can disrupt autophagy. To further establish the irrelevance of autophagy in DAXX regulation of p62 body formation, a set of autophagy machinery genes including Atg5, Atg10 and Atg16L1 were knocked down in p62 stably expressing HeLa cells which were then transfected with mCherry-vector,

mCherry-DAXX and mCherry-DAXX-histone binding domain (mCherry-DAXX-HBD). The results showed that the knockdown of these autophagy machinery genes did not affect the effect of DAXX on the formation of p62 bodies (**Figure 30**). Consistently with previous results (**Figure 19**), DAXX-HBD gave a positive effect on p62 body formation when autophagy machinery genes were knocked down.

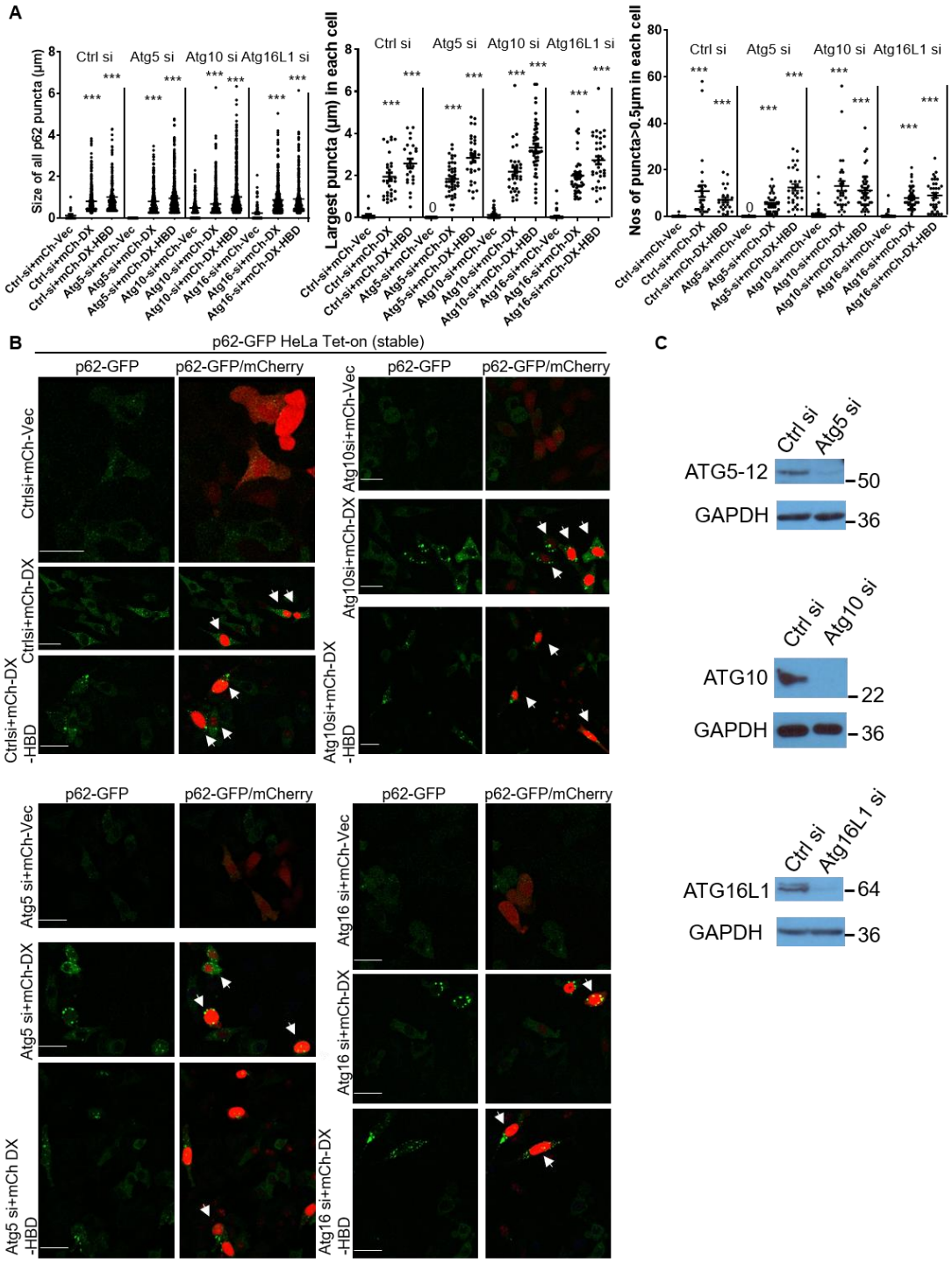

Figure 30: DAXX promotes p62 body sizes in autophagy knockdown cells.

A, B. Control siRNA, Atg5 siRNA, Atg10 siRNA or Atg16 siRNA were transfected into p62 stably expressing HeLa cells for 48 hours. Cells were then split again and transfected with mCherry vector, mCherry-DAXX or mCherry-DAXX-HBD (178-417aa). 3 hours after transfection, doxycycline was added into the medium. After 20 hours, cells were fixed. Images were acquired with Leica confocal microscopy. The size (diameter) of all p62-GFP puncta (μm) in each cell, the size (diameter) of largest p62-GFP puncta (μm) in each cell and the number of p62-GFP puncta > 0.5 μm in each cell were measured with ImageJ. Bar: 20 μm. Statistical analysis was performed by one-way ANOVA. Tukey's test was used for the comparison. Data are shown as mean ± sem.

The arrow shows p62-GFP puncta. **C.** Immunoblots show Atg5 siRNA, Atg10 siRNA and Atg16 siRNA knockdown efficiency.

Figure 31 confirmed the knocked down efficiency of Atg5, Atg10 and Atg16L1, and LC3-II levels were reduced while p62 levels were increased, suggesting that the autophagy flux was blocked successfully. Together, these data indicate that DAXX increases the formation of p62 bodies independently of autophagy.

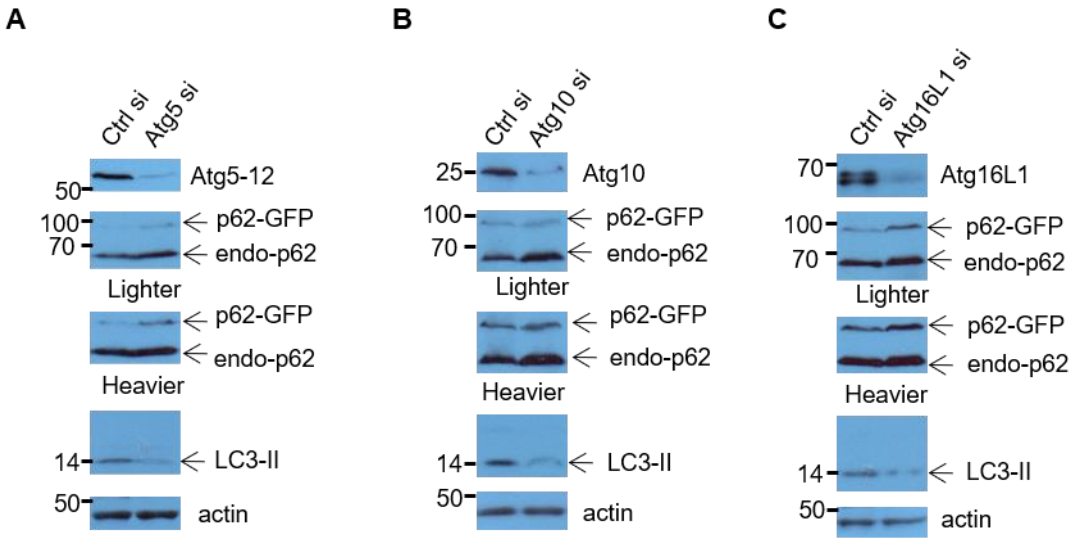

Figure 31: ATG machinery gene knockdown reduces LC3-II levels and increases p62 levels in HeLa cells.

Control siRNA, Atg5 siRNA, Atg10 siRNA or Atg16 siRNA were transfected into p62-GFP stably expressing HeLa cells for 24 hours. Doxycycline was added into the medium. After 24 hours, cells were harvested and immunoblot with Atg5 (**A**), Atg10 (**B**) or Atg16 (**C**) antibody to confirm knockdown efficiency. LC3, p62 and β-actin antibodies were used for immunoblot.

3.4 DAXX drives p62 phase condensation

Previous work found that DAXX interacted with p62 and confirmed that this interaction promoted the formation of p62 bodies. p62 bodies can dynamically exchange materials with surroundings, and DAXX could play a role in this process.

Fluorescence Recovery After Photobleaching (FRAP) assay shows exchanges of molecules between droplets and the surrounding solution, and the fluorescence recovery rate indicates the motile ability of the droplet.

First, the performance of FRAP was pretested on Leica Dmi8 confocal microscopy. **Figure 32** confirmed that GFP-p62 fluorescence in HeLa cells could achieve recovery and reach 80% of the initial fluorescence intensity in 5 minutes after photobleaching.

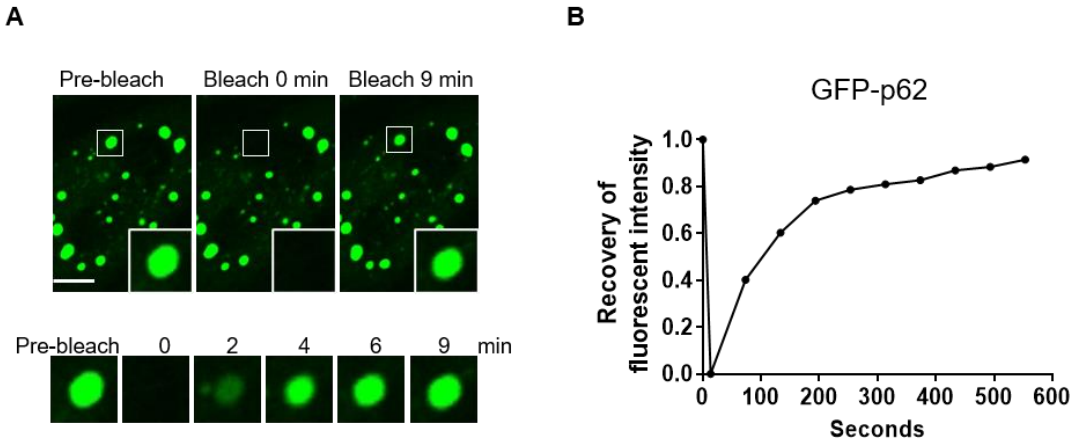

Figure 32: Confirmation of GFP-p62 undergoing fluorescence recovery after photobleaching (FRAP).

Hela cells were plated in a glass-bottom 96-well plate overnight and then transfected with GFP-p62. After 20 hours, cells were subjected to FRAP (see methods for more details) with Leica Confocal Microscopy. The boxed punctum was subjected to photobleaching. **A.** The images of pre-bleaching, bleaching and post-bleaching are shown. Bar: 10 μm. **B.** Relative fluorescence intensity of GFP-p62 at the bleaching time course.

Following experiments were performed on HeLa cells and autophagy-deficient MEFs. Given that DAXX promotes p62 body formation, it is worth testing if DAXX drove p62 body phase condensation. As shown in **Figure 33A**, in the presence of DAXX, the fluorescence intensity of GFP-p62 recovered more slowly after photobleaching than that in the absence of DAXX, suggesting that DAXX could

induce p62 bodies to condensed structures. Another important factor to consider is whether the effect of DAXX on p62 phase condensation is dependent on autophagy. **Figure 33B, C** shows that in both WT MEFs and Atg7KO MEFs, DAXX significantly reduced the fluorescence recovery levels after photobleaching, indicating that the role of DAXX in p62 condensate formation is independent of autophagy.

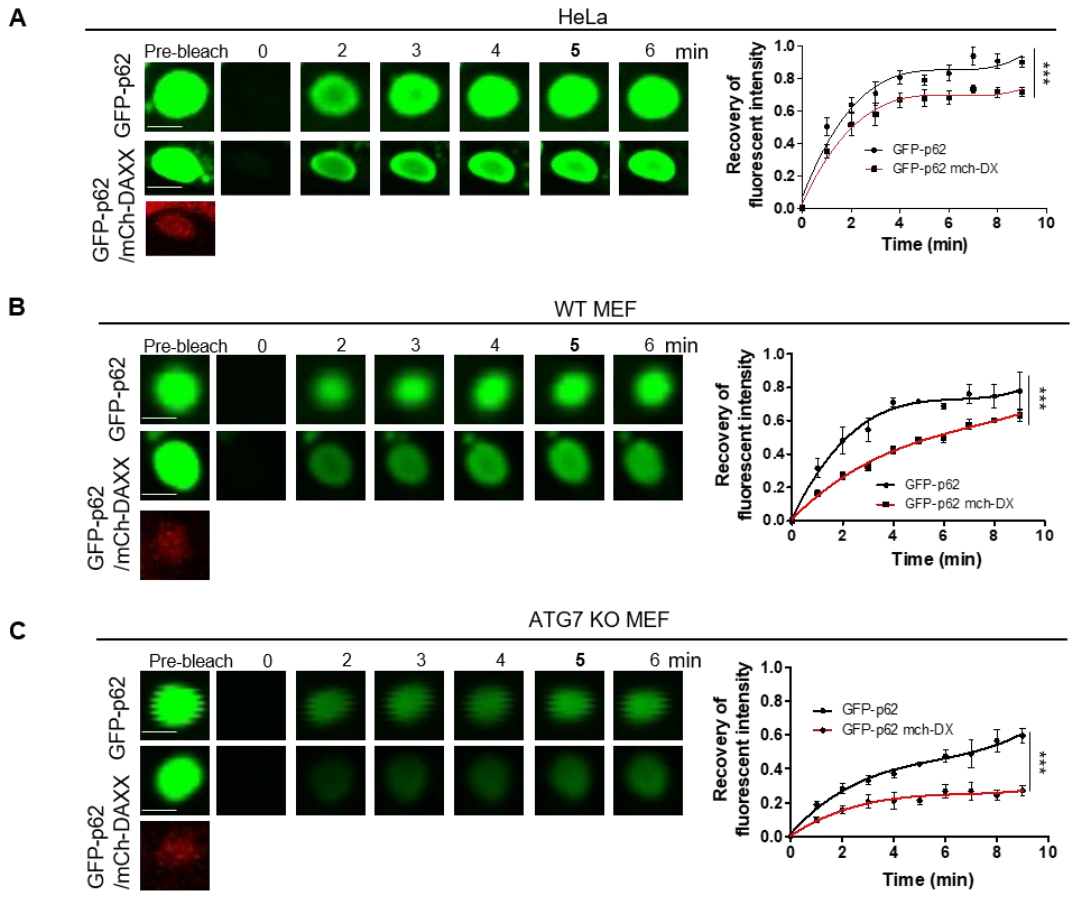

Figure 33: DAXX-induced p62 phase condensation has a lower fluorescence recovery rate.

HeLa (**A**), WT MEFs (**B**) and ATG7 knockdown (KO) MEFs (**C**) were plated in a glass-bottom 96-well plate overnight and then transfected with GFP-p62 or GFP-p62/mCherry-DAXX. After 24 hours, cells were subjected to live imaging and FRAP with Leica Confocal Microscopy. n=6 for each group. Data were plotted and analysed with Graphpad Prism V5 using nonlinear regression (curve fit). Statistical analysis was performed by two-way ANOVA. Tukey's test was used for the comparison. Data are shown as mean ± sem. ***P < 0.0001. Bar: 2 μm. mCh: mCherry. DX: DAXX.

Proteinase K treatment is often used to examine the density of protein aggregates/bodies because highly dense protein bodies resist the breakdown of proteinase K digestion. **Figure 34A** shows that the sizes of proteinase K-treated GFP-p62 bodies in the presence of DAXX were significantly larger than those in the absence of DAXX.

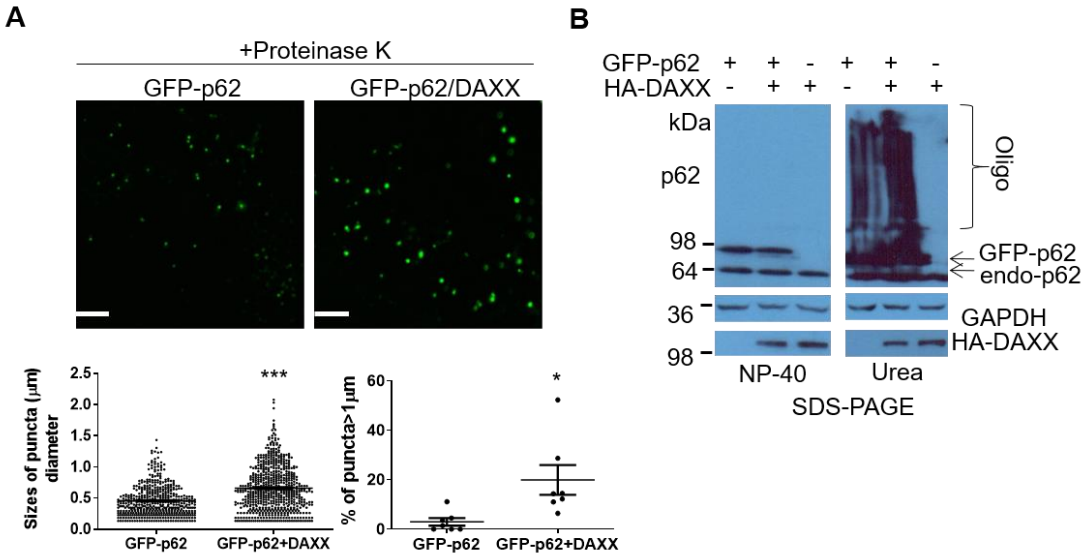

Figure 34: DAXX-induced p62 phase condensation is resistant to proteinase K digestion.

A. HeLa cells were transfected with GFP-p62/vector or GFP-p62/mCherry-DAXX. After 20 hours, cells were treated with proteinase K (50 μg/ml) at 37℃ for 30 minutes. Images were acquired with Leica im8 Microscopy. The size (diameter) of all puncta (μm) and the percentage of GFP-p62 puncta > 1 μm were measured with ImageJ. Data are shown as mean ± sem. Statistical analysis was performed by T-test. **B.** Oligomerised p62 induced by DAXX is urea-soluble. Hela cells were transfected with GFP-p62/vector, GFP-p62/HA-DAXX or HA-DAXX/vector. After 20 hours, cells were extracted in Buffer A with NP-40. The supernatants and the pellets dissolved with Buffer A containing 8M urea were subjected to SDS-PAGE and probed with p62 and other antibodies as indicated. Oligo: oligomers

Given that oligomerised/aggregated proteins could be soluble in 8M urea-containing buffers [331], the solubility of GFP-p62 with or without DAXX should be tested. **Figure 34B** showed that most p62 oligomers and DAXX-induced p62

oligomers were Nonidet P-40 (NP-40) insoluble but were soluble in 8M urea buffer, and DAXX could induce p62 oligomerisation.

Based on these findings, it appears that DAXX drives p62 phase condensation.

3.5 DAXX promotes p62 phase separation *in vitro*

In vitro studies are vital to consolidate that DAXX indeed promotes phase separation. To this end, recombinant p62 and DAXX proteins from BL21 Competent *E. coli* were purified (**Figure 35A**), and *in vitro* experiment were done to examine if DAXX could promote p62 droplet formation. Differential interference contrast (DIC) images showed that p62 proteins just had a few droplets in phase separation buffer, while there were a lot more droplets formed with the presence of DAXX. However, neither DAXX alone nor buffer-only produced any visible droplets. Considering that p62 alone only exhibits a low phase separation level [148, 172], **Figure 35B** indicated that p62 droplets formed markedly because of the existence of DAXX.

Interestingly, *in vitro*-formed p62 droplets exhibited the fusion characteristic, and this confirmed that these droplets had liquid-like properties (**Figure 36A**). To consolidate the result that DAXX could drive p62 phase separation, phase separation assays of different concentrations of DAXX were performed. The result indicated that the number of p62 droplets increased when increasing the amount of DAXX added (**Figure 36B**). This showed that DAXX is critical to drive p62 droplets formation.

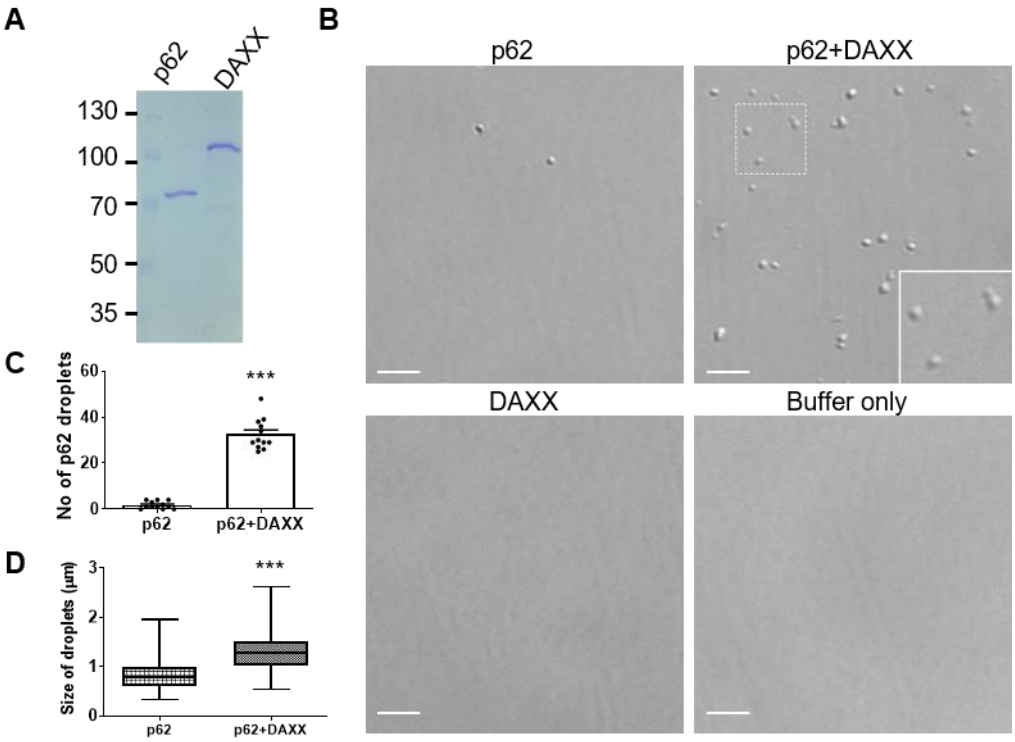

Figure 35: DAXX promotes p62 phase separation *in vitro*.

A. The purified bacteria-expressed p62 and DAXX. **B.** p62 forms more and bigger droplets with DAXX. The stocking concentration of purified p62 and DAXX were 10 μM. The mixture of 5 μl p62, p62 and DAXX, DAXX were subjected to *in vitro* phase separation at the final concentration of 5 μM in 0.2 mL microcentrifuge tube for 1 h before transferring to glass slides. Buffer only was used as a control. DIC images were acquired with Leica im8 Microscopy. The number of p62 droplets (**C**) and the size (diameter) of p62 droplets (μm) (**D**) in each image (40 μm x 40 μm) were measured with LAS AF Lite. n=12 images were used for each condition. Statistical analysis was performed with unpaired/two-tailed T-tests. Data are shown as mean ± sem. ***P < 0.0001. Bar: 5 μm; Bar (inset): 2 μm. Centre line: the median; whiskers: the minimum to maximum; box: the first to the third quartile.

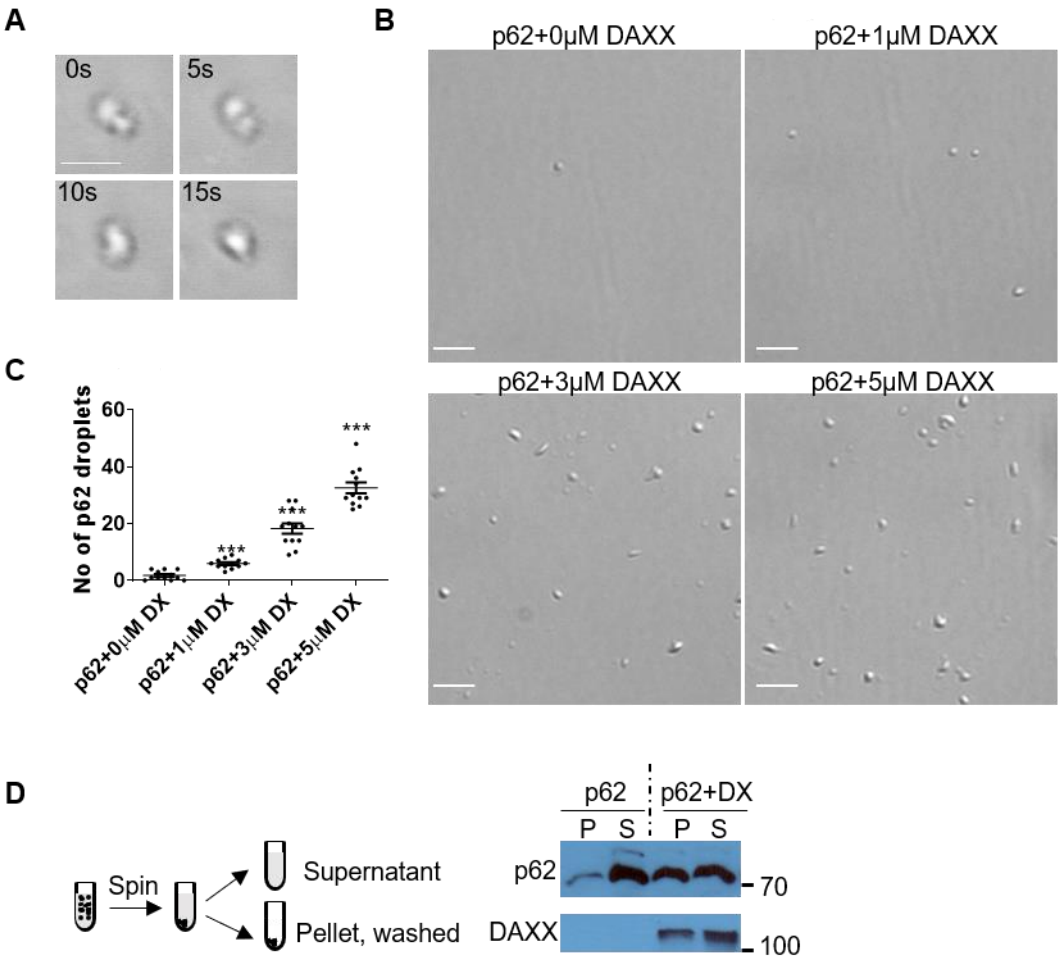

Figure 36: *In vitro* assays on p62 droplets.

A. p62 droplets undergo fusion. p62 fusion experiment was carried out in a well of a 384-well optical-bottom plate for 30 minutes at room temperature. The time-lapse DIC images were acquired with Leica confocal microscopy. Scale bar: 4 μm. **B.** The amount of DAXX affects p62 droplet formation. Purified p62 and DAXX stocking concentration were 10 μM. Different concentrations of DAXX and p62 were subjected to *in vitro* phase separation in 0.2 mL microcentrifuge tube for 1 h. DIC images were acquired with Leica DMi8 microscopy. Bar: 5 μm. **C.** The number of p62 droplets in each image (40 μm x 40 μm) were measured with LAS AF Lite. n=12 images were used for each condition. Statistical analysis was performed by one-way ANOVA (Tukey's test). Data are shown as mean ± sem. ***P < 0.0001. **D.** p62 sedimentation assay. A mixture of p62 (15 μl, 10 μM) and DAXX (15 μl, 10 μM), or p62 (15 μl, 10 μM) and buffer (15 μl) were subjected to *in vitro* sedimentation assay at room temperature for 1 h, followed by centrifugation at 16000 x *g* for 15 minutes. The pellet and the supernatant were separated. The pellet was washed once with the buffer and resuspended in 30 μl buffer. The pellet and the supernatant were subjected to immunoblot with p62 antibody and DAXX antibody. P: pellet. S: supernatant.

The sedimentation assay that separates droplets from phase separation buffer was then performed, and each fraction was immunoblotted with corresponding antibodies to test the levels of p62 and DAXX. **Figure 36C** shows that p62 exists in both pellet and supernatant, and with the existence of DAXX, p62 had a higher level in pellet, compared with p62 only condition. These data show that DAXX plays a vital role and directly promotes p62 phase separation. And this *in vitro* experiment would have the additional benefit to indicate DAXX's influence on p62 oligomerisation.

3.6 DAXX promotes p62 oligomerisation

3.6.1 p62 has more oligomers in the presence of DAXX

Individual p62 interacts with each other to form oligomers, and oligomerisation of p62 promotes its selective activity and efficiency in selective autophagy [76]. Given that DAXX promotes p62 phase separation independently of p62 transcription, further experiment were designed to test if DAXX promotes p62 oligomerisation. Immunoprecipitation of p62-HA and p62-Flag confirmed that p62-HA was pulled down by p62-Flag. Interestingly, this pulled-down capacity was increased in the presence of DAXX, suggesting that DAXX could promote p62 affinity and thus oligomerisation (**Figure 37A)**. Native gel electrophoresis, a widely used approach for protein oligomerisation assay [332], was then performed in the absence or presence of DAXX. **Figure 37B** indicated that when expressed together with DAXX, p62 could form more oligomers as well as breakdown products in HeLa cells. This suggests that DAXX-induced oligomeric p62 tends to be broken down, and it could have a critical role in autophagy. SDS-PAGE result consolidated this finding and confirmed that when transfected with

Flag-DAXX, p62-HA harboured more oligomers and breakdown products than transfected with vector (**Figure 37C**).

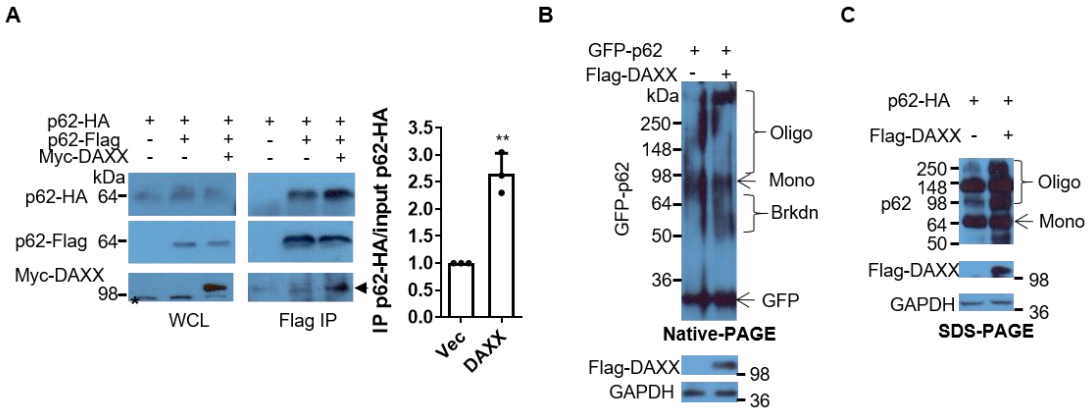

Figure 37: p62 has more oligomers and breakdown products in the presence of DAXX.

A. More p62-HA was pulled down in the presence of DAXX. p62-HA/vector, p62-HA/p62-Flag/vector and p62-HA/p62-Flag/Myc-DAXX were co-transfected into Hela cells. After 20 hours, cells were lysed and then immunoprecipitated with anti-Flag agarose beads. The whole cell lysates (WCL) and the immunoprecipitates were probed with HA antibody and Flag antibody. * denotes non-specific bands. The arrow marks Myc-DAXX. Statistical analysis was performed with unpaired two-tailed T-tests. Data are shown as mean ± sd. n = 3 independent experiments. **: P = 0.0083. **B.** p62 forms more oligomers and breakdown products in the presence of DAXX (Native-PAGE). GFP-p62/vector and GFP-p62/Flag-DAXX were co-transfected into HeLa cells. After 20 hours, cells were lysed and subjected to native PAGE, and then probed with GFP antibody. An aliquot of cell lysates was subjected to SDS-PAGE and probed with Flag antibody and GAPDH antibody. Brkdn: breakdown products. Oligo: oligomers. Mono: monomers. **C.** More oligomeric p62 was formed in the presence of DAXX (SDS-PAGE). p62-HA/vector and p62-HA/Flag-DAXX were co-transfected into HeLa cells. After 20 hours, cells were lysed and subjected to SDS-PAGE and probed with p62 antibody, Flag antibody and GAPDH antibody.

To investigate the endogenous p62 oligomerisation, SDS-PAGE on WT and DAXX KO HAP1 cells were performed. **Figure 38A** showed that WT HAP1 cells did have more oligomers and breakdown products, compared with DAXX KO HAP1 cells, which did not have any visible oligomer. Next, the relationship between the effect of DAXX on p62 oligomerisation and autophagy was investigated on autophagy-deficient MEFs. SDS-PAGE on WT and ATG5 KO

MEFs confirmed that more GFP-p62 oligomers were formed when DAXX existed, suggesting the effect of DAXX on p62 oligomerisation is independent of autophagy (**Figure 38B**). Also, the *in vitro* assay indicated that DAXX 1-250aa was sufficient for p62 oligomerisation (**Figure 38C**). These data establish that DAXX induces p62 oligomerisation.

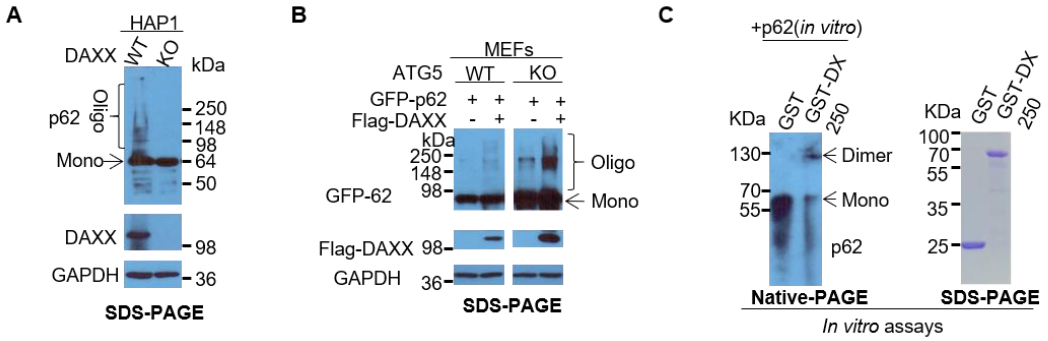

Figure 38: DAXX promotes p62 oligomerisation

A. Endogenous p62 oligomerisation in HAP1 cells. HAP1 WT and DAXX KO cells were lysed and subjected to SDS-PAGE then probed with p62, DAXX and GAPDH antibodies. **B.** DAXX induces p62 oligomerisation in both autophagy competent and autophagy-deficient MEFs. GFP-p62/vector and GFP-p62/Flag-DAXX were transfected into Atg5 WT and KO MEFs. After 20 hours, cells were lysed and subjected to SDS-PAGE, and then probed with GFP, Flag and GAPDH antibodies. **C.** DAXX 1-250aa is sufficient to induce p62 oligomerisation. *In vitro*-translated p62 was incubated with recombinant GST or GST-DAXX 1-250aa. The mixtures were subjected to native PAGE and probed with p62 antibody. An aliquot of GST or GST-DAXX 1-250aa were subjected to SDS-PAGE. DX: DAXX. Mono: monomers.

3.6.2 DAXX determines p62 oligomerisation independently of the PB1 domain

The PB1 domain (1-120aa) is known as a critical domain for p62 oligomerisation [75]. However, from our previous results, the region of p62 binds to DAXX is at its 246-300aa, not the PB1 domain. To further investigate that DAXX determines p62 oligomerisation, PB1-deleted GFP-p62 (GFP-p62ΔPB1), which is not competent for p62 self-oligomerisation, was generated and tested for its

oligomerisation. **Figure 39** showed that when co-expressed with DAXX, GFP-p62ΔPB1 formed bigger puncta-like structures and the percentage of cells having bigger puncta was increased markedly in HeLa cells. This effect appeared enhanced when puromycin treatment was performed in the cells.

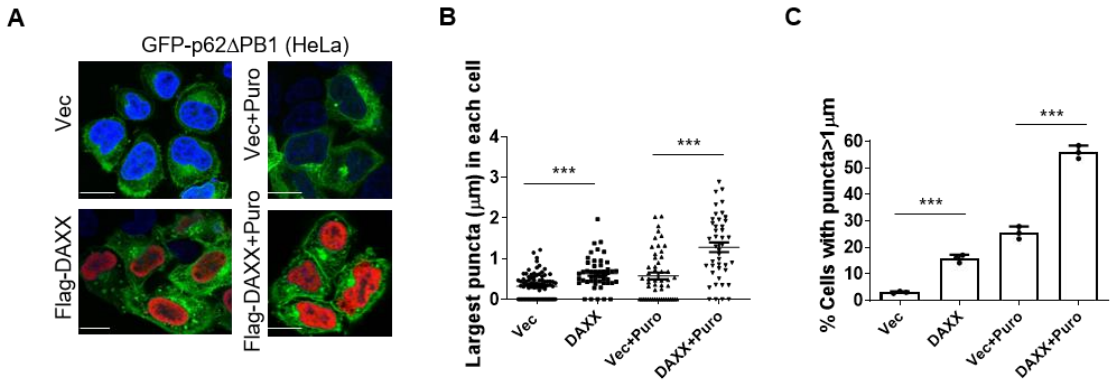

Figure 39: DAXX promotes p62ΔPB1 puncta formation.

GFP-p62 with 1-120aa deletion (GFP-p62ΔPB1) was co-transfected with vector or Flag-DAXX into HeLa cells. After 20 hours, cells were treated without or with 10 μg/ml puromycin for 5 h. Cells were fixed and stained with Flag antibody. **A.** Images were acquired with Leica confocal microscopy. Bar: 10 μm. **B.** The size (diameter) of the largest GFP-p62ΔPB1 puncta (μm) in each cell was measured with LAS AF Lite. n = 88 (Vec), 49 (DAXX), 51 (Vec + Puro), 43 cells (DAXX+ Puro). Statistical analysis was performed with unpaired two-tailed T-tests. Data are shown as mean ± sem. ***: P < 0.0001. **C.** The percentage of cells with puncta > 1 μm was measured with LAS AF Lite. n = 3 independently repeats for each group. Statistical analysis was performed with unpaired two-tailed T-tests. Data are shown as mean ± sem. ***: P = 0.0001.

To exclude the potential effect that endogenous p62 could bring to DAXX-induced GFP-p62ΔPB1 puncta formation, p62 knockout cells were utilised in the following experiment. A p62 PB1 domain-inactivated mutant, GFP-p62 K7A D69A, was used to confirm that DAXX could promote p62 puncta formation independently of the PB1 domain. In p62 KO MEFs, GFP-p62 K7A D69A was diffused in the cytoplasm, rather than formed puncta, confirming that PB1 domain inactivation leads to the failure in puncta formation and excluding the effect that endogenous p62 could bring to the results (**Figure 40**). And as expected, DAXX promoted

both GFP-p62 K7A D69A puncta and WT p62 puncta formation in p62 KO MEFs significantly, independently of endogenous p62. Interestingly, DAXX-induced GFP-p62 K7A D69A puncta were markedly smaller than DAXX-induced GFP-p62 puncta, indicating that the PB1 domain is important to p62 body formation.

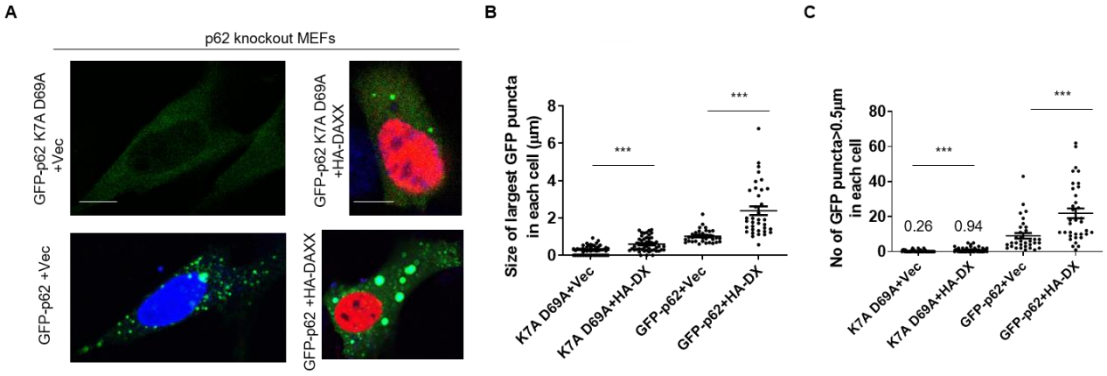

Figure 40: DAXX promotes p62 K7A D69A puncta formation in p62 knockout cells.

GFP-p62 K7A D69A/vector or GFP-p62 K7A D69A/HA-DAXX, and in parallel, GFP-p62/vector or GFP-p62/HA-DAXX, were co-transfected into p62 knockout MEFs. After 20 hours, cells were fixed and stained with HA antibody. **A.** Images were acquired with Leica confocal microscopy. Bar: 10 μm. The size (diameter) of the largest GFP-p62 puncta (μm) in each cell (**B**) and the number of GFP puncta > 0.5 μm in each cell (**C**) were measured with ImageJ. The numbers (0.26 and 0.94) represent the mean value of each column. n=53, 50, 34, 36 cells. Statistical analyses were performed by T-tests. ***: P<0.0001 (**B**); ***: P=0.0002, ***: P=0.0009 (**C**). Data are shown as mean ± sem. DX: DAXX.

Then, a native gel-electrophoresis of GFP-p62ΔPB1 with or without DAXX was performed, and the result confirmed that DAXX-induced GFP-p62ΔPB1 oligomerisation (**Figure 41A**). In SDS-PAGE, GFP-p62ΔPB1 formed oligomers when overexpressed with DAXX, but no oligomers were formed without DAXX (**Figure 41B**). Therefore, it appears that DAXX could be a factor that determines p62 oligomerisation.

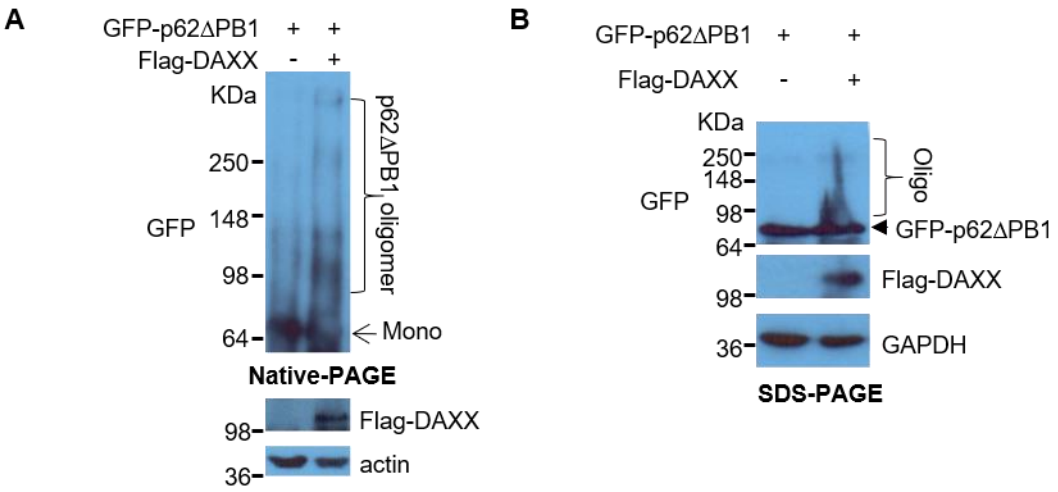

Figure 41: DAXX induces GFP-p62ΔPB1 oligomerisation.

A. DAXX induces GFP-p62ΔPB1 oligomerisation (Native-PAGE). GFP-p62 with 1-120aa deletion (GFP-p62ΔPB1) was co-transfected with vector or Flag-DAXX into HeLa cells. After 20 hours, cells were lysed and subjected to Native PAGE and probed with GFP antibody. An aliquot of cell lysates was subjected to SDS-PAGE and probed with Flag antibody and actin antibody. **B.** DAXX induces GFP-p62ΔPB1 oligomerisation (SDS-PAGE). GFP-p62ΔPB1 was co-transfected with vector or Flag-DAXX into HeLa cells. After 20 hours, cells were lysed and subjected to SDS-PAGE and probed with GFP, Flag and GAPDH antibodies.

3.7 DAXX is critical for p62 to recruit ubiquitinated proteins

p62 oligomerisation is essential to its recruitment of ubiquitinated proteins [76, 333]. Further experiments investigated if the effect of DAXX on promoting p62 oligomerisation contributes to p62 recruitment of ubiquitinated proteins. **Figure 42** showed that in the presence of DAXX, both GFP-p62 and HA-ubiquitin formed bigger puncta, and the co-localisation between p62 and ubiquitin increased significantly. It is also observed that DAXX co-localised with p62 and ubiquitin.

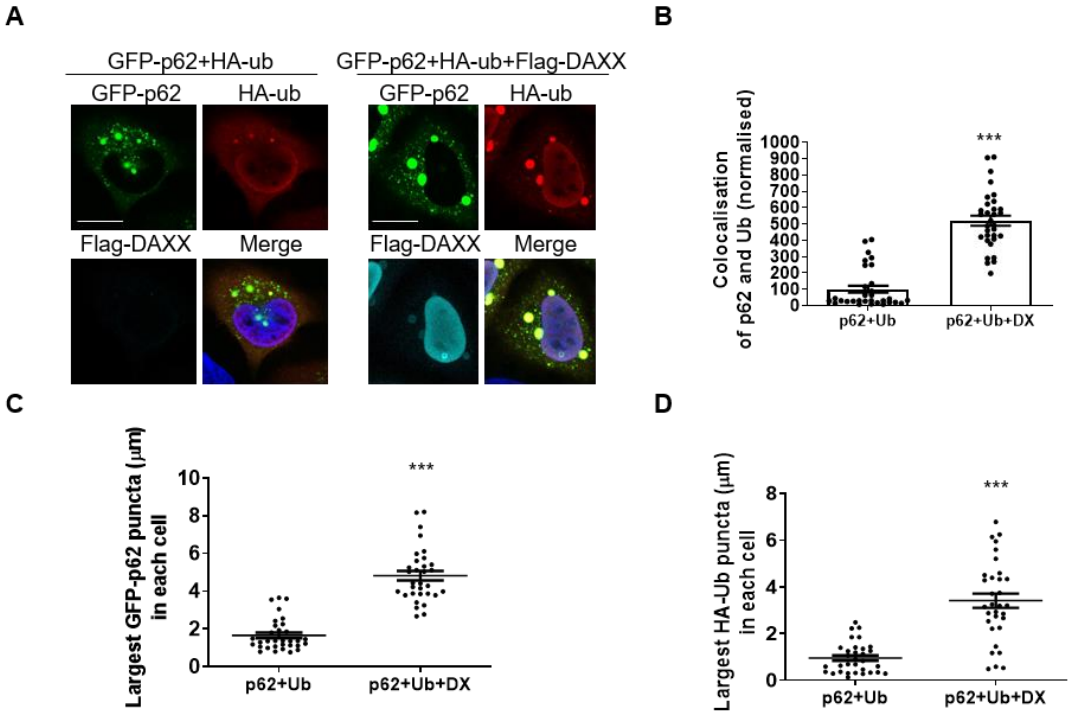

Figure 42: DAXX overexpression increases the co-localisation of p62 and ubiquitin.

GFP-p62/HA-ubiquitin were co-transfected with vector or Flag-DAXX into HeLa cells. After 20 hours, cells were fixed and stained with HA antibody and Flag antibody. **A.** Images were acquired with Leica confocal microscopy. Bar: 10 μm. **B.** The co-localisation between GFP-p62 and HA-ubiquitin was quantified by line-profile measurements of the four largest co-localised puncta in each cell with LAS AF Lite, and data were normalised with the mean of controls as 100. The size (diameter) of the largest GFP-p62 puncta (μm) (**C**) and the size of the largest HA-ubiquitin puncta (μm) (**D**) in each cell were measured with LAS AF Lite. n=32 cells. Statistical analyses were performed by T-tests. Data are shown as mean ± sem. ***: P<0.0001. ub: ubiquitin. DX: DAXX.

Endogenous staining of ubiquitin, p62 and DAXX in WT and DAXX KO HAP1 cells showed the sizes of ubiquitin-positive puncta were markedly lower in DAXX KO HAP1 cells, compared with those in WT HAP1 cells (**Figure 43**).

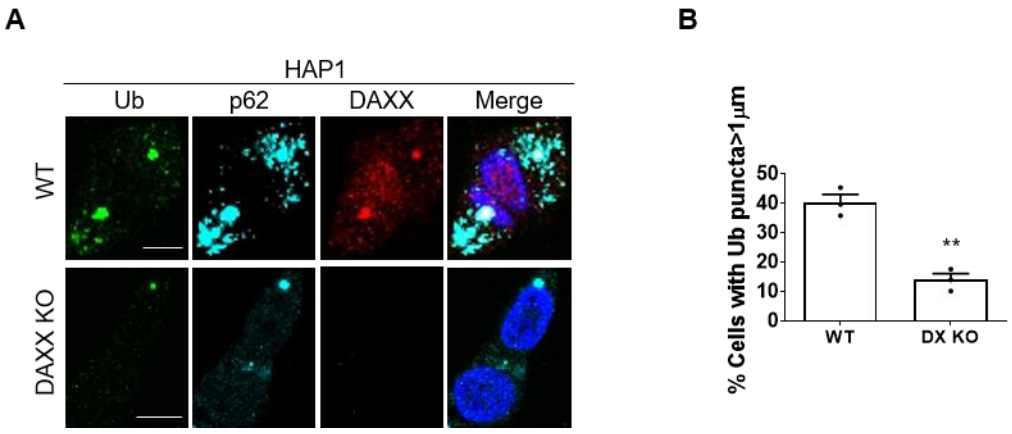

Figure 43: Endogenous ubiquitin puncta are smaller in DAXX knockout HAP1 cells.

WT and DAXX KO HAP1 cells were treated with 10 µg/ml puromycin for 5 hours. Cells were fixed and stained with ubiquitin, p62 and DAXX antibodies. **A.** Images were acquired with Leica confocal microscopy. Bar: 5 µm. **B.** The size of the largest ubiquitin puncta (µm) in each cell was measured with LAS AF Lite, and the percentage of cells with ubiquitin puncta > 1 µm was assessed. n =3 replicates. Statistical analyses were performed by T-tests. **: P=0.0093. DX: DAXX.

Similar results were received from WT and DAXX KO MEFs. In DAXX KO cells, p62 and ubiquitin had lower levels of co-localisation, and both of them formed smaller sized puncta, compared with those in WT cells (**Figure 44**).

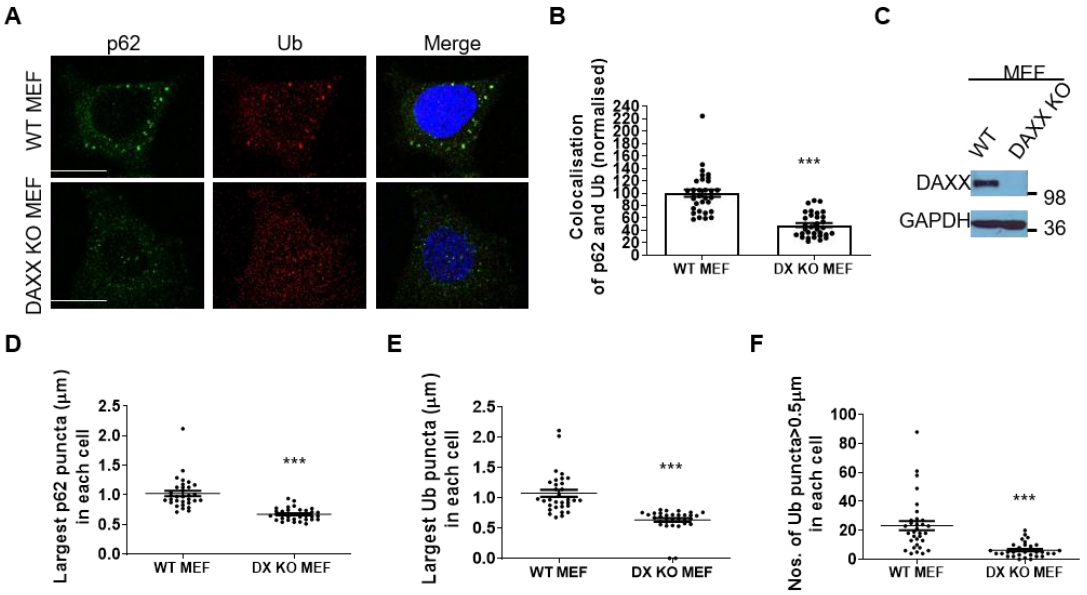

Figure 44: Endogenous p62 puncta and ubiquitin puncta are smaller in DAXX knockout MEFs.

WT and DAXX KO MEFs were fixed and stained with p62 and ubiquitin antibodies. **A.** Images were acquired with Leica confocal microscopy. Bar: 10 µm. **B.** The co-localisation between p62 and ubiquitin was quantified by line-profile measurements of the largest co-localised puncta in each cell with LAS AF Lite. Data were normalised with the mean of controls to 100. **C.** Immunoblot confirmed no DAXX expression in DAXX knockout MEFs. The diameter of the largest p62 puncta (**D**), ubiquitin puncta (**E**) and the number of ubiquitin puncta > 0.5 µm (**F**) in each cell was quantified with Image J. n=32. Statistical analysis was performed with unpaired/two-tailed T-tests. Data are shown as mean ± sem. ***: P < 0.0001. DX: DAXX. Ub: ubiquitin.

Then, the role of DAXX in ubiquitin puncta formation *in vivo* was investigated. *Drosophila* lines with wild-type (WT, W1118) and UAS-DLP (DAXX-like protein in *Drosophila*, mainly expressed in neurons in brains) shRNA (62353) were from Bloomington. These two lines were crossed with *Elav*-GAL4 driver line which is known to express in the nervous system, including neurons and glial cells, to induce control or DLP knockdown in the *Drosophila* [334, 335]. The whole brains were dissected and stained with ubiquitin antibodies. **Figure 45** showed that in DAXX/DLP knocked down brains, ubiquitin had fewer and smaller puncta than in WT brains. This suggested that DAXX could reduce p62 recruitment of ubiquitin.

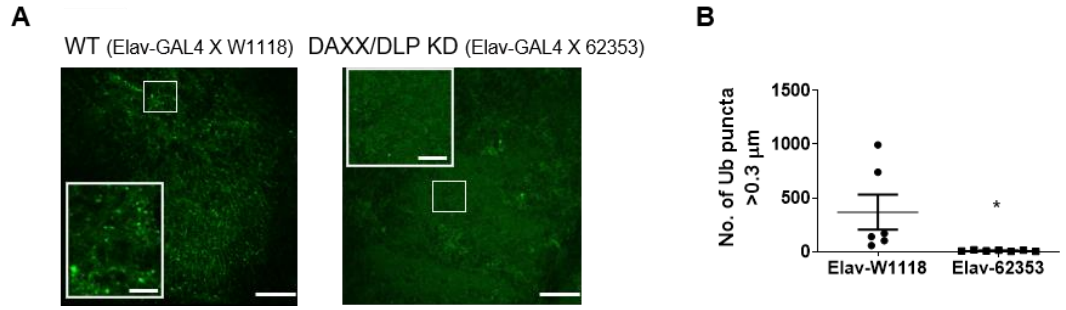

Figure 45: The sizes of ubiquitin puncta are reduced in DAXX knockdown *Drosophila* brains.

The UAS-control shRNA or UAS-DAXX shRNA *Drosophila* were crossed with *Elav*-GAL4 *Drosophila* to induce control or DAXX knockdown in the nervous system. **A.** The brains of the flies with DAXX-shRNA expression were dissected and stained with ubiquitin antibody. Bar: 20 µm; bar (insets): 5 µm. **B.** Sizes of ubiquitin puncta were quantified by ImageJ. Statistical analysis was performed with unpaired/two-tailed T-tests. n = 6 (WT), 7 (KD) biologically independent samples. Data are shown as mean ± sem. *: P = 0.0348. KD: knockdown.

Endogenous p62 and ubiquitin interactions were tested directly by immunoprecipitation in WT and DAXX KO HAP1 cells. As shown in **Figure 46A**, less ubiquitinated proteins were pulled down by p62 in DAXX KO cells, indicating that interactions between endogenous p62 and ubiquitinated proteins in DAXX KO cells were weaker than the interactions in WT cells. To consolidate this result, DAXX was knocked down in HeLa cells, and ubiquitinated proteins were pulled down by p62 immunoprecipitation. **Figure 46B** showed that less ubiquitinated proteins were pulled down when DAXX knocked down, in the absence or presence of puromycin treatment conditions. These data suggested that DAXX positively regulates p62-mediated ubiquitinated proteins recruitment.

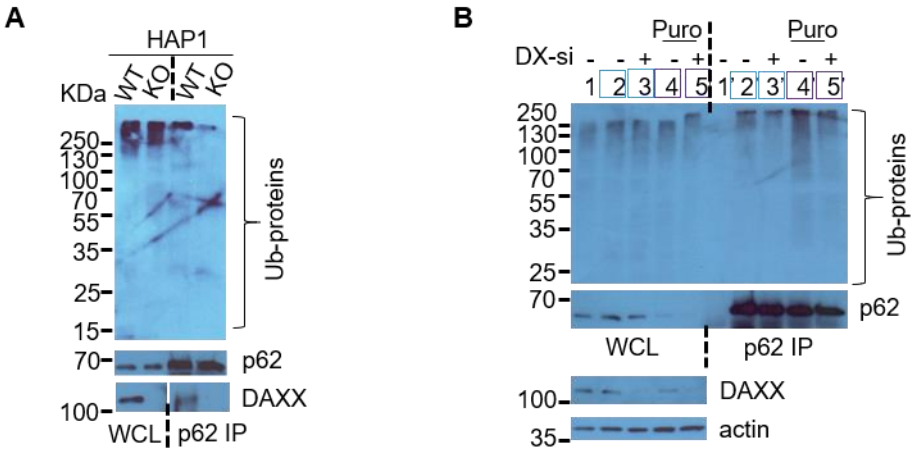

Figure 46: Less ubiquitinated proteins were pulled down in the absence of DAXX.

A. Less ubiquitinated proteins were pulled down in DAXX knockout HAP1 cells. WT and DAXX KO HAP1 cells were lysed and subjected to immunoprecipitation with p62 antibody. The whole cell lysates (WCL) and the immunoprecipitates were probed with ubiquitin, p62 and DAXX antibodies. The dot line separate the WCL and IP samples. **B.** Less ubiquitinated proteins were pulled down in DAXX knockdown HeLa cells. Control siRNA or DAXX siRNA were transfected into HeLa cells. After 48 hours, cells were treated with (lane 4, 5/lane 4', 5') or without (lane 2, 3/lane 2', 3') 10 μg/ml puromycin for 5 hours. Cells were lysed and subjected to immunoprecipitation with p62 antibody. The whole cell lysates (WCL) and the immunoprecipitates were probed with ubiquitin and p62 antibodies.

3.8 Cytoplasmic DAXX drives Nrf2-mediated stress response

Given that DAXX induced p62 oligomerisation and phase condensation, it is worth investigating the functional consequence of this effect. Increased reactive oxygen species (ROS) generation results in oxidative stress and cellular damage when it excesses the detoxification capacity of the cell [336], and p62 oligomerisation was reported to reduce ROS by recruiting Keap1 and subsequently activating Nrf2 [80, 140]. Hence, the role that DAXX plays in redox homoeostasis was tested. BFP-p62, dsRed-Keap1 and GFP-DAXX were overexpressed in HeLa cells, and it appeared that DAXX co-localised with p62

and Keap1, indicating that DAXX could contribute to the Keap1-Nrf2 pathway (**Figure 47A**). The endogenous staining also suggested that DAXX co-localised with p62 and Keap1 in HeLa cells (**Figure 47B**).

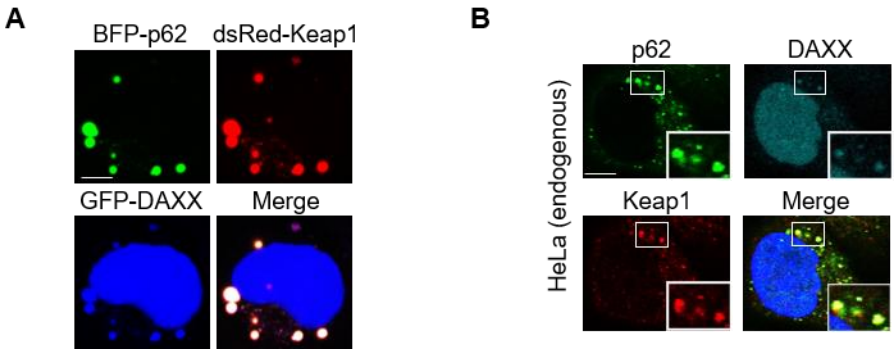

Figure 47: p62, DAXX and Keap1 co-localise in HeLa cells.

A. Overexpressed p62, DAXX and Keap1 co-localise in HeLa cells. BFP-p62, dsRed-Keap1 and GFP-DAXX were co-transfected into HeLa cells. After 20 hours, cells were fixed. Images were acquired with Leica confocal microscopy. Bar: 10 μm. **B.** Endogenous p62, DAXX and Keap1 co-localise in HeLa cells. HeLa cells were fixed and stained with p62, DAXX and Keap1 antibodies. Images were acquired with Leica confocal microscopy. Bar: 10 μm. Boxed areas are magnified at the right bottom.

In **Figure 48A**, DAXX ablation decreased not only p62 puncta formation but also p62-Keap1 co-localisation, indicating that DAXX could affect the p62-Keap1 interaction. Immunoblot also confirmed that DAXX knockdown increased the Keap1 protein level (**Figure 48B**), which could result from reduced p62 recruitment and further autophagic clearance. Indeed, less Nrf2 in nuclei was seen when DAXX or p62 was knocked down (**Figure 49A**).

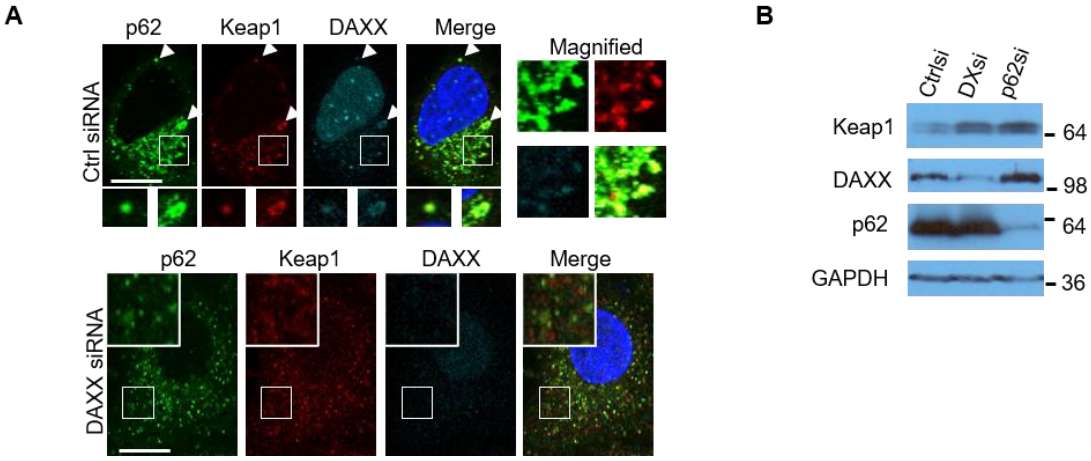

Figure 48: DAXX knockdown reduces p62-Keap1 co-localisation.

A. Control siRNA and DAXX siRNA were transfected into HeLa cells. After 48 hours, cells were fixed and stained with p62, Keap1 and DAXX antibodies. Images were acquired with Leica confocal microscopy. Arrowheads point to the condensed signals, which are magnified at bottom panels. Boxed areas are magnified at right panels or left top. Bar: 10 μm. Bar(inset): 2 μm. **B.** Control, p62 and DAXX siRNAs were transfected into HeLa cells. After 48 hours, cells were lysed and subjected to immunoblot with p62, Keap1 and DAXX antibodies.

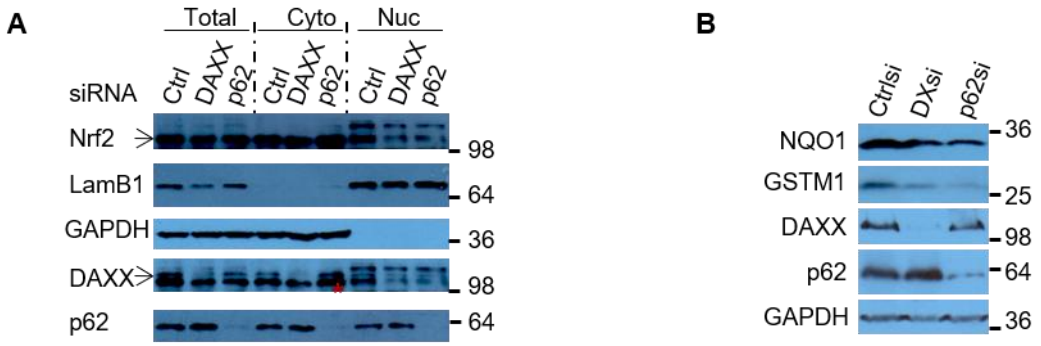

Figure 49: DAXX knockdown reduces the levels of nuclear Nrf2 and its downstream products in HeLa cells.

A. DAXX knockdown leads to reduced nuclear Nrf2 levels. Control, p62 and DAXX siRNAs were transfected into HeLa cells. After 48 hours, whole cell lysates, cytoplasmic (Cyto) and nuclear (Nuc) fractions were subjected to immunoblot with Nrf2, LaminB1, GAPDH, DAXX and p62 antibodies. The red star points to the remaining Nrf2 signals from the previous blot. LamB1: Lamin B1, nuclear marker. **B.** DAXX knockdown leads to reduced NQO1 and GSTM1 levels. Control, p62 and DAXX siRNAs were transfected into HeLa cells. After 48 hours, cells were lysed and subjected to immunoblot with NQO1, GSTM1, DAXX, p62 and GAPDH antibodies.

Transcription factor Nrf2 is found to bind to Antioxidant Response Elements (ARE) with high affinity and therefore regulate the expression of detoxifying enzymes [131]. It regulates the transcription of a series of antioxidant and detoxifying genes, such as NAD(P)H dehydrogenase quinone 1 (NQO1) and glutathione S-transferase Mu1 (GSTM1) [337]. **Figure 49B** showed that DAXX knockdown decreased NQO1 and GSTM1 protein levels, which was similar to p62 knockdown. Consistently, in DAXX knockout (KO) HAP1 cells, Nrf2 levels were reduced in nuclei (**Figure 50A**). DAXX KO also decreased the protein and mRNA levels of NQO1 and GSTM1 as downstream products of Nrf2 in HAP1 cells (**Figure 50B, C**).

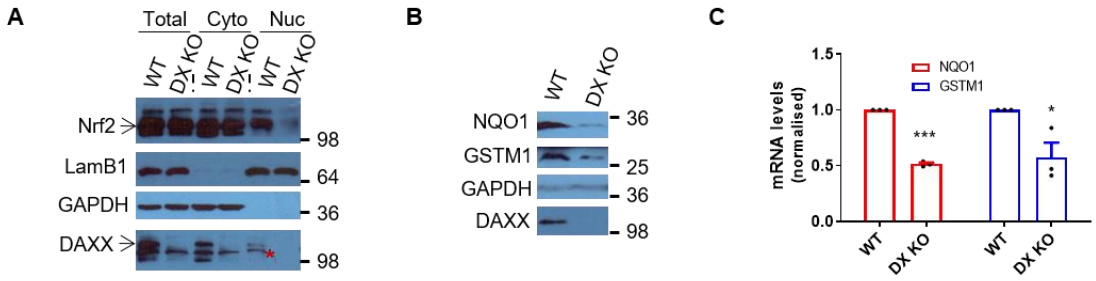

Figure 50: DAXX knockout reduces the levels of nuclear Nrf2 and its downstream products in HAP1 cells.

A. DAXX knockout leads to reduced nuclear Nrf2 levels. WT and DAXX KO HAP1 cells were lysed. Whole cell lysates, cytoplasmic (Cyto) and nuclear (Nuc) fractions were subjected to immunoblot with Nrf2, LaminB1, GAPDH and DAXX antibodies. The red star denotes the remaining Nrf2 signals from the previous blot. LamB1: Lamin B1, nuclear marker. **B.** DAXX knockout leads to reduced NQO1 and GSTM1 protein levels. WT and DAXX KO HAP1 cells were lysed and subjected to immunoblot with NQO1, GSTM1, GAPDH and DAXX antibodies. **C.** DAXX knockout leads to reduced NQO1 and GSTM1 mRNA levels. WT and DAXX KO HAP1 cells were subjected to RNA extraction and qPCR. n = 3 technical repeats. Statistical analyses were performed by T-tests. ***: P=0.0008; *: P=0.0444.

Multiple approaches have been used to measure ROS production, and among these, fluorescent probe 2', 7' dichlorodihydrofluorescein diacetate ($DCFH_2$-DA)

is widely used [338, 339]. $DCFH_2$-DA is colourless and lipophilic, and is deacetylate into $DCFH_2$ while crossing the cell membrane, followed by oxidised into DCF by ROS [340]. DCF can be detected by flow cytometry. **Figure 51** showed the gating strategy of flow cytometry, with unstained samples as the negative control, and the gates were used for the ROS assay.

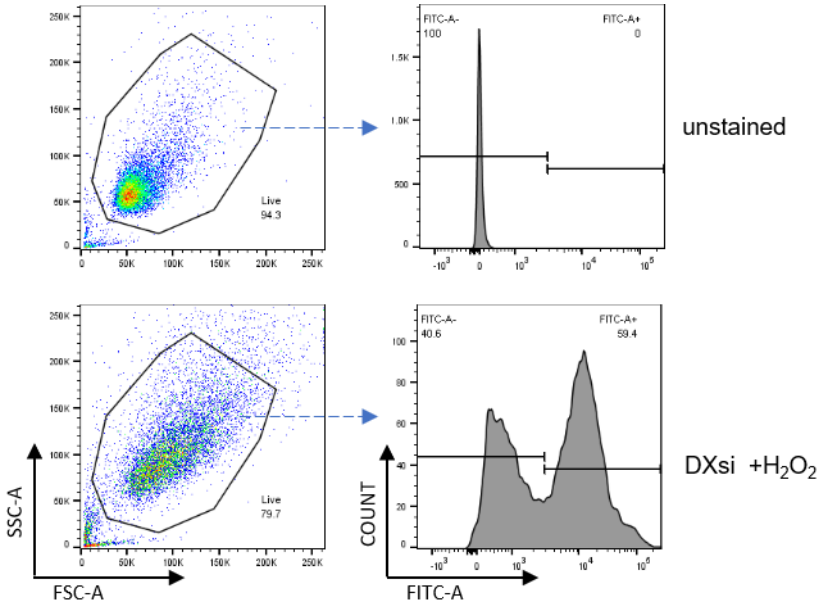

Figure 51: Gating strategy for flow cytometry.

HeLa cells were transfected with control siRNA or DAXX siRNA and treated with control or H_2O_2, then collected for H_2DCFDA (DCF) staining. Representative examples are shown. In the preliminary FSC/SSC gating, the main population was gated to exclude debris and abnormal sized cells. The main population was subjected to the ROS assay. The unstained sample was used as the negative control for DCF staining. **Figure 52** was performed with the same standard, as shown in this figure.

Figure 52A, B confirmed that both DAXX knockdown and p62 knockdown increased ROS levels in the absence and presence of H_2O_2. Of note, dual knockdown of p62 and DAXX did not increase ROS level, indicating that p62 and DAXX were in the same pathway for redox homoeostasis and the effect of DAXX was dependent on p62. Together, these experiments suggest that DAXX is a

critical factor in Nrf2-mediated detoxification by driving p62 separation/condensation.

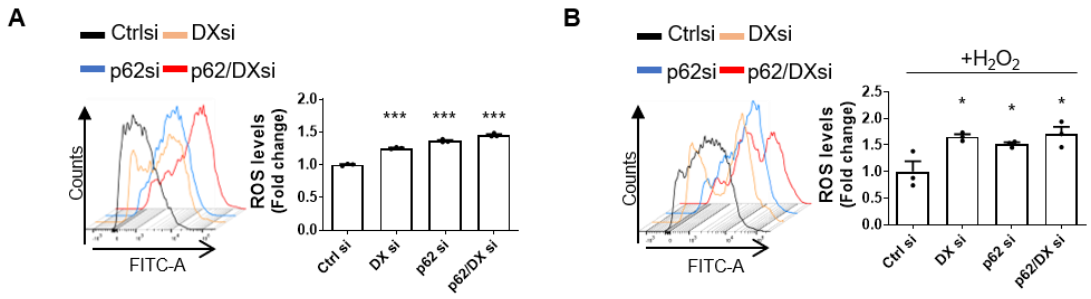

Figure 52: DAXX knockdown increases ROS levels.

HeLa cells were transfected with control, p62, DAXX and p62/DAXX siRNAs. After 48 hours, cells were treated with (**A**) or without (**B**) 300 μM H_2O_2 for 16 hours, then subjected to H_2DCFDA (DCF) staining and flow cytometry. Statistical analysis was performed by one-way ANOVA and Tukey's test. n = 3 independently treated samples. Data are shown as mean ± sem. ***: P < 0.0001; *: P < 0.05. DX: DAXX.

It is possible that the effect of DAXX on p62 recruitment of Keap1 could result in subsequent Nrf2 activation. The ARE reporters, including a Firefly luciferase gene and a constitutively-expressing *Renilla* luciferase gene, are designed for monitoring the activity of the Nrf2 antioxidant pathway. Dual-luciferase assays were performed to study the effect of DAXX on the activity of the Nrf2 pathway. The results showed that under basal conditions, DAXX or p62 knockdown caused a mild reduction in Nrf2 activity (**Figure 53A**). However, when cells were under oxidative stress by excess H_2O_2, Nrf2 activity decreased markedly in DAXX or p62 knockdown conditions (**Figure 53B**). Double knockdown of DAXX and p62 did not give a more pronounced reduction of Nrf2 activity, suggesting that the effect of DAXX on Nrf2 activity was dependent on p62.

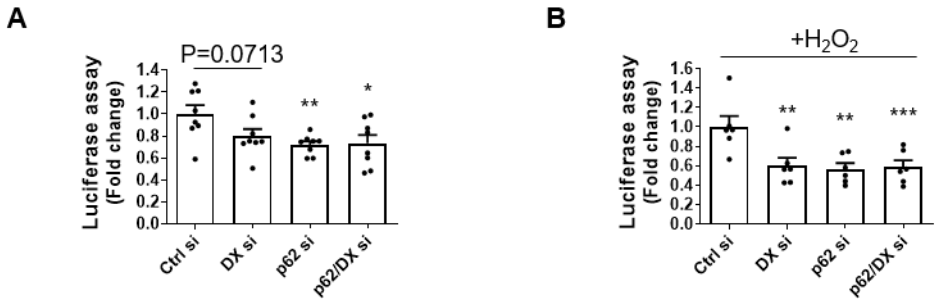

Figure 53: Nrf2 activity is reduced when DAXX knocked down.

HeLa cells were transfected with control, p62, DAXX and p62/DAXX siRNAs and subsequently transfected with luciferase reporter components. Cells were treated with (**A**) or without (**B**) 200 μM H_2O_2 for 6 hours then subjected to dual-luciferase assays. n = 8 (**A**) and n = 6 (**B**) independently plated samples. Statistical analysis was performed by one-way ANOVA and Tukey's test. Data are shown as mean ± sem. *: $P < 0.05$; **: $P < 0.01$.

To further examine the effect of DAXX on Nrf2 activity, DAXX variants were generated. Among DAXX variants, DAXX D349A mutant reduced p62 and DAXX interaction significantly (**Figure 54A**). **Figure 54B** showed that while WT DAXX increased Nrf2 activity largely, DAXX D349A mutant just gave a slight increase to Nrf2 activity, consistent with the reduced interaction of p62 and DAXX mutants. Interestingly, DAXX mutants did not have a significant effect on Nrf2 activity compared with WT DAXX in p62 knockdown cells, consolidating that the effect of DAXX on Nrf2 activity was dependent on p62.

These results established that DAXX promotes p62 phase condensation and oligomerisation, and further modulates the p62-Keap1-Nrf2 pathway.

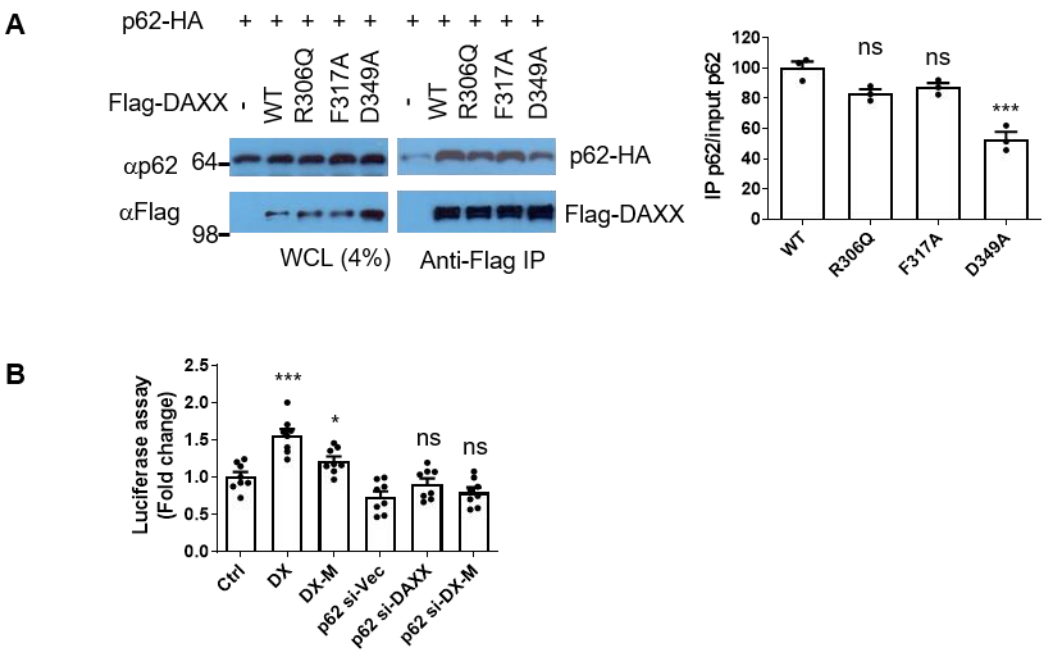

Figure 54: DAXX D349A mutant slightly increases Nrf2 activity compared with wild-type DAXX.

A. p62-HA was co-transfected with vector, Flag-DAXX, Flag-DAXX R306Q, Flag-DAXX F317A and Flag-DAXX D349A into HeLa cells. After 20 hours, cells were subjected to immunoprecipitation with Flag antibody. The whole cell lysates (WCL) and the immunoprecipitates were probed with p62 and Flag antibodies. The ratio of immunoprecipitated p62 versus input p62 was quantified. Statistical analysis was performed by one-way ANOVA and Tukey's test. n=3 independent experiments. ***: P<0.0001. ns: not significant. Data are shown as mean±sem. **B.** Vector, DAXX or DAXX D349A was co-transfected with luciferase reporters into WT or p62 knockdown HeLa cells. After 20 hours, cells were subjected to dual luciferase assay. Statistical analysis was performed by one-way ANOVA and Tukey's test. n=8 biological replicates. ***: P<0.0001; *: P<0.05; ns: not significant. DX: DAXX. M: mutant.

4 Discussion

Two modes of cargo sequestration by autophagosomal membranes are suggested: starvation-induced non-selective autophagy that a portion of cytoplasm is randomly engulfed, and selective autophagy that specific cargoes are recognised by receptors and exclusively enwrapped [33]. Selective autophagy contributes to the clearance of biomolecular condensates and the maintenance of cellular homeostasis, thereby preventing aggregation-induced disease potentially [341]. As a selective autophagy receptor, p62 recognises and interacts with ubiquitinated cargoes in a non-selective manner, and additional auxiliary proteins might be needed to cooperate with p62 to improve selective autophagy [79]. A recent study showed that p62 senses redox states in vertebrates, allowing activation of autophagy in response to oxidative stress [342].

The cell is the basic structural, biological and functional unit of organisms. It is important for cells to compartmentalise spatially and temporally to allow a variety of cellular activities to occur simultaneously. Membrane-bound organelles ensure confined spaces for efficient and specific cellular processes. Apart from membrane-bound organelles, cells harbour different types of membraneless compartments, also called biomacromolecular condensates. These condensates participate in a range of biological activities, such as initiating autophagosome formation sites and specifying autophagic degradation cargoes [157]. However, how these membraneless compartments assemble and function need to be investigated. Evidence has uncovered the fact that membraneless compartments are assembled via LLPS that regulates cellular processes by increasing local concentration and modulating the dynamics of the constituents [186]. It is

reported that p62 bodies are formed through LLPS and are degraded by selective autophagy [148, 172].

In this study, it is confirmed that DAXX facilitates p62 liquid phase separation and condensation. Initially, yeast two-hybrid screening showed that DAXX was a potential binding partner of p62. Physical interactions between p62 and DAXX were tested by immunoprecipitation and the GST pull-down assay, and DAXX co-localisation with p62 was further confirmed in several cell models and tissues. Intriguingly, all large-sized p62 puncta were DAXX positive and p62 puncta were always larger in the presence of DAXX, compared with in the absence of DAXX, suggesting that DAXX could promote p62 body size and could regulate p62 body formation. To consolidate these findings, Tet-on inducible p62-GFP-expressing stable cell line and DAXX-expressing stable cell line were generated, and experiments based on these two cell lines confirmed that p62 body sizes were largely increased in the presence of DAXX and that this effect was not affected by the potential influence of transfection efficiency. Also, DAXX knockout and knockdown models were used to confirm that p62 body formation was decreased with DAXX ablation. DAXX was reported suppressing autophagy [343]. In order to exclude any potential effect of DAXX on autophagy activity, autophagy-defective cells or cells with autophagy machinery gene knockdown were used for p62 body formation assay, which further confirmed that DAXX promoted p62 body formation independently of autophagy. Next, DAXX drove p62 phase condensation was confirmed with FRAP assays, and DAXX promoted p62 phase separation was confirmed with *in vitro* assays. *In vitro* assays also showed that DAXX was required to induce p62 oligomerisation independently of the PB1 domain. Moreover, DAXX played an essential role in p62 recruitment of

polyubiquitinated proteins. Evidence showed that p62 activated the Keap1-Nrf2 pathway, regulating the ROS-response for cytoprotection [80]. My findings suggest that DAXX promotes ROS responses via promoting p62 body formation and increasing Nrf2 nuclear translocation. Collectively, the data reveal a new mechanism for p62 phase condensation and separation and show that cytoplasmic DAXX plays a role in selective autophagy.

4.1 The challenges in LLPS and *in vitro* assays

LLPS is modulated by different factors that affect multivalent interactions, including composition, pH, chaperones, temperature and the concentration of key components [155, 157]. Also, post-translational modifications (PTMs) of proteins change the valency and strength of interactions, thus contribute to protein phase separation. p62 is subjected to different PTMs, and it is reported that phosphorylation of S403 promotes polyubiquitin chain-induced p62 phase separation and body formation [148]. To better understand p62 LLPS, it may be interesting to investigate whether PTMs of p62 can affect DAXX-induced p62 LLPS or other factors that could regulate p62 phase separation.

In selective autophagy, cargoes should be concentrated for effective engulfment of autophagosomal membranes. Here, the project proposes a mechanism that DAXX-induced p62 phase condensation modulates the Nrf2-mediated stress response.

There are great interests in uncovering the principles of LLPS. However, as in other emerging research fields, clear standards and experimental designs and methods need to be developed. Reconstituting a simplified assembly of the critical component *in vitro* and testing if the assembly is formed via LLPS are

practical steps [154]. If the critical component is essential, removal of it would suppress LLPS *in vitro*. Indeed, in our result **Figure 35B**, p62 forms a few droplets with the absence of DAXX, but significantly more droplets with the presence of DAXX, indicating DAXX has critical roles in p62 droplet formation.

Understanding the structures and material properties of the condensates will help get a better insight into them, however, approaches to reveal the mechanisms of the condensates are still in an early stage. High diffusivity of the molecules in condensates ensures the effective reactions, and FRAP assays are commonly used to capture the mobility of molecules. The compactness of LLPS shows the density of LLPS and can be tested by sedimentation under gravity or density gradient centrifugation method [186]. **Figure 36C** indeed shows that DAXX-induced p62 condensates reinforce the impact of centrifugation. Investigating the biophysical mechanisms at the molecular level is another research aspect. This can be achieved by force spectroscopy techniques, providing information to decode the mechanisms behind the formation of LLPS condensates and to understand the functional roles. The structural information can be obtained by nuclear magnetic resonance (NMR) spectroscopy [344]. Solution NMR can monitor protein motion and conformation changes and probe the dynamic of proteins. Solid-state NMR can characterise structures within fibrils that are related to phase transition and human diseases [345-347].

4.2 The potential clinical impact of DAXX-induced p62 LLPS

Misfolded proteins are constitutively generated by stresses and can be degraded by the cellular quality control mechanism. p62 is one of the best characterised autophagy cargo receptors in the recognition and clearance of protein aggregates [79]. Recent studies indicate that the assembly of p62 protein condensates is

mediated by LLPS. In this study, I elucidate that cytoplasmic DAXX drives p62 liquid phase condensation. As shown in **Figure 35B**, p62 and DAXX fail to undergo LLPS separately, but they form phase-separated condensates when mixed *in vitro*. Also, the DAXX-induced p62 condensates are spherical and can fuse with each other *in vitro* (**Figure 36A**).

Mutations in p62 have been suggested contributing to Paget's disease of bone (PDB). Among all the mutations, M404T and G411S are confirmed to inhibit p62 body formation and polyubiquitin chain-induced p62 phase separation [148]. In this project, I observed that the mutant P392L, which is identified in PDB, has less physical interaction with DAXX and affects its body formation (**Figure 12C** and **Figure 23**). To further investigate the mechanism of p62 LLPS, *in vitro* experiments on P392L may be applied. Mutation of M404 in the UBA domain, which reduces the affinity of p62 for ubiquitin, abolishes phase separation of polyubiquitinated protein-reduced p62 phase separation [148]. Interestingly, these p62 mutations are located in the UBA domain, indicating that the UBA domain is critical in p62 phase separation and may have crucial roles in p62-related diseases. Further studies can focus on this area of p62 and precise mechanisms by which mutations in the UBA domain cause diseases should be investigated.

Aberrant phase separation is associated with human diseases. Many proteins that have intrinsically disordered regions are also important drivers for diseases in cells. There are a number of devastating diseases that are associated with protein aggregation. Irreversible protein aggregation can cause diseases like ALS, AD and mad cow disease. The relationship between liquid states of the disordered proteins that are playing key roles and driving assembly of

physiological structures in cells, and how those same proteins under some conditions can form pathologies in disease should be further investigated. Just like water can go from gas to liquid to a solid state, biomolecules can also undergo these kinds of transitions. It is also known that liquid-like droplets can transit into more stable states over time and solidify into harmful aggregates due to stress, leading to diseases [152, 158]. Besides, high salt conditions have been confirmed to dissolve freshly prepared RNA-binding protein Whi3 droplets; however, aged droplets have elongated and salt-resistant properties and have a slower fluorescence recovery rate [183]. In this study, FRAP assays revealed that the mobility of DAXX-induced p62 condensates and the exchange rate of its molecules in droplets is low (**Figure 33**), which may have the potential to transit to a more solid state. Stress or pathology modulated phase separation and transition help protein condensates evade the surveillance of autophagy, which help cells adapt stresses, but also increase the accumulation of aggregates [348]. As p62 accumulation is found in several diseases, it is possible that at certain conditions DAXX-induced p62 condensates transit into a solid state which cannot be degraded by autophagy. Future work is needed in this area to reveal the link between LLPS of p62, accumulation of p62 aggregates and diseases.

The discovery that selective autophagy effectively eliminates protein droplets but not protein aggregates provides a new idea that drugs that can change aggregates to droplets may be effective in therapeutic medication for neurodegenerative diseases and other diseases caused by the accumulation of protein aggregates [167]. Drugs target LLPS in either suspending the transition into a solid-like state or transiting a solid-like state to a liquid-like state, will

hopefully be of help. The discovery in this study provides new insights into disease mechanisms as well as new frameworks for treatment.

4.3 p62 and *in vitro* assays

Recent studies revealed the widespread natural phenomenon about stress adaptation through protein phase separation, and proteins that undergo phase separation are associated with diseases. Studies in this thesis provide insights into this biological phenomena.

p62 has a role in mediating autophagic degradation of stress granules which are condensates resulting from phase separation. Based on the results that DAXX interacts with p62 and promotes phase condensation in cells, I continue to exclude the possibility that this process could be achieved by ubiquitin or other proteins *in vivo*. To prove the project hypothesis, *in vitro* studies were implemented, and the results confirmed that purified recombinant DAXX promotes p62 droplet formation.

Phase separation is a potential way to concentrate enzymes and substrates [155]. It is confirmed in several non-membrane compartments that phase separation enhances polymerisation; for example, condensed BugZ droplets enhance tubulin polymerisation, and Nephrin/Grb2 phase separation enhances actin polymerisation [203, 349, 350]. Recent studies have demonstrated the non-membrane-bound liquid character of several intracellular body structures, including p62 bodies, nucleoli and P granules. These droplet structures are formed through liquid-liquid phase separation in which biomacromolecules are organised in a dynamic manner and separate from solution with a separated liquid phase [147, 152, 351]. Like membrane-bound structures, these non-

membrane-bound assemblies play essential roles in maintaining intracellular homeostasis. While these droplets comprise hundreds of proteins, only a small portion of proteins execute their formation and condensation. It is necessary to investigate the roles of these critical proteins in the process [352].

The autophagy receptor p62 is reported undergoing liquid-liquid phase separation, which can be induced by polyubiquitin chains, and p62 droplets show a viscous liquid-like property [148, 172]. The liquid-like p62 droplets are spherical and undergo fusion, and can exchange with the surroundings. Interestingly, previous studies indicated that the induction of polyubiquitin chains in p62 phase separation requires its PB1 domain. However, this project reveals that the role of DAXX in p62 phase separation/condensation is independent of the PB1 domain. DAXX confers p62 condensates gel-like characteristic by increasing its condensation. Both previous studies and results in this study show that p62 alone undergoes basal phase separation, and this study indicates that DAXX regulates p62 oligomerisation and promotes p62 phase separation.

As phase separation is induced through multivalent macromolecular interactions of different interacting proteins, and the interactions between molecules are different, intracellular liquid phase condensates often harbour multi-layered structures [155, 350]. p62 condensates concentrate specific sets of proteins, like LC3 and ubiquitinated proteins, for selective autophagic clearance. Hence it is speculated that the phase separation of p62 is dynamically regulated to meet its multi-functions for cellular homeostasis.

Liquid-liquid phase separation appears to be a common mechanism for the generation of biomolecular condensates involved in diverse cellular processes.

For p62, it would be worth isolating p62 condensates, extract ubiquitinated cargoes and analyse the protein composition.

4.4 p62 levels and the redox state

Autophagy selectively degrades different types of cargoes, and the selectivity is largely dependent on autophagy receptors. Among autophagy receptors, p62 is well studied and is responsible for ubiquitinated protein degradation. When autophagy is disrupted, p62 is accumulated with ubiquitin-positive aggregates, a condition reminiscent to that of degenerative disorders. Besides, the accumulation of p62 induces cellular stress response that leads to diseases in liver cells [94]. p62 mRNA and protein levels increase after oxygen radical stress, suggesting an induced transcription of p62 [353].

The Keap1-Nrf2 pathway is a cellular defence mechanism against oxidative stress, regulating the reactive oxygen species (ROS)-response gene transcription, and this process is activated by p62 [80]. Nrf2 is a transcription factor that is involved in the activation of cytoprotective genes. Under normal conditions, Keap1 acts as a key regulator of Nrf2, mediating Nrf2 degradation in proteasomes; Under oxidative conditions, p62 interrupts Keap1-Nrf2 pathway by interacting with Keap1, freeing Nrf2 for its nuclear translocation and subsequent activation of its downstream gene expression. In this study, it appears that p62 knockdown reduces the level of Nrf2 in the nucleus and find that DAXX knockdown also decreases the nuclear Nrf2 level. Given that less p62 puncta are formed in the absence of DAXX, more Nrf2 remains in the cytoplasm by Keap1 binding. In this way, DAXX promotes ROS response by increasing Nrf2 nuclear localisation.

In order to confirm the effect of DAXX does not result from transcriptional alterations, mRNA levels of p62 were checked in DAXX knockdown and DAXX overexpression cells. The results showed that DAXX knockdown or overexpression did not increase p62 mRNA levels. It is also confirmed that the p62 protein levels are not affected by DAXX knockdown or overexpression.

4.5 p62 mutations and diseases

p62 is a major component in Mallory-Denk bodies (MDB) and intracellular hyaline bodies that are hallmarks of chronic liver disease and enhance hepatocellular carcinoma (HCC) risk significantly, and elevated p62 is shown in HCC progenitor cells and is known to accumulate in most chronic liver diseases that progress to HCC [354-356]. High p62 expression activates Nrf2 and mTORC1, protecting ROS-containing HCC-initiating cells from oxidative stress-induced death [357]. Nrf2, inducing the expression of antioxidant and detoxifying enzymes, is regulated by E3 ligase Keap1. Interestingly, in HCC, p62 levels are increased in hepatocytes but decreased in hepatic stellate cells (HSCs), and loss of p62 in HSCs promotes HCC development [358]. However, p62-positive inclusions accumulated in liver was reported as a major cause of liver injury, including alcoholic hepatitis and hepatocellular carcinoma, due to upregulating detoxifying enzyme [80]. p62 has the ability to shuttle between the nucleus and the cytoplasm, and is essential to accumulate polyubiquitinated proteins in promyelocytic leukaemia bodies by inhibiting of nuclear protein export [77]. It is possible that p62 turnover is dynamically regulated to meet its multi-functions for cellular homeostasis.

Mutations in p62 contribute to various diseases such as Paget's disease of bone (PDB) and amyotrophic lateral sclerosis (ALS) [359, 360]. This project reveals

that the p62 mutant, p62 P392L, which is associated with PDB, exhibited a reduced interaction with DAXX. Notably, the effect of DAXX on p62 P392L body formation was also decreased significantly.

4.6 Other methods used in this study

4.6.1 Different cell models

Experiments were initially performed on DAXX knockout HAP1 cells as they were generated at the earlier stage of the project. HAP1 is a near-haloid human cell line derived from a patient with chronic myelogenous leukaemia, with one copy of almost every chromosome and is widely used in biomedical and genetic research [361]. To complete and corroborate the data from HAP1 cells, DAXX KO MEFs were generated to confirm the results with different models. Indeed, DAXX KO MEFs gave the result that corresponds to what DAXX KO HAP1 cells had shown. Different models were used to acquire complementary and comprehensive results toward the conclusions.

The p62 stable cell line was generated previously and kept in our cell bank, so most experiments based on stable cells were carried out with it. To investigate the effect of DAXX on p62 body formation comprehensively, tet-on DAXX stable cell line was generated and used to confirm the effect of DAXX on p62 puncta formation.

Inhibition of autophagy leads to p62 accumulation in cells which can be easily observed by western blot or immunofluorescent staining. In this project, when cells were knocked down with Atg10 or Atg16L1, the overall p62-GFP exhibits bigger puncta compared with cells with control siRNA, as shown in **Figure 30**. This result suggested that the sizes of p62 puncta were modulated by autophagy.

However, an unexpected result was observed that the size of p62-GFP puncta was markedly decreased in Atg5 knockdown cells, which is indeed contradictory to the published results in Atg knockdown cells. It is possible that Atg5 has a direct role in p62 puncta formation.

4.6.2 Structure and measurement of p62 bodies

I initially found that DAXX promoted p62 puncta size and measured the size of puncta with ImageJ or LAS AF LITE. Though p62 bodies exhibited the spherical 3D shape, as previously published [148], it was technically challenging to quantify the actual volume of each p62 body accurately in our experimental settings. Therefore, diameters of p62 puncta were adopted to measure the size of p62 bodies, as used previously [105, 148, 362]. In order to reveal the most precise circumstance of p62 bodies, p62 puncta were quantified from different aspects, like the size of largest puncta in each cell, the number of puncta over a certain size in each cell and the percentage of cells with puncta over a certain size, to show the overall size extent of p62 bodies.

4.6.3 Site mutagenesis

Deletion of large regions may affect intrinsic functions of p62 or DAXX. Thus I narrowed down the region and generated p62 K7A D69A in addition to the p62 with the PB1 domain deletion. For determination of the p62-DAXX interaction, point mutants, like p62 P392L or DAXX D349A, were used to investigate the region required for p62-DAXX binding or Nrf2 activity.

Given that the PB1 domain is a ubiquitin-like domain that can non-covalently interact with the C-terminal UBA domain, the interactions between the PB1 domain and the UBA domain in different p62 molecules exist [363]. To exclude

the possibility that PB1 mutants interact with endogenous p62 through the UBA domain, the experiment with PB1 deficient mutants (p62 K7A D69A) in p62 KO MEFs was conducted for the effect of DAXX in the context.

The p62 P392L mutant that reduced the p62-DAXX interaction, formed smaller sized puncta than full-length p62, indicating that the physical interaction of p62-DAXX is required for p62 body formation. Likewise, DAXX D349A mutant, which significantly reduced the p62-DAXX interaction, had a lower effect on DAXX-induced Nrf2 transcriptional activity than WT DAXX.

4.7 UPS and autophagy activity

Autophagy and the ubiquitin-proteasome system (UPS) are two major protein degradation mechanisms for cellular homeostasis in eukaryotes. Ubiquitilation targets substrates for degradation of both pathways, and while the UPS is responsible for the degradation of short-lived protein and soluble misfolded proteins, autophagy recycles long-lived proteins, insoluble protein aggregates and damaged organelles. Although activities are not interdependent, there are interconnections and crosstalks between autophagy and the UPS, and the inhibition in the flux of either pathway affects the activity of the other system. To maintain cellular homeostasis, accumulated materials from inhibition of one of these degradation systems need to be eliminated by the other. For example, impairment of proteasome activity was observed to active autophagy as a compensatory mechanism to reduce UPS substrates [230]. The UBA domain of p62 allows its capacity to bind to ubiquitin chains, and p62 has a higher affinity for K63-linked ubiquitin for autophagic degradation, compared with K48-linked ubiquitin that is generally degraded through the UPS [78, 364]. This dual ubiquitin-binding characteristic makes p62 in the middle of autophagy and the

UPS, and might inhibit the UPS to some extent [1]. As p62 deficiency has been seen to enhance the proteasomal activity, it is possible that the effect of DAXX mediated p62 phase condensation could result from the proteasomal activity and further increase p62 puncta formation. There is no significant change in p62 levels in DAXX knockdown condition or overexpression condition, indicating that DAXX promotes p62 puncta formation independently of p62 proteasomal turnover.

4.8 DAXX

DAXX was first found as a signalling protein binding to a cell death receptor, Fas, to activate apoptosis [188]. It was then found to directly and specifically bind to one of the histone variants, H3.3, expressed in the cell cycle continuously, and to assemble H3.3-containing nucleosomes [191]. Nucleosome turnover is crucial in epigenome maintenance and the assembly of chromosomal DNA acts as a constitutive way in eukaryotic chromatin, and loss of DAXX cause embryonic lethality in early mouse development [195, 197]. Mutations in DAXX are associated with cancers and it inhibits hypoxia-induced lung cancer cell metastasis through HIF/HDAC1/slug pathway [365, 366].

When it was first discovered, DAXX was reported to induce apoptosis by initiating FADD-independent activation of the JNK pathway. However, DAXX shows an anti-apoptotic function in embryo, and its expression is vital for embryonic development; disruption of DAXX in mouse leads to early embryonic lethality [197]. During this study, I also found that while all p62 puncta co-localised with DAXX, not all DAXX puncta were positive for p62. This suggests that DAXX is required for efficient p62 phase separation, and it also plays p62-independent roles in the cytoplasm.

DAXX is also known to interact with PML bodies and co-localise with PML bodies [200]. The membraneless PML bodies are formed via phase separation and exhibit multi-layered structures [149]. These condensates may consist of hundreds of proteins, but very few of them are predicted to promote liquid droplets formation. DAXX offers p62 condensates gel-like properties by increasing its condensation. Different from recent studies that polyubiquitin chain-induced p62 phase separation requires the PB1 domain, the role of DAXX in p62 phase condensation/separation is independent of the PB1 domain. It would be intriguing to investigate if DAXX has the characteristic to promote phase separation of other proteins, and it would be worth finding out other DAXX interacting proteins. Since DAXX works as an H3.3 chaperone, it would also be worth investigating if the interaction between p62 and DAXX affects the activity of DAXX as an H3.3 chaperone.

DAXX has been suggested vital for cell survival, but its prosurvival role is not well understood. This study also offers a mechanistic insight into the prosurvival role of DAXX.

5 Conclusions and future work

5.1 Concluding remarks

The major aim of the work undertaken in this thesis was to characterise cytoplasmic DAXX as a chaperone of autophagy receptor p62 phase condensation which activates Nrf2-mediated stress response. DAXX is a known chaperone for histone H3.3 deposition in the nucleolus. This project has described a new mechanism for p62 puncta formation and phase separation, and revealed a role of DAXX in selective autophagy in the cytoplasm.

Initially, the direct interaction between p62 and DAXX is confirmed in different models and this interaction has a functional effect of p62 puncta formation. p62 puncta formation is required for its role of autophagy receptor which interacts with ubiquitinated cargoes and LC3 simultaneously, and this project confirms that this process is enhanced by DAXX. Next, by using autophagy-deficient models, this project reveals that DAXX promotes p62 puncta formation independently of autophagy. This study also provides insight into the underlying mechanisms of p62 liquid-liquid phase separation. It is also revealed that DAXX enhances p62 phase condensation, and these p62 condensates can exchange molecules with surroundings. *In vitro* constituting system firmly indicates the critical role of DAXX in p62 phase separation. The p62 droplets formed in the presence of DAXX show liquid-like properties and fusion characteristic. The implications of these findings are not limited to the identification of a p62 interacting protein DAXX; it is also observed that the p62 mutation, p62 P392L, which associated with Paget's disease of bone (PDB), has reduced interaction with DAXX. This may be a new area of study the mechanism of PDB. Further, the observation that DAXX drives

p62 phase condensation is confirmed both *in vivo* and *in vitro*. DAXX promotes p62 recruitment of Keap1 and subsequent Nrf2-mediated stress response. Besides, DAXX mutation which has a decreased interaction with p62 affects the Nrf2 transcription. Given the diverse range of diseases that autophagy has been linked with, these findings may suggest a potential implication of the p62-DAXX interaction in disease. Upon further investigation, the regulation of autophagy based on the p62-DAXX interaction may provide a potential opportunity for a novel target towards medical treatment.

Specific conclusions are as follows:

5.1.1 DAXX has a physical interaction with p62

The p62-DAXX interaction occurs in different cell models and mouse striata. The regions for the p62-DAXX interaction locate in p62 246-300aa and DAXX 182-230aa. Also, endogenous p62 and DAXX co-localise in HeLa cells, HAP1 cells and mouse striata, and the co-localisation of them is dependent on their interaction.

5.1.2 DAXX promotes the formation of p62 bodies independently of autophagy

Based on the result that p62 and DAXX have a direct interaction, I further find that sizes and numbers of p62 bodies are largely increased where DAXX is overexpressed. Experiments on Tet-on inducible p62 stably expressing cells and DAXX stably expressing cells exclude the potential effect of transcription and p62 expression. Moreover, DAXX expression does not affect p62 proteasomal turnover or mRNA expression. DAXX promotes p62 body formation in autophagy-

deficient cells or autophagy-inhibited conditions. These findings together indicate that DAXX-induced p62 body formation is independent of autophagy.

5.1.3 DAXX drives p62 phase condensation both *in vivo* and *in vitro*

FRAP assays show that DAXX induces p62 phase condensation *in vivo*, independently of autophagy, and these DAXX-induced p62 condensates are able to resist Proteinase K digestion. *In vitro* experiments give a straightforward view of the liquid-like properties of DAXX-induced p62 condensates that are sphere-like and undergo fusion. The numbers of p62 condensates increase when the amount of DAXX increases. The sedimentation assay also confirms DAXX is critical in p62 phase condensation. These *in vivo* and *in vitro* experiments have been successfully verified that DAXX drives p62 phase condensation.

5.1.4 DAXX promotes p62 oligomerisation independently of the PB1 domain

Immunoprecipitation, native gel electrophoresis and SDS-PAGE confirm that DAXX enhances p62-p62 interaction affinity and promotes p62 oligomerisation. This effect is also independent of autophagy. The PB1 domain of p62 is critical for p62 oligomerisation and polyubiquitin chain-induced p62 phase separation. DAXX markedly promotes the formation of p62ΔPB1 and p62 K7A D69A body-like structures. Native gel electrophoresis results show that DAXX induces p62ΔPB1 oligomerisation.

5.1.5 DAXX drives p62 recruitment of the Keap1-Nrf2 pathway in response to stress

The functional consequence of DAXX-induced p62 phase condensation is also examined in this study. DAXX co-localises with p62 and Keap1 in cells and promotes the p62-Keap1 co-localisation. DAXX knockdown decreases Nrf2

levels in nuclei and causes a reduction in the protein levels of Nrf2 downstream proteins, NQO1 and GSTM1, which play the antioxidant role in cellular protection. Consequently, DAXX or p62 knockdown increases the levels of cellular ROS in either the absence or the presence of H_2O_2. Dual knockdown of p62 and DAXX did not cause a further increase in ROS levels, suggesting that DAXX is critical in Nrf2-mediated detoxification via driving p62 phase condensation. The Nrf2 activity, tested by luciferase assays, is also reduced in DAXX or p62 knockdown conditions. Together, DAXX drives p62 phase condensation and regulates the Keap1-Nrf2 pathway in response to stress.

5.2 Future work

This study provides evidence for a role of cytoplasmic DAXX in p62 phase condensation, suggesting an interesting mechanism for further exploration in p62. DAXX is essential for cell survival, but the mechanism of its prosurvival function is not well understood. This study offers insight into the prosurvival role of DAXX to protect against oxidative stress.

DAXX-induced p62 phase condensation could be involved in yet more aspects of human diseases. It is yet unknown if protein components, in addition to DAXX and ubiquitinated proteins, can drive p62 phase separation, and it would be interesting to investigate if other factors could also contribute to p62 phase separation. It would be interesting to investigate the composition, assembly and physical properties of p62 droplets in order to better understand the biochemical and cellular functions of this important structure, and it is also tempting to examine negative regulators of p62 puncta formation.

6 Appendices

Publications associated with this study:

Yang, Y., Willis, T. L., Button, R. W., Strang, C. J., Fu, Y., Wen, X., Grayson, P. R. C., Evans, T., Sipthorpe, R. J., Roberts, S. L., Hu, B., Zhang, J., Lu, B., & Luo, S. (2019). Cytoplasmic DAXX drives SQSTM1/p62 phase condensation to activate Nrf2-mediated stress response. Nat Commun, 10(1), 3759. doi:10.1038/s41467-019-11671-2

Yang, Y., Valionyte, E., Kelly, J., & Luo, S. (2020). Histone H3F3/H3.3 chaperone DAXX converts to modulate SQSTM1 phase condensation for NFE2L2 activation. Autophagy, 16(1), 171-172. doi:10.1080/15548627.2019.1677323

Please note full texts have not been included due to copyright restrictions.

6.1 Appendix i: Yang *et al*., (2019) Nature Communications

Yang, Y., Willis, T. L., Button, R. W., Strang, C. J., Fu, Y., Wen, X., Grayson, P. R. C., Evans, T., Sipthorpe, R. J., Roberts, S. L., Hu, B., Zhang, J., Lu, B., & Luo, S. (2019). Cytoplasmic DAXX drives SQSTM1/p62 phase condensation to activate Nrf2-mediated stress response. Nat Commun, 10(1), 3759. doi:10.1038/s41467-019-11671-2

Autophagy cargo recognition and clearance are essential for intracellular protein quality control. SQSTM1/p62 sequesters intracellular aberrant proteins and mediates cargo delivery for their selective autophagic degradation. The formation of p62 non-membrane-bound liquid compartments is critical for its function as a cargo receptor. The regulation of p62 phase separation/condensation has yet been poorly characterised. Using an unbiased yeast two-hybrid screening and complementary approaches, we found that DAXX physically interacts with p62. Cytoplasmic DAXX promotes p62 puncta formation. We further elucidate that DAXX drives p62 liquid phase condensation by inducing p62 oligomerisation. This effect promotes p62 recruitment of Keap1 and subsequent Nrf2-mediated stress response. The present study suggests a mechanism of p62 phase condensation by a protein interaction, and indicates that DAXX regulates redox homoeostasis, providing a mechanistic insight into the prosurvival function of DAXX.

6.2 Appendix ii: Yang *et al*., (2020) Autophagy

Yang, Y., Valionyte, E., Kelly, J., & Luo, S. (2020). Histone H3F3/H3.3 chaperone DAXX converts to modulate SQSTM1 phase condensation for NFE2L2 activation. Autophagy, 16(1), 171-172. doi:10.1080/15548627.2019.1677323

Macroautophagy/autophagy cargo receptor SQSTM1/p62 puncta or clustering formation is critical for its function in cargo recognition and LC3 interaction. Evidence suggests that SQSTM1 puncta formation is a process of liquid-liquid phase separation. It is poorly understood how SQSTM1 liquid-liquid phase separation is regulated. We found that cytoplasmic DAXX enhances SQSTM1 puncta formation, and further demonstrated that DAXX drives SQSTM1 liquid phase condensation through increasing SQSTM1 oligomerisation. DAXX promotes SQSTM1 recruitment of KEAP1, subsequently activating an NFE2L2/NRF2-mediated stress response. This study suggests a new mechanism of SQSTM1 phase condensation by a protein-protein interaction, and indicates that cytoplasmic DAXX can play a role to regulate redox homeostasis

.

7 References

1. Korolchuk, V.I., et al., *Autophagy inhibition compromises degradation of ubiquitin-proteasome pathway substrates.* Mol Cell, 2009. **33**(4): p. 517-27.
2. Rock, K.L., et al., *Inhibitors of the proteasome block the degradation of most cell proteins and the generation of peptides presented on MHC class I molecules.* Cell, 1994. **78**(5): p. 761-71.
3. Kocaturk, N.M. and D. Gozuacik, *Crosstalk Between Mammalian Autophagy and the Ubiquitin-Proteasome System.* Front Cell Dev Biol, 2018. **6**: p. 128.
4. Zhao, J., et al., *mTOR inhibition activates overall protein degradation by the ubiquitin proteasome system as well as by autophagy.* Proc Natl Acad Sci U S A, 2015. **112**(52): p. 15790-7.
5. Hershko, A. and A. Ciechanover, *The ubiquitin system.* Annu Rev Biochem, 1998. **67**: p. 425-79.
6. Finley, D., *Recognition and processing of ubiquitin-protein conjugates by the proteasome.* Annu Rev Biochem, 2009. **78**: p. 477-513.
7. Collins, G.A. and A.L. Goldberg, *The Logic of the 26S Proteasome.* Cell, 2017. **169**(5): p. 792-806.
8. Danieli, A. and S. Martens, *p62-mediated phase separation at the intersection of the ubiquitin-proteasome system and autophagy.* J Cell Sci, 2018. **131**(19).
9. Kuma, A., et al., *The role of autophagy during the early neonatal starvation period.* Nature, 2004. **432**(7020): p. 1032-6.
10. Mizushima, N., et al., *Autophagy fights disease through cellular self-digestion.* Nature, 2008. **451**(7182): p. 1069-75.
11. Yang, Z. and D.J. Klionsky, *Eaten alive: a history of macroautophagy.* Nat Cell Biol, 2010. **12**(9): p. 814-22.
12. Lamark, T. and T. Johansen, *Aggrephagy: selective disposal of protein aggregates by macroautophagy.* Int J Cell Biol, 2012. **2012**: p. 736905.
13. De Duve, C. and R. Wattiaux, *Functions of lysosomes.* Annu Rev Physiol, 1966. **28**: p. 435-92.
14. Mijaljica, D., M. Prescott, and R.J. Devenish, *Microautophagy in mammalian cells: revisiting a 40-year-old conundrum.* Autophagy, 2011. **7**(7): p. 673-82.
15. Sahu, R., et al., *Microautophagy of cytosolic proteins by late endosomes.* Dev Cell, 2011. **20**(1): p. 131-9.
16. Mejlvang, J., et al., *Starvation induces rapid degradation of selective autophagy receptors by endosomal microautophagy.* J Cell Biol, 2018. **217**(10): p. 3640-3655.
17. Olsvik, H.L., et al., *Endosomal microautophagy is an integrated part of the autophagic response to amino acid starvation.* Autophagy, 2019. **15**(1): p. 182-183.
18. Cuervo, A.M. and E. Wong, *Chaperone-mediated autophagy: roles in disease and aging.* Cell Res, 2014. **24**(1): p. 92-104.
19. Chiang, H.L., et al., *A role for a 70-kilodalton heat shock protein in lysosomal degradation of intracellular proteins.* Science, 1989. **246**(4928): p. 382-5.
20. Cuervo, A.M. and J.F. Dice, *A receptor for the selective uptake and degradation of proteins by lysosomes.* Science, 1996. **273**(5274): p. 501-3.
21. Kaushik, S. and A.M. Cuervo, *Chaperone-mediated autophagy: a unique way to enter the lysosome world.* Trends Cell Biol, 2012. **22**(8): p. 407-17.
22. Cuervo, A.M., *Chaperone-mediated autophagy: selectivity pays off.* Trends Endocrinol Metab, 2010. **21**(3): p. 142-50.
23. Shen, H.M. and N. Mizushima, *At the end of the autophagic road: an emerging understanding of lysosomal functions in autophagy.* Trends Biochem Sci, 2014. **39**(2): p. 61-71.

24. Reggiori, F. and D.J. Klionsky, *Autophagy in the eukaryotic cell.* Eukaryot Cell, 2002. **1**(1): p. 11-21.
25. Mizushima, N., T. Yoshimori, and Y. Ohsumi, *The role of Atg proteins in autophagosome formation.* Annu Rev Cell Dev Biol, 2011. **27**: p. 107-32.
26. Kim, P.K., et al., *Ubiquitin signals autophagic degradation of cytosolic proteins and peroxisomes.* Proc Natl Acad Sci U S A, 2008. **105**(52): p. 20567-74.
27. Rogov, V., et al., *Interactions between autophagy receptors and ubiquitin-like proteins form the molecular basis for selective autophagy.* Mol Cell, 2014. **53**(2): p. 167-78.
28. Levine, B. and D.J. Klionsky, *Development by self-digestion: molecular mechanisms and biological functions of autophagy.* Dev Cell, 2004. **6**(4): p. 463-77.
29. Xie, Z. and D.J. Klionsky, *Autophagosome formation: core machinery and adaptations.* Nat Cell Biol, 2007. **9**(10): p. 1102-9.
30. Kraft, C. and S. Martens, *Mechanisms and regulation of autophagosome formation.* Curr Opin Cell Biol, 2012. **24**(4): p. 496-501.
31. Romanov, J., et al., *Mechanism and functions of membrane binding by the Atg5-Atg12/Atg16 complex during autophagosome formation.* EMBO J, 2012. **31**(22): p. 4304-17.
32. Huang, J. and D.J. Klionsky, *Autophagy and human disease.* Cell Cycle, 2007. **6**(15): p. 1837-49.
33. Nakatogawa, H., et al., *Dynamics and diversity in autophagy mechanisms: lessons from yeast.* Nat Rev Mol Cell Biol, 2009. **10**(7): p. 458-67.
34. Itakura, E. and N. Mizushima, *Characterization of autophagosome formation site by a hierarchical analysis of mammalian Atg proteins.* Autophagy, 2010. **6**(6): p. 764-76.
35. Grasso, D., F.J. Renna, and M.I. Vaccaro, *Initial Steps in Mammalian Autophagosome Biogenesis.* Front Cell Dev Biol, 2018. **6**: p. 146.
36. Chen, Y. and D.J. Klionsky, *The regulation of autophagy - unanswered questions.* J Cell Sci, 2011. **124**(Pt 2): p. 161-70.
37. Gwinn, D.M., et al., *AMPK phosphorylation of raptor mediates a metabolic checkpoint.* Mol Cell, 2008. **30**(2): p. 214-26.
38. Funderburk, S.F., Q.J. Wang, and Z. Yue, *The Beclin 1-VPS34 complex--at the crossroads of autophagy and beyond.* Trends Cell Biol, 2010. **20**(6): p. 355-62.
39. Liang, X.H., et al., *Induction of autophagy and inhibition of tumorigenesis by beclin 1.* Nature, 1999. **402**(6762): p. 672-6.
40. Hurley, J.H. and L.N. Young, *Mechanisms of Autophagy Initiation.* Annu Rev Biochem, 2017. **86**: p. 225-244.
41. Itakura, E., et al., *Beclin 1 forms two distinct phosphatidylinositol 3-kinase complexes with mammalian Atg14 and UVRAG.* Mol Biol Cell, 2008. **19**(12): p. 5360-72.
42. Noda, T., et al., *Apg9p/Cvt7p is an integral membrane protein required for transport vesicle formation in the Cvt and autophagy pathways.* J Cell Biol, 2000. **148**(3): p. 465-80.
43. Young, A.R., et al., *Starvation and ULK1-dependent cycling of mammalian Atg9 between the TGN and endosomes.* J Cell Sci, 2006. **119**(Pt 18): p. 3888-900.
44. Takahashi, Y., et al., *Bif-1 regulates Atg9 trafficking by mediating the fission of Golgi membranes during autophagy.* Autophagy, 2011. **7**(1): p. 61-73.
45. Webber, J.L. and S.A. Tooze, *Coordinated regulation of autophagy by p38alpha MAPK through mAtg9 and p38IP.* EMBO J, 2010. **29**(1): p. 27-40.
46. Lamb, C.A., T. Yoshimori, and S.A. Tooze, *The autophagosome: origins unknown, biogenesis complex.* Nat Rev Mol Cell Biol, 2013. **14**(12): p. 759-74.
47. Mizushima, N., et al., *A protein conjugation system essential for autophagy.* Nature, 1998. **395**(6700): p. 395-8.

48. Nakatogawa, H., Y. Ichimura, and Y. Ohsumi, *Atg8, a ubiquitin-like protein required for autophagosome formation, mediates membrane tethering and hemifusion.* Cell, 2007. **130**(1): p. 165-78.
49. Kabeya, Y., et al., *LC3, GABARAP and GATE16 localize to autophagosomal membrane depending on form-II formation.* J Cell Sci, 2004. **117**(Pt 13): p. 2805-12.
50. Hanada, T., et al., *The Atg12-Atg5 conjugate has a novel E3-like activity for protein lipidation in autophagy.* J Biol Chem, 2007. **282**(52): p. 37298-302.
51. Suzuki, K., et al., *The pre-autophagosomal structure organized by concerted functions of APG genes is essential for autophagosome formation.* EMBO J, 2001. **20**(21): p. 5971-81.
52. Mizushima, N., et al., *Mouse Apg16L, a novel WD-repeat protein, targets to the autophagic isolation membrane with the Apg12-Apg5 conjugate.* J Cell Sci, 2003. **116**(Pt 9): p. 1679-88.
53. Kabeya, Y., et al., *LC3, a mammalian homologue of yeast Apg8p, is localized in autophagosome membranes after processing.* EMBO J, 2000. **19**(21): p. 5720-8.
54. Tanaka, Y., et al., *Accumulation of autophagic vacuoles and cardiomyopathy in LAMP-2-deficient mice.* Nature, 2000. **406**(6798): p. 902-6.
55. Itakura, E., C. Kishi-Itakura, and N. Mizushima, *The hairpin-type tail-anchored SNARE syntaxin 17 targets to autophagosomes for fusion with endosomes/lysosomes.* Cell, 2012. **151**(6): p. 1256-69.
56. Feng, Y., et al., *The machinery of macroautophagy.* Cell Res, 2014. **24**(1): p. 24-41.
57. Parzych, K.R. and D.J. Klionsky, *An overview of autophagy: morphology, mechanism, and regulation.* Antioxid Redox Signal, 2014. **20**(3): p. 460-73.
58. Gatica, D., V. Lahiri, and D.J. Klionsky, *Cargo recognition and degradation by selective autophagy.* Nat Cell Biol, 2018. **20**(3): p. 233-242.
59. Kumsta, C., et al., *The autophagy receptor p62/SQST-1 promotes proteostasis and longevity in C. elegans by inducing autophagy.* Nat Commun, 2019. **10**(1): p. 5648.
60. Jin, M., X. Liu, and D.J. Klionsky, *SnapShot: Selective autophagy.* Cell, 2013. **152**(1-2): p. 368-368 e2.
61. Lamark, T., S. Svenning, and T. Johansen, *Regulation of selective autophagy: the p62/SQSTM1 paradigm.* Essays Biochem, 2017. **61**(6): p. 609-624.
62. Chen, R.H., Y.H. Chen, and T.Y. Huang, *Ubiquitin-mediated regulation of autophagy.* J Biomed Sci, 2019. **26**(1): p. 80.
63. Johansen, T. and T. Lamark, *Selective autophagy mediated by autophagic adapter proteins.* Autophagy, 2011. **7**(3): p. 279-96.
64. Thurston, T.L., et al., *The TBK1 adaptor and autophagy receptor NDP52 restricts the proliferation of ubiquitin-coated bacteria.* Nat Immunol, 2009. **10**(11): p. 1215-21.
65. Kirkin, V., et al., *A role for NBR1 in autophagosomal degradation of ubiquitinated substrates.* Mol Cell, 2009. **33**(4): p. 505-16.
66. Wild, P., et al., *Phosphorylation of the autophagy receptor optineurin restricts Salmonella growth.* Science, 2011. **333**(6039): p. 228-33.
67. Newman, A.C., et al., *TBK1 kinase addiction in lung cancer cells is mediated via autophagy of Tax1bp1/Ndp52 and non-canonical NF-kappaB signalling.* PLoS One, 2012. **7**(11): p. e50672.
68. Pankiv, S., et al., *p62/SQSTM1 binds directly to Atg8/LC3 to facilitate degradation of ubiquitinated protein aggregates by autophagy.* J Biol Chem, 2007. **282**(33): p. 24131-45.
69. Ichimura, Y., et al., *Structural basis for sorting mechanism of p62 in selective autophagy.* J Biol Chem, 2008. **283**(33): p. 22847-57.
70. Novak, I., et al., *Nix is a selective autophagy receptor for mitochondrial clearance.* EMBO Rep, 2010. **11**(1): p. 45-51.
71. Mancias, J.D., et al., *Quantitative proteomics identifies NCOA4 as the cargo receptor mediating ferritinophagy.* Nature, 2014. **509**(7498): p. 105-9.

72. Chauhan, S., et al., *TRIMs and Galectins Globally Cooperate and TRIM16 and Galectin-3 Co-direct Autophagy in Endomembrane Damage Homeostasis.* Dev Cell, 2016. **39**(1): p. 13-27.
73. Khaminets, A., et al., *Regulation of endoplasmic reticulum turnover by selective autophagy.* Nature, 2015. **522**(7556): p. 354-8.
74. Sanchez-Martin, P. and M. Komatsu, *p62/SQSTM1 - steering the cell through health and disease.* J Cell Sci, 2018. **131**(21).
75. Lamark, T., et al., *Interaction codes within the family of mammalian Phox and Bem1p domain-containing proteins.* J Biol Chem, 2003. **278**(36): p. 34568-81.
76. Wurzer, B., et al., *Oligomerization of p62 allows for selection of ubiquitinated cargo and isolation membrane during selective autophagy.* Elife, 2015. **4**: p. e08941.
77. Pankiv, S., et al., *Nucleocytoplasmic shuttling of p62/SQSTM1 and its role in recruitment of nuclear polyubiquitinated proteins to promyelocytic leukemia bodies.* J Biol Chem, 2010. **285**(8): p. 5941-53.
78. Long, J., et al., *Ubiquitin recognition by the ubiquitin-associated domain of p62 involves a novel conformational switch.* J Biol Chem, 2008. **283**(9): p. 5427-40.
79. Komatsu, M., et al., *Homeostatic levels of p62 control cytoplasmic inclusion body formation in autophagy-deficient mice.* Cell, 2007. **131**(6): p. 1149-63.
80. Komatsu, M., et al., *The selective autophagy substrate p62 activates the stress responsive transcription factor Nrf2 through inactivation of Keap1.* Nat Cell Biol, 2010. **12**(3): p. 213-23.
81. Zhang, J., Z. Yang, and J. Dong, *P62: An emerging oncotarget for osteolytic metastasis.* J Bone Oncol, 2016. **5**(1): p. 30-7.
82. Knaevelsrud, H. and A. Simonsen, *Fighting disease by selective autophagy of aggregate-prone proteins.* FEBS Lett, 2010. **584**(12): p. 2635-45.
83. Fracchiolla, D., et al., *Mechanism of cargo-directed Atg8 conjugation during selective autophagy.* Elife, 2016. **5**.
84. Bjorkoy, G., et al., *p62/SQSTM1 forms protein aggregates degraded by autophagy and has a protective effect on huntingtin-induced cell death.* J Cell Biol, 2005. **171**(4): p. 603-14.
85. Khaminets, A., C. Behl, and I. Dikic, *Ubiquitin-Dependent And Independent Signals In Selective Autophagy.* Trends Cell Biol, 2016. **26**(1): p. 6-16.
86. Ciuffa, R., et al., *The selective autophagy receptor p62 forms a flexible filamentous helical scaffold.* Cell Rep, 2015. **11**(5): p. 748-58.
87. Itakura, E. and N. Mizushima, *p62 Targeting to the autophagosome formation site requires self-oligomerization but not LC3 binding.* J Cell Biol, 2011. **192**(1): p. 17-27.
88. Jain, A., et al., *p62/SQSTM1 is a target gene for transcription factor NRF2 and creates a positive feedback loop by inducing antioxidant response element-driven gene transcription.* J Biol Chem, 2010. **285**(29): p. 22576-91.
89. Villeneuve, N.F., A. Lau, and D.D. Zhang, *Regulation of the Nrf2-Keap1 antioxidant response by the ubiquitin proteasome system: an insight into cullin-ring ubiquitin ligases.* Antioxid Redox Signal, 2010. **13**(11): p. 1699-712.
90. Sanz, L., et al., *The atypical PKC-interacting protein p62 channels NF-kappaB activation by the IL-1-TRAF6 pathway.* EMBO J, 2000. **19**(7): p. 1576-86.
91. Moscat, J. and M.T. Diaz-Meco, *p62 at the crossroads of autophagy, apoptosis, and cancer.* Cell, 2009. **137**(6): p. 1001-4.
92. Ling, J., et al., *KrasG12D-induced IKK2/beta/NF-kappaB activation by IL-1alpha and p62 feedforward loops is required for development of pancreatic ductal adenocarcinoma.* Cancer Cell, 2012. **21**(1): p. 105-20.
93. Dupont, N., et al., *Shigella phagocytic vacuolar membrane remnants participate in the cellular response to pathogen invasion and are regulated by autophagy.* Cell Host Microbe, 2009. **6**(2): p. 137-49.

94. Rusten, T.E. and H. Stenmark, *p62, an autophagy hero or culprit?* Nat Cell Biol, 2010. **12**(3): p. 207-9.
95. Finley, D., A. Ciechanover, and A. Varshavsky, *Ubiquitin as a central cellular regulator.* Cell, 2004. **116**(2 Suppl): p. S29-32, 2 p following S32.
96. Moremen, K.W., M. Tiemeyer, and A.V. Nairn, *Vertebrate protein glycosylation: diversity, synthesis and function.* Nat Rev Mol Cell Biol, 2012. **13**(7): p. 448-62.
97. Bononi, A., et al., *Protein kinases and phosphatases in the control of cell fate.* Enzyme Res, 2011. **2011**: p. 329098.
98. Wani, W.Y., et al., *Regulation of autophagy by protein post-translational modification.* Lab Invest, 2015. **95**(1): p. 14-25.
99. Long, J., et al., *Dimerisation of the UBA domain of p62 inhibits ubiquitin binding and regulates NF-kappaB signalling.* J Mol Biol, 2010. **396**(1): p. 178-94.
100. Lim, J., et al., *Proteotoxic stress induces phosphorylation of p62/SQSTM1 by ULK1 to regulate selective autophagic clearance of protein aggregates.* PLoS Genet, 2015. **11**(2): p. e1004987.
101. Matsumoto, G., et al., *Serine 403 phosphorylation of p62/SQSTM1 regulates selective autophagic clearance of ubiquitinated proteins.* Mol Cell, 2011. **44**(2): p. 279-89.
102. Ichimura, Y., et al., *Phosphorylation of p62 activates the Keap1-Nrf2 pathway during selective autophagy.* Mol Cell, 2013. **51**(5): p. 618-31.
103. Ishimura, R., K. Tanaka, and M. Komatsu, *Dissection of the role of p62/Sqstm1 in activation of Nrf2 during xenophagy.* FEBS Lett, 2014. **588**(5): p. 822-8.
104. Peng, H., et al., *Ubiquitylation of p62/sequestosome1 activates its autophagy receptor function and controls selective autophagy upon ubiquitin stress.* Cell Res, 2017. **27**(5): p. 657-674.
105. Lee, Y., et al., *Keap1/Cullin3 Modulates p62/SQSTM1 Activity via UBA Domain Ubiquitination.* Cell Rep, 2017. **19**(1): p. 188-202.
106. Pan, J.A., et al., *TRIM21 Ubiquitylates SQSTM1/p62 and Suppresses Protein Sequestration to Regulate Redox Homeostasis.* Mol Cell, 2016. **62**(1): p. 149-51.
107. Norman, J.M., G.M. Cohen, and E.T. Bampton, *The in vitro cleavage of the hAtg proteins by cell death proteases.* Autophagy, 2010. **6**(8): p. 1042-56.
108. Jin, Z., et al., *Cullin3-based polyubiquitination and p62-dependent aggregation of caspase-8 mediate extrinsic apoptosis signaling.* Cell, 2009. **137**(4): p. 721-35.
109. Duran, A., et al., *The signaling adaptor p62 is an important NF-kappaB mediator in tumorigenesis.* Cancer Cell, 2008. **13**(4): p. 343-54.
110. Duran, A., et al., *p62 is a key regulator of nutrient sensing in the mTORC1 pathway.* Mol Cell, 2011. **44**(1): p. 134-46.
111. Storz, G. and J.A. Imlay, *Oxidative stress.* Curr Opin Microbiol, 1999. **2**(2): p. 188-94.
112. Nohl, H., et al., *Cell respiration and formation of reactive oxygen species: facts and artefacts.* Biochem Soc Trans, 2003. **31**(Pt 6): p. 1308-11.
113. Ding, B., et al., *Role of p53 in antioxidant defense of HPV-positive cervical carcinoma cells following H2O2 exposure.* J Cell Sci, 2007. **120**(Pt 13): p. 2284-94.
114. Driessens, N., et al., *Hydrogen peroxide induces DNA single- and double-strand breaks in thyroid cells and is therefore a potential mutagen for this organ.* Endocr Relat Cancer, 2009. **16**(3): p. 845-56.
115. Ameziane-El-Hassani, R., et al., *Role of H2O2 in RET/PTC1 chromosomal rearrangement produced by ionizing radiation in human thyroid cells.* Cancer Res, 2010. **70**(10): p. 4123-32.
116. Freitas, M., et al., *Oxidative stress adaptation in aggressive prostate cancer may be counteracted by the reduction of glutathione reductase.* FEBS Open Bio, 2012. **2**: p. 119-28.

117. Sauer, H., M. Wartenberg, and J. Hescheler, *Reactive oxygen species as intracellular messengers during cell growth and differentiation.* Cell Physiol Biochem, 2001. **11**(4): p. 173-86.
118. Martindale, J.L. and N.J. Holbrook, *Cellular response to oxidative stress: signaling for suicide and survival.* J Cell Physiol, 2002. **192**(1): p. 1-15.
119. Turpaev, K.T., *Reactive oxygen species and regulation of gene expression.* Biochemistry (Mosc), 2002. **67**(3): p. 281-92.
120. Finkel, T., *Signal transduction by reactive oxygen species.* J Cell Biol, 2011. **194**(1): p. 7-15.
121. Schieber, M. and N.S. Chandel, *ROS function in redox signaling and oxidative stress.* Curr Biol, 2014. **24**(10): p. R453-62.
122. Waris, G. and H. Ahsan, *Reactive oxygen species: role in the development of cancer and various chronic conditions.* J Carcinog, 2006. **5**: p. 14.
123. Dikalov, S.I. and D.G. Harrison, *Methods for detection of mitochondrial and cellular reactive oxygen species.* Antioxid Redox Signal, 2014. **20**(2): p. 372-82.
124. Shehat, M.G. and J. Tigno-Aranjuez, *Flow Cytometric Measurement Of ROS Production In Macrophages In Response To FcgammaR Cross-linking.* J Vis Exp, 2019(145).
125. Tammariello, S.P., M.T. Quinn, and S. Estus, *NADPH oxidase contributes directly to oxidative stress and apoptosis in nerve growth factor-deprived sympathetic neurons.* J Neurosci, 2000. **20**(1): p. RC53.
126. Bass, D.A., et al., *Flow cytometric studies of oxidative product formation by neutrophils: a graded response to membrane stimulation.* J Immunol, 1983. **130**(4): p. 1910-7.
127. Eruslanov, E. and S. Kusmartsev, *Identification of ROS using oxidized DCFDA and flow-cytometry.* Methods Mol Biol, 2010. **594**: p. 57-72.
128. Baird, L. and A.T. Dinkova-Kostova, *The cytoprotective role of the Keap1-Nrf2 pathway.* Arch Toxicol, 2011. **85**(4): p. 241-72.
129. Kovac, S., et al., *Nrf2 regulates ROS production by mitochondria and NADPH oxidase.* Biochim Biophys Acta, 2015. **1850**(4): p. 794-801.
130. Holmstrom, K.M., et al., *Nrf2 impacts cellular bioenergetics by controlling substrate availability for mitochondrial respiration.* Biol Open, 2013. **2**(8): p. 761-70.
131. Itoh, K., et al., *An Nrf2/small Maf heterodimer mediates the induction of phase II detoxifying enzyme genes through antioxidant response elements.* Biochem Biophys Res Commun, 1997. **236**(2): p. 313-22.
132. Motohashi, H. and M. Yamamoto, *Nrf2-Keap1 defines a physiologically important stress response mechanism.* Trends Mol Med, 2004. **10**(11): p. 549-57.
133. Venugopal, R. and A.K. Jaiswal, *Nrf1 and Nrf2 positively and c-Fos and Fra1 negatively regulate the human antioxidant response element-mediated expression of NAD(P)H:quinone oxidoreductase1 gene.* Proc Natl Acad Sci U S A, 1996. **93**(25): p. 14960-5.
134. Ma, Q., *Role of nrf2 in oxidative stress and toxicity.* Annu Rev Pharmacol Toxicol, 2013. **53**: p. 401-26.
135. Itoh, K., et al., *Keap1 represses nuclear activation of antioxidant responsive elements by Nrf2 through binding to the amino-terminal Neh2 domain.* Genes Dev, 1999. **13**(1): p. 76-86.
136. He, X., et al., *Arsenic induces NAD(P)H-quinone oxidoreductase I by disrupting the Nrf2 x Keap1 x Cul3 complex and recruiting Nrf2 x Maf to the antioxidant response element enhancer.* J Biol Chem, 2006. **281**(33): p. 23620-31.
137. Wakabayashi, N., et al., *Keap1-null mutation leads to postnatal lethality due to constitutive Nrf2 activation.* Nat Genet, 2003. **35**(3): p. 238-45.
138. Zhang, D.D., et al., *Keap1 is a redox-regulated substrate adaptor protein for a Cul3-dependent ubiquitin ligase complex.* Mol Cell Biol, 2004. **24**(24): p. 10941-53.

139. Taguchi, K., H. Motohashi, and M. Yamamoto, *Molecular mechanisms of the Keap1-Nrf2 pathway in stress response and cancer evolution.* Genes Cells, 2011. **16**(2): p. 123-40.
140. Lau, A., et al., *A noncanonical mechanism of Nrf2 activation by autophagy deficiency: direct interaction between Keap1 and p62.* Mol Cell Biol, 2010. **30**(13): p. 3275-85.
141. Lo, S.C. and M. Hannink, *PGAM5 tethers a ternary complex containing Keap1 and Nrf2 to mitochondria.* Exp Cell Res, 2008. **314**(8): p. 1789-803.
142. Chen, W., et al., *Direct interaction between Nrf2 and p21(Cip1/WAF1) upregulates the Nrf2-mediated antioxidant response.* Mol Cell, 2009. **34**(6): p. 663-73.
143. Bossy-Wetzel, E., R. Schwarzenbacher, and S.A. Lipton, *Molecular pathways to neurodegeneration.* Nat Med, 2004. **10 Suppl**: p. S2-9.
144. Finkel, T., *Radical medicine: treating ageing to cure disease.* Nat Rev Mol Cell Biol, 2005. **6**(12): p. 971-6.
145. Vargas, M.R., et al., *Nrf2 activation in astrocytes protects against neurodegeneration in mouse models of familial amyotrophic lateral sclerosis.* J Neurosci, 2008. **28**(50): p. 13574-81.
146. Clements, C.M., et al., *DJ-1, a cancer- and Parkinson's disease-associated protein, stabilizes the antioxidant transcriptional master regulator Nrf2.* Proc Natl Acad Sci U S A, 2006. **103**(41): p. 15091-6.
147. Brangwynne, C.P., et al., *Germline P granules are liquid droplets that localize by controlled dissolution/condensation.* Science, 2009. **324**(5935): p. 1729-32.
148. Sun, D., et al., *Polyubiquitin chain-induced p62 phase separation drives autophagic cargo segregation.* Cell Res, 2018. **28**(4): p. 405-415.
149. Boeynaems, S., et al., *Protein Phase Separation: A New Phase in Cell Biology.* Trends Cell Biol, 2018. **28**(6): p. 420-435.
150. Handwerger, K.E., J.A. Cordero, and J.G. Gall, *Cajal bodies, nucleoli, and speckles in the Xenopus oocyte nucleus have a low-density, sponge-like structure.* Mol Biol Cell, 2005. **16**(1): p. 202-11.
151. Brangwynne, C.P., T.J. Mitchison, and A.A. Hyman, *Active liquid-like behavior of nucleoli determines their size and shape in Xenopus laevis oocytes.* Proc Natl Acad Sci U S A, 2011. **108**(11): p. 4334-9.
152. Aguzzi, A. and M. Altmeyer, *Phase Separation: Linking Cellular Compartmentalization to Disease.* Trends Cell Biol, 2016. **26**(7): p. 547-558.
153. Feric, M., et al., *Coexisting Liquid Phases Underlie Nucleolar Subcompartments.* Cell, 2016. **165**(7): p. 1686-1697.
154. Alberti, S., A. Gladfelter, and T. Mittag, *Considerations and Challenges in Studying Liquid-Liquid Phase Separation and Biomolecular Condensates.* Cell, 2019. **176**(3): p. 419-434.
155. Banani, S.F., et al., *Biomolecular condensates: organizers of cellular biochemistry.* Nat Rev Mol Cell Biol, 2017. **18**(5): p. 285-298.
156. Yoshizawa, T., et al., *Biological phase separation: cell biology meets biophysics.* Biophys Rev, 2020.
157. Noda, N.N., Z. Wang, and H. Zhang, *Liquid-liquid phase separation in autophagy.* J Cell Biol, 2020. **219**(8).
158. Kaganovich, D., *There Is an Inclusion for That: Material Properties of Protein Granules Provide a Platform for Building Diverse Cellular Functions.* Trends Biochem Sci, 2017. **42**(10): p. 765-776.
159. Alberti, S. and D. Dormann, *Liquid-Liquid Phase Separation in Disease.* Annu Rev Genet, 2019. **53**: p. 171-194.
160. Noda, N.N. and Y. Fujioka, *Atg1 family kinases in autophagy initiation.* Cell Mol Life Sci, 2015. **72**(16): p. 3083-96.
161. Fujioka, Y., et al., *Phase separation organizes the site of autophagosome formation.* Nature, 2020. **578**(7794): p. 301-305.

162. Suzuki, K., et al., *Hierarchy of Atg proteins in pre-autophagosomal structure organization.* Genes Cells, 2007. **12**(2): p. 209-18.
163. Yamamoto, H., et al., *The Intrinsically Disordered Protein Atg13 Mediates Supramolecular Assembly of Autophagy Initiation Complexes.* Dev Cell, 2016. **38**(1): p. 86-99.
164. Noda, T., *Regulation of Autophagy through TORC1 and mTORC1.* Biomolecules, 2017. **7**(3).
165. Takahara, T. and T. Maeda, *Transient sequestration of TORC1 into stress granules during heat stress.* Mol Cell, 2012. **47**(2): p. 242-52.
166. Yang, Y.S., et al., *Yeast Ataxin-2 Forms an Intracellular Condensate Required for the Inhibition of TORC1 Signaling during Respiratory Growth.* Cell, 2019. **177**(3): p. 697-710 e17.
167. Yamasaki, A., et al., *Liquidity Is a Critical Determinant for Selective Autophagy of Protein Condensates.* Mol Cell, 2020. **77**(6): p. 1163-1175 e9.
168. Lynch-Day, M.A. and D.J. Klionsky, *The Cvt pathway as a model for selective autophagy.* FEBS Lett, 2010. **584**(7): p. 1359-66.
169. Shintani, T., et al., *Mechanism of cargo selection in the cytoplasm to vacuole targeting pathway.* Dev Cell, 2002. **3**(6): p. 825-37.
170. Zatloukal, K., et al., *p62 Is a common component of cytoplasmic inclusions in protein aggregation diseases.* Am J Pathol, 2002. **160**(1): p. 255-63.
171. Kuusisto, E., A. Salminen, and I. Alafuzoff, *Ubiquitin-binding protein p62 is present in neuronal and glial inclusions in human tauopathies and synucleinopathies.* Neuroreport, 2001. **12**(10): p. 2085-90.
172. Zaffagnini, G., et al., *p62 filaments capture and present ubiquitinated cargos for autophagy.* EMBO J, 2018. **37**(5).
173. Wegmann, S., et al., *Tau protein liquid-liquid phase separation can initiate tau aggregation.* EMBO J, 2018. **37**(7).
174. Shin, Y., et al., *Spatiotemporal Control of Intracellular Phase Transitions Using Light-Activated optoDroplets.* Cell, 2017. **168**(1-2): p. 159-171 e14.
175. Dao, T.P., et al., *Ubiquitin Modulates Liquid-Liquid Phase Separation of UBQLN2 via Disruption of Multivalent Interactions.* Mol Cell, 2018. **69**(6): p. 965-978 e6.
176. Zeng, M., et al., *Phase Transition in Postsynaptic Densities Underlies Formation of Synaptic Complexes and Synaptic Plasticity.* Cell, 2016. **166**(5): p. 1163-1175 e12.
177. Saha, S., et al., *Polar Positioning of Phase-Separated Liquid Compartments in Cells Regulated by an mRNA Competition Mechanism.* Cell, 2016. **166**(6): p. 1572-1584 e16.
178. Nott, T.J., et al., *Phase transition of a disordered nuage protein generates environmentally responsive membraneless organelles.* Mol Cell, 2015. **57**(5): p. 936-947.
179. Alberti, S., et al., *A User's Guide for Phase Separation Assays with Purified Proteins.* J Mol Biol, 2018. **430**(23): p. 4806-4820.
180. McQuilken, M., et al., *Polarized Fluorescence Microscopy to Study Cytoskeleton Assembly and Organization in Live Cells.* Curr Protoc Cell Biol, 2015. **67**: p. 4 29 1-4 29 13.
181. Wei, M.T., et al., *Phase behaviour of disordered proteins underlying low density and high permeability of liquid organelles.* Nat Chem, 2017. **9**(11): p. 1118-1125.
182. Fernagut, P.O., et al., *Behavioral and histopathological consequences of paraquat intoxication in mice: effects of alpha-synuclein over-expression.* Synapse, 2007. **61**(12): p. 991-1001.
183. Zhang, H., et al., *RNA Controls PolyQ Protein Phase Transitions.* Mol Cell, 2015. **60**(2): p. 220-30.
184. Molliex, A., et al., *Phase separation by low complexity domains promotes stress granule assembly and drives pathological fibrillization.* Cell, 2015. **163**(1): p. 123-33.

185. Patel, A., et al., *A Liquid-to-Solid Phase Transition of the ALS Protein FUS Accelerated by Disease Mutation.* Cell, 2015. **162**(5): p. 1066-77.
186. Zhang, H., et al., *Liquid-liquid phase separation in biology: mechanisms, physiological functions and human diseases.* Sci China Life Sci, 2020. **63**(7): p. 953-985.
187. Cai, D., et al., *Phase separation of YAP reorganizes genome topology for long-term YAP target gene expression.* Nat Cell Biol, 2019. **21**(12): p. 1578-1589.
188. Yang, X., et al., *Daxx, a novel Fas-binding protein that activates JNK and apoptosis.* Cell, 1997. **89**(7): p. 1067-76.
189. Santiago, A., et al., *Identification of two independent SUMO-interacting motifs in Daxx: evolutionary conservation from Drosophila to humans and their biochemical functions.* Cell Cycle, 2009. **8**(1): p. 76-87.
190. Escobar-Cabrera, E., et al., *Structural characterization of the DAXX N-terminal helical bundle domain and its complex with Rassf1C.* Structure, 2010. **18**(12): p. 1642-53.
191. Lewis, P.W., et al., *Daxx is an H3.3-specific histone chaperone and cooperates with ATRX in replication-independent chromatin assembly at telomeres.* Proc Natl Acad Sci U S A, 2010. **107**(32): p. 14075-80.
192. Elsasser, S.J., et al., *DAXX envelops a histone H3.3-H4 dimer for H3.3-specific recognition.* Nature, 2012. **491**(7425): p. 560-5.
193. Jenstad, M., et al., *System A transporter SAT2 mediates replenishment of dendritic glutamate pools controlling retrograde signaling by glutamate.* Cereb Cortex, 2009. **19**(5): p. 1092-106.
194. Deal, R.B., J.G. Henikoff, and S. Henikoff, *Genome-wide kinetics of nucleosome turnover determined by metabolic labeling of histones.* Science, 2010. **328**(5982): p. 1161-4.
195. Ng, R.K. and J.B. Gurdon, *Epigenetic memory of an active gene state depends on histone H3.3 incorporation into chromatin in the absence of transcription.* Nat Cell Biol, 2008. **10**(1): p. 102-9.
196. Mahmud, I. and D. Liao, *DAXX in cancer: phenomena, processes, mechanisms and regulation.* Nucleic Acids Res, 2019. **47**(15): p. 7734-7752.
197. Michaelson, J.S., et al., *Loss of Daxx, a promiscuously interacting protein, results in extensive apoptosis in early mouse development.* Genes Dev, 1999. **13**(15): p. 1918-23.
198. Pan, W.W., et al., *Death domain-associated protein DAXX promotes ovarian cancer development and chemoresistance.* J Biol Chem, 2013. **288**(19): p. 13620-30.
199. Tang, J., et al., *Critical role for Daxx in regulating Mdm2.* Nat Cell Biol, 2006. **8**(8): p. 855-62.
200. Ishov, A.M., et al., *PML is critical for ND10 formation and recruits the PML-interacting protein daxx to this nuclear structure when modified by SUMO-1*. J Cell Biol, 1999. **147**(2): p. 221-34.
201. Salomoni, P. and A.F. Khelifi, *Daxx: death or survival protein?* Trends Cell Biol, 2006. **16**(2): p. 97-104.
202. Zhong, S., et al., *Promyelocytic leukemia protein (PML) and Daxx participate in a novel nuclear pathway for apoptosis.* J Exp Med, 2000. **191**(4): p. 631-40.
203. Bouchard, J.J., et al., *Cancer Mutations of the Tumor Suppressor SPOP Disrupt the Formation of Active, Phase-Separated Compartments.* Mol Cell, 2018. **72**(1): p. 19-36 e8.
204. Singh, B. and S. Bhaskar, *Methods for Detection of Autophagy in Mammalian Cells.* Methods Mol Biol, 2019. **2045**: p. 245-258.
205. Mizushima, N., T. Yoshimori, and B. Levine, *Methods in mammalian autophagy research.* Cell, 2010. **140**(3): p. 313-26.
206. Kroemer, G. and B. Levine, *Autophagic cell death: the story of a misnomer.* Nat Rev Mol Cell Biol, 2008. **9**(12): p. 1004-10.
207. Ruska, E., *Nobel lecture. The development of the electron microscope and of electron microscopy.* Biosci Rep, 1987. **7**(8): p. 607-29.

208. Eskelinen, E.L., et al., *Seeing is believing: the impact of electron microscopy on autophagy research.* Autophagy, 2011. **7**(9): p. 935-56.
209. Clark, S.L., Jr., *Cellular differentiation in the kidneys of newborn mice studies with the electron microscope.* J Biophys Biochem Cytol, 1957. **3**(3): p. 349-62.
210. Novikoff, A.B., *The proximal tubule cell in experimental hydronephrosis.* J Biophys Biochem Cytol, 1959. **6**(1): p. 136-8.
211. Novikoff, A.B. and E. Essner, *Cytolysomes and mitochondrial degeneration.* J Cell Biol, 1962. **15**: p. 140-6.
212. Lucocq, J.M. and C. Hacker, *Cutting a fine figure: On the use of thin sections in electron microscopy to quantify autophagy.* Autophagy, 2013. **9**(9): p. 1443-8.
213. Eskelinen, E.L., *To be or not to be? Examples of incorrect identification of autophagic compartments in conventional transmission electron microscopy of mammalian cells.* Autophagy, 2008. **4**(2): p. 257-60.
214. Kovacs, A.L., A. Reith, and P.O. Seglen, *Accumulation of autophagosomes after inhibition of hepatocytic protein degradation by vinblastine, leupeptin or a lysosomotropic amine.* Exp Cell Res, 1982. **137**(1): p. 191-201.
215. Melendez, A., et al., *Autophagy genes are essential for dauer development and life-span extension in C. elegans.* Science, 2003. **301**(5638): p. 1387-91.
216. Mizushima, N., et al., *In vivo analysis of autophagy in response to nutrient starvation using transgenic mice expressing a fluorescent autophagosome marker.* Mol Biol Cell, 2004. **15**(3): p. 1101-11.
217. Tasdemir, E., et al., *Methods for assessing autophagy and autophagic cell death.* Methods Mol Biol, 2008. **445**: p. 29-76.
218. Loos, B., A. du Toit, and J.H. Hofmeyr, *Defining and measuring autophagosome flux-concept and reality.* Autophagy, 2014. **10**(11): p. 2087-96.
219. Zhang, X.J., et al., *Why should autophagic flux be assessed?* Acta Pharmacol Sin, 2013. **34**(5): p. 595-9.
220. Fass, E., et al., *Microtubules support production of starvation-induced autophagosomes but not their targeting and fusion with lysosomes.* J Biol Chem, 2006. **281**(47): p. 36303-16.
221. Tanida, I., et al., *Lysosomal turnover, but not a cellular level, of endogenous LC3 is a marker for autophagy.* Autophagy, 2005. **1**(2): p. 84-91.
222. Ju, J.S., et al., *Quantitation of "autophagic flux" in mature skeletal muscle.* Autophagy, 2010. **6**(7): p. 929-35.
223. Zhang, Z., R. Singh, and M. Aschner, *Methods for the Detection of Autophagy in Mammalian Cells.* Curr Protoc Toxicol, 2016. **69**: p. 20 12 1-20 12 26.
224. Rubinsztein, D.C., et al., *In search of an "autophagomometer".* Autophagy, 2009. **5**(5): p. 585-9.
225. Yoshii, S.R. and N. Mizushima, *Monitoring and Measuring Autophagy.* Int J Mol Sci, 2017. **18**(9).
226. Lippai, M. and P. Low, *The role of the selective adaptor p62 and ubiquitin-like proteins in autophagy.* Biomed Res Int, 2014. **2014**: p. 832704.
227. Bjorkoy, G., et al., *Monitoring autophagic degradation of p62/SQSTM1.* Methods Enzymol, 2009. **452**: p. 181-97.
228. Kim, J.H., et al., *Raf/MEK/ERK can regulate cellular levels of LC3B and SQSTM1/p62 at expression levels.* Exp Cell Res, 2014. **327**(2): p. 340-52.
229. Bardag-Gorce, F., et al., *Modifications in P62 occur due to proteasome inhibition in alcoholic liver disease.* Life Sci, 2005. **77**(20): p. 2594-602.
230. Korolchuk, V.I., F.M. Menzies, and D.C. Rubinsztein, *Mechanisms of cross-talk between the ubiquitin-proteasome and autophagy-lysosome systems.* FEBS Lett, 2010. **584**(7): p. 1393-8.

231. Seibenhener, M.L., et al., *Sequestosome 1/p62 is a polyubiquitin chain binding protein involved in ubiquitin proteasome degradation.* Mol Cell Biol, 2004. **24**(18): p. 8055-68.
232. Bampton, E.T., et al., *The dynamics of autophagy visualized in live cells: from autophagosome formation to fusion with endo/lysosomes.* Autophagy, 2005. **1**(1): p. 23-36.
233. Kimura, S., T. Noda, and T. Yoshimori, *Dissection of the autophagosome maturation process by a novel reporter protein, tandem fluorescent-tagged LC3.* Autophagy, 2007. **3**(5): p. 452-60.
234. Gump, J.M. and A. Thorburn, *Sorting cells for basal and induced autophagic flux by quantitative ratiometric flow cytometry.* Autophagy, 2014. **10**(7): p. 1327-34.
235. Kopitz, J., et al., *Nonselective autophagy of cytosolic enzymes by isolated rat hepatocytes.* J Cell Biol, 1990. **111**(3): p. 941-53.
236. Bauvy, C., A.J. Meijer, and P. Codogno, *Assaying of autophagic protein degradation.* Methods Enzymol, 2009. **452**: p. 47-61.
237. Kroemer, G. and M. Jaattela, *Lysosomes and autophagy in cell death control.* Nat Rev Cancer, 2005. **5**(11): p. 886-97.
238. Maiuri, M.C., et al., *Functional and physical interaction between Bcl-X(L) and a BH3-like domain in Beclin-1.* EMBO J, 2007. **26**(10): p. 2527-39.
239. Rubinsztein, D.C., et al., *Potential therapeutic applications of autophagy.* Nat Rev Drug Discov, 2007. **6**(4): p. 304-12.
240. Sarkar, S., et al., *Trehalose, a novel mTOR-independent autophagy enhancer, accelerates the clearance of mutant huntingtin and alpha-synuclein.* J Biol Chem, 2007. **282**(8): p. 5641-52.
241. Hosseinpour-Moghaddam, K., M. Caraglia, and A. Sahebkar, *Autophagy induction by trehalose: Molecular mechanisms and therapeutic impacts.* J Cell Physiol, 2018. **233**(9): p. 6524-6543.
242. Ding, W.X., et al., *Linking of autophagy to ubiquitin-proteasome system is important for the regulation of endoplasmic reticulum stress and cell viability.* Am J Pathol, 2007. **171**(2): p. 513-24.
243. Seglen, P.O. and P.B. Gordon, *3-Methyladenine: specific inhibitor of autophagic/lysosomal protein degradation in isolated rat hepatocytes.* Proc Natl Acad Sci U S A, 1982. **79**(6): p. 1889-92.
244. Fuertes, G., et al., *Changes in the proteolytic activities of proteasomes and lysosomes in human fibroblasts produced by serum withdrawal, amino-acid deprivation and confluent conditions.* Biochem J, 2003. **375**(Pt 1): p. 75-86.
245. Blommaart, E.F., et al., *The phosphatidylinositol 3-kinase inhibitors wortmannin and LY294002 inhibit autophagy in isolated rat hepatocytes.* Eur J Biochem, 1997. **243**(1-2): p. 240-6.
246. Yamamoto, A., et al., *Bafilomycin A1 prevents maturation of autophagic vacuoles by inhibiting fusion between autophagosomes and lysosomes in rat hepatoma cell line, H-4-II-E cells.* Cell Struct Funct, 1998. **23**(1): p. 33-42.
247. Klionsky, D.J., et al., *Does bafilomycin A1 block the fusion of autophagosomes with lysosomes?* Autophagy, 2008. **4**(7): p. 849-50.
248. de Duve, C., et al., *Commentary. Lysosomotropic agents.* Biochem Pharmacol, 1974. **23**(18): p. 2495-531.
249. Yue, Z., et al., *Beclin 1, an autophagy gene essential for early embryonic development, is a haploinsufficient tumor suppressor.* Proc Natl Acad Sci U S A, 2003. **100**(25): p. 15077-82.
250. Komatsu, M., et al., *Impairment of starvation-induced and constitutive autophagy in Atg7-deficient mice.* J Cell Biol, 2005. **169**(3): p. 425-34.
251. Boya, P., et al., *Inhibition of macroautophagy triggers apoptosis.* Mol Cell Biol, 2005. **25**(3): p. 1025-40.

252. Rubinsztein, D.C., *The roles of intracellular protein-degradation pathways in neurodegeneration.* Nature, 2006. **443**(7113): p. 780-6.
253. Menzies, F.M., A. Fleming, and D.C. Rubinsztein, *Compromised autophagy and neurodegenerative diseases.* Nat Rev Neurosci, 2015. **16**(6): p. 345-57.
254. Sturrock, A. and B.R. Leavitt, *The clinical and genetic features of Huntington disease.* J Geriatr Psychiatry Neurol, 2010. **23**(4): p. 243-59.
255. Vonsattel, J.P., C. Keller, and E.P. Cortes Ramirez, *Huntington's disease - neuropathology.* Handb Clin Neurol, 2011. **100**: p. 83-100.
256. Landles, C. and G.P. Bates, *Huntingtin and the molecular pathogenesis of Huntington's disease. Fourth in molecular medicine review series.* EMBO Rep, 2004. **5**(10): p. 958-63.
257. Croce, K.R. and A. Yamamoto, *A role for autophagy in Huntington's disease.* Neurobiol Dis, 2019. **122**: p. 16-22.
258. Scherzinger, E., et al., *Huntingtin-encoded polyglutamine expansions form amyloid-like protein aggregates in vitro and in vivo.* Cell, 1997. **90**(3): p. 549-58.
259. DiFiglia, M., et al., *Therapeutic silencing of mutant huntingtin with siRNA attenuates striatal and cortical neuropathology and behavioral deficits.* Proc Natl Acad Sci U S A, 2007. **104**(43): p. 17204-9.
260. Yamamoto, A., J.J. Lucas, and R. Hen, *Reversal of neuropathology and motor dysfunction in a conditional model of Huntington's disease.* Cell, 2000. **101**(1): p. 57-66.
261. Ravikumar, B., R. Duden, and D.C. Rubinsztein, *Aggregate-prone proteins with polyglutamine and polyalanine expansions are degraded by autophagy.* Hum Mol Genet, 2002. **11**(9): p. 1107-17.
262. Zheng, S., et al., *Deletion of the huntingtin polyglutamine stretch enhances neuronal autophagy and longevity in mice.* PLoS Genet, 2010. **6**(2): p. e1000838.
263. Rui, Y.N., et al., *Huntingtin functions as a scaffold for selective macroautophagy.* Nat Cell Biol, 2015. **17**(3): p. 262-75.
264. Olanow, C.W. and K. McNaught, *Parkinson's disease, proteins, and prions: milestones.* Mov Disord, 2011. **26**(6): p. 1056-71.
265. Anglade, P., et al., *Apoptosis and autophagy in nigral neurons of patients with Parkinson's disease.* Histol Histopathol, 1997. **12**(1): p. 25-31.
266. Hara, T., et al., *Suppression of basal autophagy in neural cells causes neurodegenerative disease in mice.* Nature, 2006. **441**(7095): p. 885-9.
267. Komatsu, M., et al., *Loss of autophagy in the central nervous system causes neurodegeneration in mice.* Nature, 2006. **441**(7095): p. 880-4.
268. Alegre-Abarrategui, J. and R. Wade-Martins, *Parkinson disease, LRRK2 and the endocytic-autophagic pathway.* Autophagy, 2009. **5**(8): p. 1208-10.
269. Bandyopadhyay, U. and A.M. Cuervo, *Chaperone-mediated autophagy in aging and neurodegeneration: lessons from alpha-synuclein.* Exp Gerontol, 2007. **42**(1-2): p. 120-8.
270. Lynch-Day, M.A., et al., *The role of autophagy in Parkinson's disease.* Cold Spring Harb Perspect Med, 2012. **2**(4): p. a009357.
271. Cuervo, A.M., et al., *Impaired degradation of mutant alpha-synuclein by chaperone-mediated autophagy.* Science, 2004. **305**(5688): p. 1292-5.
272. Martinez-Vicente, M., et al., *Dopamine-modified alpha-synuclein blocks chaperone-mediated autophagy.* J Clin Invest, 2008. **118**(2): p. 777-88.
273. McBride, H.M., M. Neuspiel, and S. Wasiak, *Mitochondria: more than just a powerhouse.* Curr Biol, 2006. **16**(14): p. R551-60.
274. Wallace, D.C., *A mitochondrial paradigm of metabolic and degenerative diseases, aging, and cancer: a dawn for evolutionary medicine.* Annu Rev Genet, 2005. **39**: p. 359-407.
275. Schapira, A.H., *Mitochondria in the aetiology and pathogenesis of Parkinson's disease.* Lancet Neurol, 2008. **7**(1): p. 97-109.
276. Geisler, S., et al., *PINK1/Parkin-mediated mitophagy is dependent on VDAC1 and p62/SQSTM1.* Nat Cell Biol, 2010. **12**(2): p. 119-31.

277. Narendra, D., et al., *Parkin is recruited selectively to impaired mitochondria and promotes their autophagy.* J Cell Biol, 2008. **183**(5): p. 795-803.
278. Matsuda, N., et al., *PINK1 stabilized by mitochondrial depolarization recruits Parkin to damaged mitochondria and activates latent Parkin for mitophagy.* J Cell Biol, 2010. **189**(2): p. 211-21.
279. Valente, E.M., et al., *Hereditary early-onset Parkinson's disease caused by mutations in PINK1.* Science, 2004. **304**(5674): p. 1158-60.
280. Kitada, T., et al., *Mutations in the parkin gene cause autosomal recessive juvenile parkinsonism.* Nature, 1998. **392**(6676): p. 605-8.
281. Moreau, K., et al., *PICALM modulates autophagy activity and tau accumulation.* Nat Commun, 2014. **5**: p. 4998.
282. LaFerla, F.M., K.N. Green, and S. Oddo, *Intracellular amyloid-beta in Alzheimer's disease.* Nat Rev Neurosci, 2007. **8**(7): p. 499-509.
283. Cummings, J., et al., *Alzheimer's disease drug development pipeline: 2019.* Alzheimers Dement (N Y), 2019. **5**: p. 272-293.
284. Nixon, R.A., et al., *Extensive involvement of autophagy in Alzheimer disease: an immuno-electron microscopy study.* J Neuropathol Exp Neurol, 2005. **64**(2): p. 113-22.
285. Nixon, R.A. and D.S. Yang, *Autophagy failure in Alzheimer's disease--locating the primary defect.* Neurobiol Dis, 2011. **43**(1): p. 38-45.
286. Lee, S., Y. Sato, and R.A. Nixon, *Primary lysosomal dysfunction causes cargo-specific deficits of axonal transport leading to Alzheimer-like neuritic dystrophy.* Autophagy, 2011. **7**(12): p. 1562-3.
287. Pickford, F., et al., *The autophagy-related protein beclin 1 shows reduced expression in early Alzheimer disease and regulates amyloid beta accumulation in mice.* J Clin Invest, 2008. **118**(6): p. 2190-9.
288. Nixon, R.A., *The role of autophagy in neurodegenerative disease.* Nat Med, 2013. **19**(8): p. 983-97.
289. Deverman, B.E., et al., *Gene therapy for neurological disorders: progress and prospects.* Nat Rev Drug Discov, 2018. **17**(10): p. 767.
290. Perez-Gonzalez, R., et al., *Leptin gene therapy attenuates neuronal damages evoked by amyloid-beta and rescues memory deficits in APP/PS1 mice.* Gene Ther, 2014. **21**(3): p. 298-308.
291. Carty, N., et al., *Intracranial injection of AAV expressing NEP but not IDE reduces amyloid pathology in APP+PS1 transgenic mice.* PLoS One, 2013. **8**(3): p. e59626.
292. Colella, P., G. Ronzitti, and F. Mingozzi, *Emerging Issues in AAV-Mediated In Vivo Gene Therapy.* Mol Ther Methods Clin Dev, 2018. **8**: p. 87-104.
293. Guo, Q., et al., *Small interfering RNA delivery to the neurons near the amyloid plaques for improved treatment of Alzheimers disease.* Acta Pharm Sin B, 2019. **9**(3): p. 590-603.
294. Levine, B., *Cell biology: autophagy and cancer.* Nature, 2007. **446**(7137): p. 745-7.
295. White, E. and R.S. DiPaola, *The double-edged sword of autophagy modulation in cancer.* Clin Cancer Res, 2009. **15**(17): p. 5308-16.
296. Janku, F., et al., *Autophagy as a target for anticancer therapy.* Nat Rev Clin Oncol, 2011. **8**(9): p. 528-39.
297. Kang, M.R., et al., *Frameshift mutations of autophagy-related genes ATG2B, ATG5, ATG9B and ATG12 in gastric and colorectal cancers with microsatellite instability.* J Pathol, 2009. **217**(5): p. 702-6.
298. Marino, G., et al., *Tissue-specific autophagy alterations and increased tumorigenesis in mice deficient in Atg4C/autophagin-3.* J Biol Chem, 2007. **282**(25): p. 18573-83.
299. Guo, J.Y., et al., *Autophagy suppresses progression of K-ras-induced lung tumors to oncocytomas and maintains lipid homeostasis.* Genes Dev, 2013. **27**(13): p. 1447-61.
300. Rao, S., et al., *A dual role for autophagy in a murine model of lung cancer.* Nat Commun, 2014. **5**: p. 3056.

301. Mathew, R., et al., *Autophagy suppresses tumorigenesis through elimination of p62.* Cell, 2009. **137**(6): p. 1062-75.
302. Karantza-Wadsworth, V., et al., *Autophagy mitigates metabolic stress and genome damage in mammary tumorigenesis.* Genes Dev, 2007. **21**(13): p. 1621-35.
303. White, E., *Deconvoluting the context-dependent role for autophagy in cancer.* Nat Rev Cancer, 2012. **12**(6): p. 401-10.
304. Ma, Y., et al., *Autophagy and cellular immune responses.* Immunity, 2013. **39**(2): p. 211-27.
305. Coussens, L.M., L. Zitvogel, and A.K. Palucka, *Neutralizing tumor-promoting chronic inflammation: a magic bullet?* Science, 2013. **339**(6117): p. 286-91.
306. Degenhardt, K., et al., *Autophagy promotes tumor cell survival and restricts necrosis, inflammation, and tumorigenesis.* Cancer Cell, 2006. **10**(1): p. 51-64.
307. Lum, J.J., et al., *Growth factor regulation of autophagy and cell survival in the absence of apoptosis.* Cell, 2005. **120**(2): p. 237-48.
308. DeYoung, M.P., et al., *Hypoxia regulates TSC1/2-mTOR signaling and tumor suppression through REDD1-mediated 14-3-3 shuttling.* Genes Dev, 2008. **22**(2): p. 239-51.
309. Bellot, G., et al., *Hypoxia-induced autophagy is mediated through hypoxia-inducible factor induction of BNIP3 and BNIP3L via their BH3 domains.* Mol Cell Biol, 2009. **29**(10): p. 2570-81.
310. Lock, R., et al., *Autophagy facilitates glycolysis during Ras-mediated oncogenic transformation.* Mol Biol Cell, 2011. **22**(2): p. 165-78.
311. Guo, J.Y., et al., *Activated Ras requires autophagy to maintain oxidative metabolism and tumorigenesis.* Genes Dev, 2011. **25**(5): p. 460-70.
312. Gong, C., et al., *Beclin 1 and autophagy are required for the tumorigenicity of breast cancer stem-like/progenitor cells.* Oncogene, 2013. **32**(18): p. 2261-72, 2272e 1-11.
313. Wolf, J., et al., *A mammosphere formation RNAi screen reveals that ATG4A promotes a breast cancer stem-like phenotype.* Breast Cancer Res, 2013. **15**(6): p. R109.
314. Galluzzi, L., et al., *Autophagy in malignant transformation and cancer progression.* EMBO J, 2015. **34**(7): p. 856-80.
315. Levy, J.M., et al., *Autophagy inhibition improves chemosensitivity in BRAF(V600E) brain tumors.* Cancer Discov, 2014. **4**(7): p. 773-80.
316. Amaravadi, R.K., et al., *Autophagy inhibition enhances therapy-induced apoptosis in a Myc-induced model of lymphoma.* J Clin Invest, 2007. **117**(2): p. 326-36.
317. Mathew, R., V. Karantza-Wadsworth, and E. White, *Role of autophagy in cancer.* Nat Rev Cancer, 2007. **7**(12): p. 961-7.
318. Lazova, R., et al., *Punctate LC3B expression is a common feature of solid tumors and associated with proliferation, metastasis, and poor outcome.* Clin Cancer Res, 2012. **18**(2): p. 370-9.
319. Mikhaylova, O., et al., *VHL-regulated MiR-204 suppresses tumor growth through inhibition of LC3B-mediated autophagy in renal clear cell carcinoma.* Cancer Cell, 2012. **21**(4): p. 532-46.
320. Yang, S., et al., *Pancreatic cancers require autophagy for tumor growth.* Genes Dev, 2011. **25**(7): p. 717-29.
321. Yazbeck, V.Y., et al., *Temsirolimus downregulates p21 without altering cyclin D1 expression and induces autophagy and synergizes with vorinostat in mantle cell lymphoma.* Exp Hematol, 2008. **36**(4): p. 443-50.
322. Crazzolara, R., K.F. Bradstock, and L.J. Bendall, *RAD001 (Everolimus) induces autophagy in acute lymphoblastic leukemia.* Autophagy, 2009. **5**(5): p. 727-8.
323. Zhu, K., K. Dunner, Jr., and D.J. McConkey, *Proteasome inhibitors activate autophagy as a cytoprotective response in human prostate cancer cells.* Oncogene, 2010. **29**(3): p. 451-62.

324. Czyzyk-Krzeska, M.F., J. Meller, and D.R. Plas, *Not all autophagy is equal.* Autophagy, 2012. **8**(7): p. 1155-6.
325. Morselli, E., et al., *Anti- and pro-tumor functions of autophagy.* Biochim Biophys Acta, 2009. **1793**(9): p. 1524-32.
326. Yang, Y., et al., *Cytoplasmic DAXX drives SQSTM1/p62 phase condensation to activate Nrf2-mediated stress response.* Nat Commun, 2019. **10**(1): p. 3759.
327. Laurin, N., et al., *Recurrent mutation of the gene encoding sequestosome 1 (SQSTM1/p62) in Paget disease of bone.* Am J Hum Genet, 2002. **70**(6): p. 1582-8.
328. Kwok, C.T., A. Morris, and J.S. de Belleroche, *Sequestosome-1 (SQSTM1) sequence variants in ALS cases in the UK: prevalence and coexistence of SQSTM1 mutations in ALS kindred with PDB.* Eur J Hum Genet, 2014. **22**(4): p. 492-6.
329. Fecto, F., et al., *SQSTM1 mutations in familial and sporadic amyotrophic lateral sclerosis.* Arch Neurol, 2011. **68**(11): p. 1440-6.
330. Li, J., et al., *Daxx plays a novel role in T cell survival but is dispensable in Fas-induced apoptosis.* PLoS One, 2017. **12**(3): p. e0174011.
331. Marston, F.A. and D.L. Hartley, *Solubilization of protein aggregates.* Methods Enzymol, 1990. **182**: p. 264-76.
332. Braz, V.A. and K.J. Howard, *Separation of protein oligomers by blue native gel electrophoresis.* Anal Biochem, 2009. **388**(1): p. 170-2.
333. Lu, K., F. den Brave, and S. Jentsch, *Receptor oligomerization guides pathway choice between proteasomal and autophagic degradation.* Nat Cell Biol, 2017. **19**(6): p. 732-739.
334. Berger, C., et al., *The commonly used marker ELAV is transiently expressed in neuroblasts and glial cells in the Drosophila embryonic CNS.* Dev Dyn, 2007. **236**(12): p. 3562-8.
335. Hwang, S., et al., *Drosophila DJ-1 decreases neural sensitivity to stress by negatively regulating Daxx-like protein through dFOXO.* PLoS Genet, 2013. **9**(4): p. e1003412.
336. Schmitt, F.J., et al., *Reactive oxygen species: re-evaluation of generation, monitoring and role in stress-signaling in phototrophic organisms.* Biochim Biophys Acta, 2014. **1837**(6): p. 835-48.
337. Holtzclaw, W.D., A.T. Dinkova-Kostova, and P. Talalay, *Protection against electrophile and oxidative stress by induction of phase 2 genes: the quest for the elusive sensor that responds to inducers.* Adv Enzyme Regul, 2004. **44**: p. 335-67.
338. Chen, X., et al., *2',7'-Dichlorodihydrofluorescein as a fluorescent probe for reactive oxygen species measurement: Forty years of application and controversy.* Free Radic Res, 2010. **44**(6): p. 587-604.
339. Woolley, J.F., J. Stanicka, and T.G. Cotter, *Recent advances in reactive oxygen species measurement in biological systems.* Trends Biochem Sci, 2013. **38**(11): p. 556-65.
340. Zielonka, J. and B. Kalyanaraman, *Hydroethidine- and MitoSOX-derived red fluorescence is not a reliable indicator of intracellular superoxide formation: another inconvenient truth.* Free Radic Biol Med, 2010. **48**(8): p. 983-1001.
341. Deng, Z., et al., *Autophagy Receptors and Neurodegenerative Diseases.* Trends Cell Biol, 2017. **27**(7): p. 491-504.
342. Carroll, B., et al., *Oxidation of SQSTM1/p62 mediates the link between redox state and protein homeostasis.* Nat Commun, 2018. **9**(1): p. 256.
343. Puto, L.A., J. Brognard, and T. Hunter, *Transcriptional Repressor DAXX Promotes Prostate Cancer Tumorigenicity via Suppression of Autophagy.* J Biol Chem, 2015. **290**(25): p. 15406-20.
344. Murthy, A.C. and N.L. Fawzi, *The (un)structural biology of biomolecular liquid-liquid phase separation using NMR spectroscopy.* J Biol Chem, 2020. **295**(8): p. 2375-2384.
345. Murthy, A.C., et al., *Molecular interactions underlying liquid-liquid phase separation of the FUS low-complexity domain.* Nat Struct Mol Biol, 2019. **26**(7): p. 637-648.

346. Conicella, A.E., et al., *ALS Mutations Disrupt Phase Separation Mediated by alpha-Helical Structure in the TDP-43 Low-Complexity C-Terminal Domain.* Structure, 2016. **24**(9): p. 1537-49.
347. Murray, D.T., et al., *Structure of FUS Protein Fibrils and Its Relevance to Self-Assembly and Phase Separation of Low-Complexity Domains.* Cell, 2017. **171**(3): p. 615-627 e16.
348. Guzikowski, A.R., Y.S. Chen, and B.M. Zid, *Stress-induced mRNP granules: Form and function of processing bodies and stress granules.* Wiley Interdiscip Rev RNA, 2019. **10**(3): p. e1524.
349. Jiang, H., et al., *Phase transition of spindle-associated protein regulate spindle apparatus assembly.* Cell, 2015. **163**(1): p. 108-22.
350. Li, P., et al., *Phase transitions in the assembly of multivalent signalling proteins.* Nature, 2012. **483**(7389): p. 336-40.
351. Bergeron-Sandoval, L.P., N. Safaee, and S.W. Michnick, *Mechanisms and Consequences of Macromolecular Phase Separation.* Cell, 2016. **165**(5): p. 1067-1079.
352. Elbaum-Garfinkle, S., et al., *The disordered P granule protein LAF-1 drives phase separation into droplets with tunable viscosity and dynamics.* Proc Natl Acad Sci U S A, 2015. **112**(23): p. 7189-94.
353. Ishii, T., et al., *Low micromolar levels of hydrogen peroxide and proteasome inhibitors induce the 60-kDa A170 stress protein in murine peritoneal macrophages.* Biochem Biophys Res Commun, 1997. **232**(1): p. 33-7.
354. Nakagawa, H., et al., *ER stress cooperates with hypernutrition to trigger TNF-dependent spontaneous HCC development.* Cancer Cell, 2014. **26**(3): p. 331-343.
355. Denk, H., et al., *Are the Mallory bodies and intracellular hyaline bodies in neoplastic and non-neoplastic hepatocytes related?* J Pathol, 2006. **208**(5): p. 653-61.
356. Zatloukal, K., et al., *From Mallory to Mallory-Denk bodies: what, how and why?* Exp Cell Res, 2007. **313**(10): p. 2033-49.
357. Umemura, A., et al., *p62, Upregulated during Preneoplasia, Induces Hepatocellular Carcinogenesis by Maintaining Survival of Stressed HCC-Initiating Cells.* Cancer Cell, 2016. **29**(6): p. 935-948.
358. Duran, A., et al., *p62/SQSTM1 by Binding to Vitamin D Receptor Inhibits Hepatic Stellate Cell Activity, Fibrosis, and Liver Cancer.* Cancer Cell, 2016. **30**(4): p. 595-609.
359. Rea, S.L., et al., *New insights into the role of sequestosome 1/p62 mutant proteins in the pathogenesis of Paget's disease of bone.* Endocr Rev, 2013. **34**(4): p. 501-24.
360. Chamoux, E., et al., *The p62 P392L mutation linked to Paget's disease induces activation of human osteoclasts.* Mol Endocrinol, 2009. **23**(10): p. 1668-80.
361. Olbrich, T., et al., *A p53-dependent response limits the viability of mammalian haploid cells.* Proc Natl Acad Sci U S A, 2017. **114**(35): p. 9367-9372.
362. Sanchez-Martin, P., et al., *NBR1-mediated p62-liquid droplets enhance the Keap1-Nrf2 system.* EMBO Rep, 2020. **21**(3): p. e48902.
363. Isogai, S., et al., *Crystal structure of the ubiquitin-associated (UBA) domain of p62 and its interaction with ubiquitin.* J Biol Chem, 2011. **286**(36): p. 31864-74.
364. Wooten, M.W., et al., *Essential role of sequestosome 1/p62 in regulating accumulation of Lys63-ubiquitinated proteins.* J Biol Chem, 2008. **283**(11): p. 6783-9.
365. Lin, C.W., et al., *Daxx inhibits hypoxia-induced lung cancer cell metastasis by suppressing the HIF-1alpha/HDAC1/Slug axis.* Nat Commun, 2016. **7**: p. 13867.
366. Heaphy, C.M., et al., *Altered telomeres in tumors with ATRX and DAXX mutations.* Science, 2011. **333**(6041): p. 425.